A REVIEW OF POLISH AERONAUTICAL FATIGUE AND STRUCTURAL INTEGRITY INVESTIGATIONS DURING MAY 2019 TO APRIL 2023

by

Antoni Niepokólczycki

Lukasiewicz Research Network - Institute of Aviation, Warsaw, POLAND

(Investigations in Civil Aviation)

and

Marcin Kurdelski

Air Force Institute of Technology, Warsaw, POLAND

(Investigations in Military Aviation)

ICAF 2023

The 38th Conference and the 31st Symposium of the International Committee on Aeronautical Fatigue and Structural Integrity, Delft, The Netherlands, June 26 - 29, 2023

Contents

INVESTIGATIONS IN CIVIL AVIATION

1. JOINTS

1.1. *Investigation into the effect of RFSSW parameters on tensile shear fracture load of 7075-T6 Alclad aluminium alloy joints* – A. Kubit, T. Trzepieciński, E. Gadalińska, J. Slota, W. Bochnowski [Rzeszów University of Technology, Ł-ILOT, Technical University of Košice, University of Rzeszów]

The aim of the investigations was to determine the effect of parameters of refill friction stir spot welding (RFSSW) on the fracture load and failure mechanisms of the resulting joint. RFSSW joints were made in 7075-T6 Alclad aluminium alloy sheets using different welding parameters. The load capacity of joints was determined under tensile/shear loadings. Finite element-based numerical simulations of the joint-loading process were carried out, taking into account the variability of elasto-plastic properties of weld material through the joint cross-section. The influence of welding parameters on selected phenomena occurring during the destruction of the joint was presented. The considerations were supported by a fractographic analysis based on SEM images of fractures. It was found that there is a certain optimal amount of heat generated, which is necessary to produce the correct joint in terms of its load capacity. This value should not be exceeded, because it leads to weakening of the base material and thus to a reduction in the strength of the joint. Samples subjected to uniaxial tensile shear load showed three types of failure mode (tensile fracture, shear fracture, plug type fracture) depending on the tool rotational speed and duration of welding. Prediction of the fracture mode using FE-based numerical modelling was consistent with the experimental results. The samples that were damaged due to the tensile fracture of the lower sheet revealed a load capacity (LC) of 5.76 KN. The average value of LC for the shear fracture failure mechanism was 5.24 kN. The average value of the LC for plug-type fracture mode was 5.02 kN. It was found that there is an optimal amount of heat generated, which is necessary to produce the correct joint in terms of its LC. Excessive overheating of the joint leads to a weakening of the base metal and thus a reduction in the strength of the joint. Measurements of residual stresses along the axis specimens showed the presence of stresses with a certain constant value for the welded area on the side of the 1.6 mm thick plate.

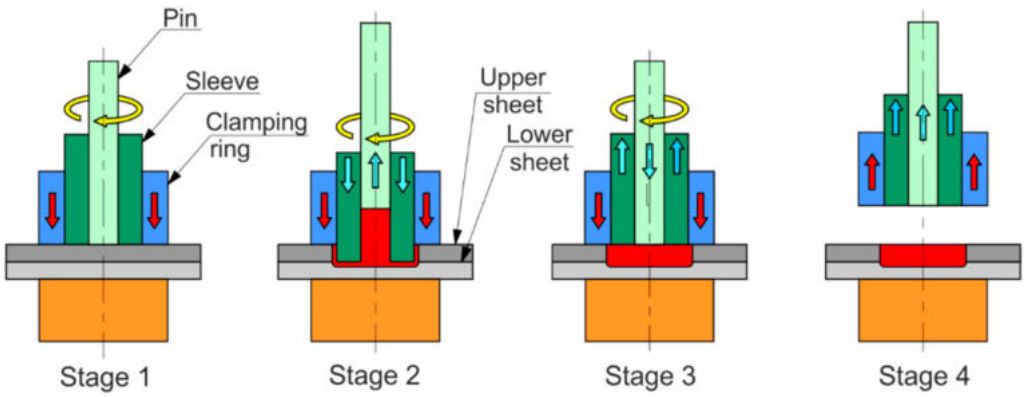

Fig. 1 Stages of refill friction stir spot welding.

Consequently, the effect of RFSSW parameters on tensile shear fracture load of 7075T6 Alclad aluminium alloy joint was investigated. Based on the results of the investigations, the following conclusions could be drawn:

1. The s ample produced at the tool rotational speed n = 2400 rpm and duration of welding t = 3.5 s had the highest load capacity. The results of the tensile shear test revealed tensile fracture mode for this specimen.
2. As a result of insufficient plasticisation of the materials being joined during the RFSSW process with the parameters n = 2000 rpm and t = 2.5 s, a joint was produced, which showed the shear fracture mode. Microstructural analysis showed a fine-grained structure in the area of operation of the pin; however, the peripheral zone of the weld was subjected to less heat, which was associated with a weakening of the joint. The fracture initiated in this zone.
3. Destruction of the weld through plug-type fracture mode is a weld defect associated with a weakened or insufficient mixing of material near the circumference of the weld in the upper sheet.
4. The samples that were damaged due to the tensile fracture of the lower sheet were showed load capacity of 5.76 KN. The average value of load capacity for the shear fracture failure mechanism was 5.24 kN. The average value of the load capacity for plug-type fracture mode was 5.02 kN.
5. The highest values of tool rotation speed as well as welding time that were considered lead to the generation of an excessive amount of heat in the joining process, which in turn led to a significant expansion of the HAZ in both upper and lower sheets.
6. It was found that there is an optimal amount of heat generated, which is necessary to produce the correct joint in terms of its load capacity. Excessive overheating of the joint leads to a weakening of the base metal and thus a reduction in the strength of the joint.
7. The processes taking place during thermo-mechanical joint formation change the value of the modulus of elasticity and the hardness of the weld nugget in relation to the base material.
8. Measurements of residual stresses along the axis specimens showed the presence of stresses with a certain constant value for the welded area on the side of the 1.6 mm thick plate. In the case of thinner sheet (0.8 mm), the stress value relaxed at a distance of about 3 mm from the centre of the weld. Precise determination of the stress values in the plate's base material was disabled by the relatively coarse grain size of the material.
9. For each specimen, for each plate and for each stress direction tested, the stress values were similar and ranged from about −60 MPa to about 40 MPa.
10. In the case of stresses in the radial direction, for both the thicker and the thinner sheets, the stress values in the central area of the weld are similar, being compressive and approx. −40 MPa.
11. It is worth considering more in-depth diffraction studies to determine the full stress tensor and to determine von Mises stress values to make the comparison with numerical modelling possible.

Acknowledgment
The authors are grateful for the support in the experimental work to the Slovak Research and Development Agency under project APVV-17-0381—Increasing the efficiency of forming and joining parts of hybrid car bodies; the Grant Agency of the Ministry of Education, Science, Research, and Sport of the Slovak Republic (grant number VEGA 1/0259/19). and ITMS 26220220182—University Science Park TECHNICOM for innovation applications supported by knowledge technologies.

Contact
Andrzej Kubit akubit@prz.edu.pl

1.2. *Checking the Correctness of the Process of Brazing of the Honeycomb Seal to the Base by Ultrasonic Method* - Agata Świerek, Józef Krysztofik, Wojciech Matczak, Antoni Niepokólczycki [Calisia University - Kalisz, Łukasiewicz Research Network - Institute of Aviation, Aalberts Surface Technologies]

This work is focused on the checking of the correctness of the brazing process of honeycomb seals to stationary elements of aircraft turbine engines. It describes this process, paying attention to the aspects that have a fundamental impact on whether the seal will be brazed to the base as required, or whether the unacceptable areas of non-brazing will appear.

The aim of the study was to check the possibility of using the ultrasonic method to check the correctness of the brazing process of honeycomb seals and to compare the tests carried out using this method with the mostly used visual tests.

The research carried out as part of the work showed very well that there are reasons to use the ultrasonic defectoscopy method to test the correctness of the brazing process of honeycomb seals in the elements of aircraft engines. This method also makes it possible to automate the checking process, fully document it, and objectively assess the correctness of the connection.

The results obtained in the study provide a very good starting point for further research, the aim of which will be to implement the ultrasonic defectoscopy method for testing the correctness of brazing honeycomb seals into practice in industrial conditions.

The basic, currently used method of controlling the correctness of the process of soldering of the honeycomb seals in the elements of air engines is visual control using a borescope and gravitational tightness test.

Visual control consists in checking if there is a meniscus on the edges connecting the honeycomb seal with the basic material and whether there are disqualifying damage in the structure of the seal.

Below (Fig. 1), examples of the correct and bad layout of the solder in the honeycomb seal are schematically presented.

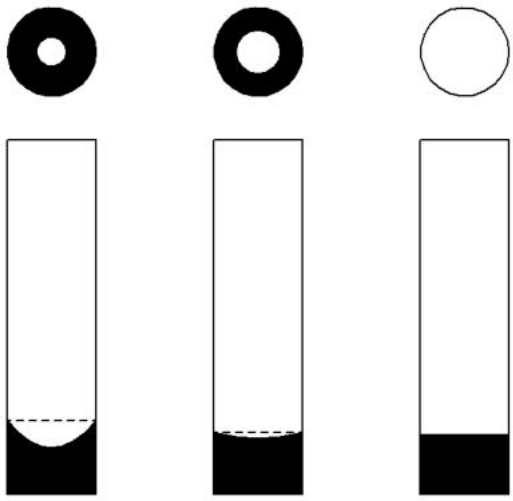

Fig. 1. Examples of the correct and bad layout of the solder in the sealant cell

Left cell - an example of correct soldering, a dark ring indicates that the solder swam on the walls of the cell to the right height.

Central cell - an example of average soldering, the dark ring is much thinner. The illustration indicates that the solder swam on the walls of the cell to a low height.

Right cell - an example of bad soldering, no solder on the cell walls.

The aim of the work was to check the possibility of using the ultrasonic method to test the correctness of the soldering process of honeycomb seals in aircraft engine components and to compare the tests carried out using this method with the currently used visual tests.

For this purpose:

- a method for testing samples of sealant soldered to the base with the use of ultrasonic detection was developed,
- ultrasonic testing of samples was carried out,
- an analysis of the obtained test results was carried out,
- the summary compares both test methods - visual and ultrasonic – in the context of testing the correctness of the soldering process of the honeycomb seal.

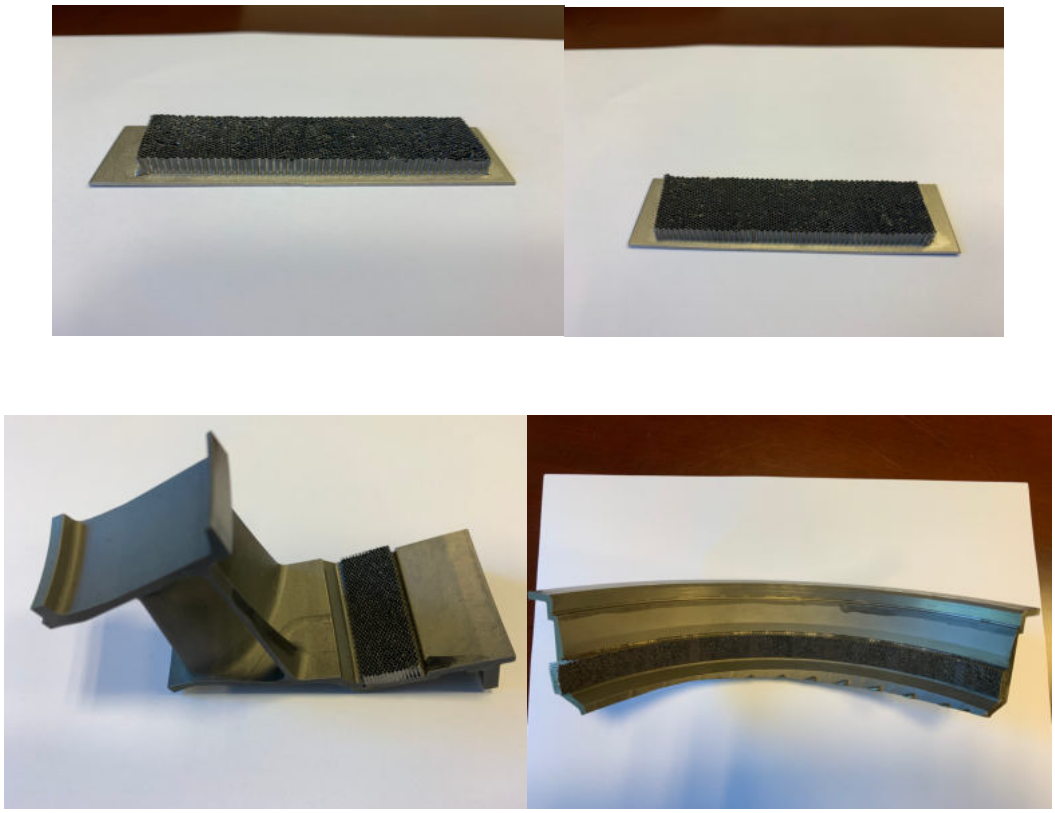

Fig. 2. Test samples

The tests were carried out using the ultrasonic method using the echo technique. The signal generated by the flaw detector transmitter is sent to the transducer located in the head. Stimulated by this signal, the transducer emits an acoustic wave. Then, this wave passes through the coupling medium - a liquid that covers the surface around its contact with the head - to the tested part of the object. At the substrate-sealer interface, the wave undergoes e.g., reflection and is received by the head transducer.

If there is a proper connection between the base and the sealant, then the wave is partly reflected and partly propagated in the walls of the sealant. The reflected wave, after processing, is visualized on the flaw detector screen in the form of pulses with specific amplitudes, located in specific places - Fig. 3, Fig. 4.

If the connection is incorrect, i.e., there is an air gap between the base and the seal, almost complete reflection of the waves occurs. This is visible on the flaw detector screen by the increased amplitude of the pulses (in relation to the proper connection) - Fig. 5, Fig. 6. Depending on the amount of "attached" remnants of filler cells, this amplitude fluctuates somewhat, but it always remains higher than in the places of proper connection.

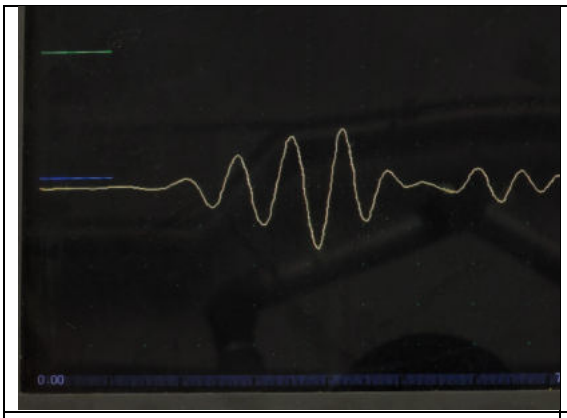

Fig. 3. The image of the reflected wave at the correct connection of the base and the sealant

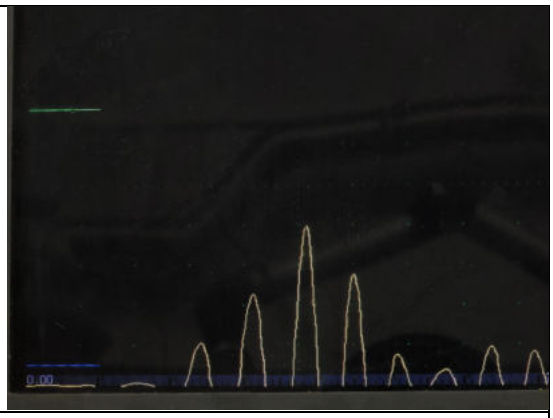

Fig. 4. The image of the reflected wave at the correct connection of the base and the sealant

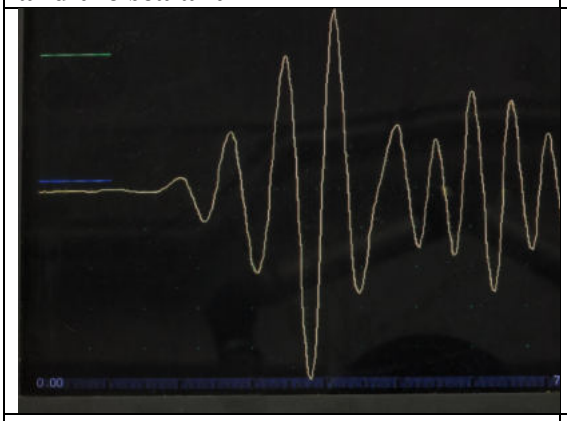

Fig. 5. The image of the reflected wave at the wrong base-sealer connection

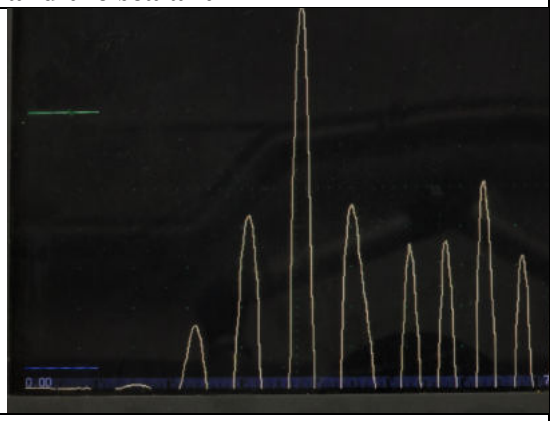

Fig. 6. The image of the reflected wave at the wrong base-sealer connection

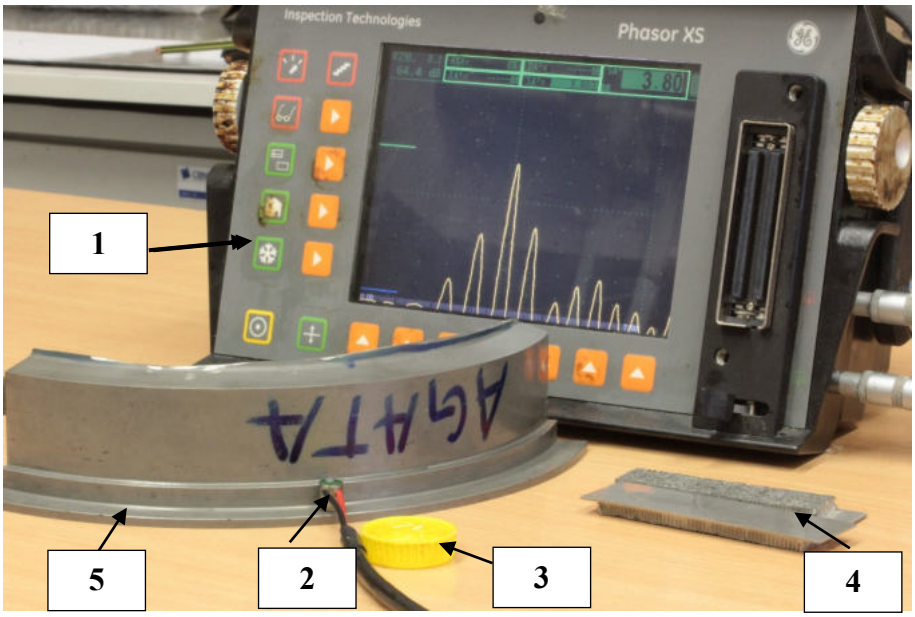

Fig.7. Test system for assessing the condition of base-cellular sealant connections: 1 - ultrasonic flaw detector, 2 - head, 3 - coupling medium, 4 - reference sample, 5 - tested object

The tests of four samples carried out using the ultrasonic flaw detection method showed very well that there are premises to use this method to test the correctness of the soldering process of honeycomb seals in aircraft engine components.

During the tests of the samples, the areas of proper connection of the sealant with the base were clearly indicated, when the wave is partially reflected and partially propagated in the walls of the sealant, as well as areas of improper connection, when there is an air gap between the base and the seal, and the waves are almost completely reflected.

Since the last sample was tested by both methods - visual and ultrasonic - the times of these tests were compared. In both cases, the time to prepare the test stand was approximately the same, i.e., about 15 minutes. The time of the visual examination alone was 10 minutes, while the time of the ultrasonic examination with the marking of areas of incorrect connection was half as long. It should be noted that a specially cut part of the engine part was tested, and the increase in the area to be checked significantly extends the time of visual inspection than that of ultrasonic inspection.

In addition, performing a visual check of the joint of the sealant with the base requires the operator's full involvement throughout the entire process and his decision regarding the correctness of the joint based on subjective observations. In the case of using the ultrasonic method, it is possible to automate the inspection process, fully document it and objectively assess the correctness of the connection.

The research and analyzes carried out in the work indicate the possibility of implementing the ultrasonic flaw detection method to test the correctness of the soldering process of honeycomb seals in aircraft engine components into practice in industrial conditions.

Contact:

Antoni Niepokólczycki Antoni.niepokolczycki@ilot.lukasiewicz.gov.pl

2. ADDITIVE MANUFACTURING (AM)

2.1. *Microstructural and Mechanical Properties of Selective Laser Melted Inconel 718 for Different Specimen Sizes* – Bartosz Madejski, Maciej Malicki, Konrad Gruber [Ł-ILOT, Wrocław University of Science and Technology]

Selective laser melting (SLM) falls into the category of additive manufacturing technologies that are being increasingly used in the aerospace industry. This study presents the results of the examination of the microstructure and mechanical properties of selective laser melted Inconel 718. The tests were carried out for samples of different geometry (thickness, shape). The investigation showed the effect of the specimen's size and the printing direction on the microstructure and mechanical properties. In the microstructural investigation, light and scanning electron microscopes were used. The microstructure investigation included measurements of the grain size and the carbides' content. In order to estimate porosity computer tomography was used. Tensile tests were carried out at room temperature. The results showed differences in mechanical and microstructural properties of different size specimens.

MATERIALS AND METHODS / PROCEDURE

Mechanical tests were performed for heat treated INCONEL 718 alloy, manufactured in three printing directions (0°, 45°, 90°) and for two specimen types (Table 1). For each test conditions, 3 samples were tested. All samples before machining and tensile tests were heat treated according to Table 2.

Table 1. Test plan for tensile tests

Alloy	Heat treatment	Printing direction	Test temp.	Drawing type	No. of the sample per one test condition	SUM
1	1	3	1	2	3	**18**
Inconel 718	HT	00 degree 45 degrees 90 degrees	22 C	D5 – d=4,06 mm D6 – d= 6,35 mm	-	

Static tensile tests were performed for two types of specimens (D5 and D6) in order to show how differences in a sample's size affect its mechanical properties. The geometry (Fig. 1) of the test specimens and tensile testing procedures were carried out in accordance with the ASTM E8/E8M-16a standard.

Table 2. Heat treatment parameters

Type	Stress relieving	HIP	Solutioning	Ageing
HT	1150°C / 6h / parts on platform / FC	N/A	1100°C / 1h / WC or AC	718°C / 8h + 621°C / to 18h / AC
HT0	1150°C / 6h / parts on platform / FC	N/A	N/A	N/A

Tensile tests were carried out at room temperature at a strain rate of 0,005 [mm/mm/min] up to yield strength (0,2%) and after that rate increased to 0,05 [mm/mm/min] and the test was performed up to rupture. The goal of performing tensile tests was to determine Yield Strength

0.2% (YS0,2%), ultimate tensile strength (UTS), Young's modulus (E), elongation, and reduction of area.

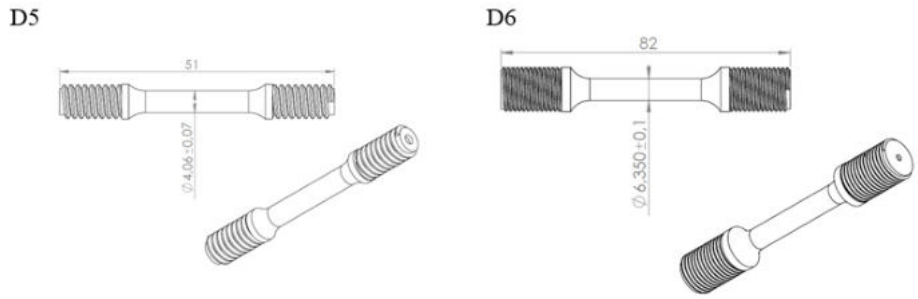

Fig. 1. Samples D5 and D6 for tensile tests.

For the microstructure investigation, the raw bars 3 and 6 mm in diameter and the plate type specimen (Fig. 2) were built. From the raw bars and the plate type specimen, the metallographic cross sections in the planes perpendicular and parallel to the longitudinal axis of the raw bars/plate type specimens were prepared.

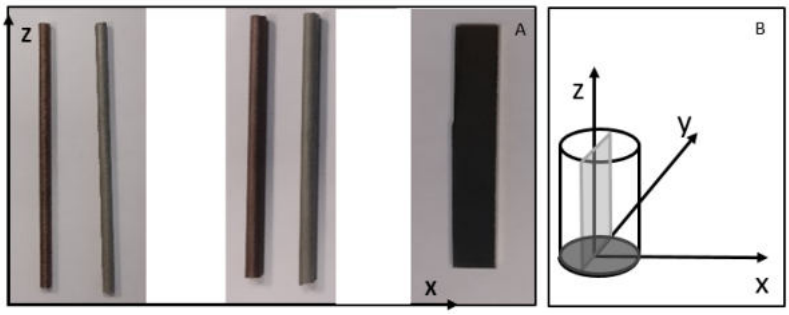

Fig. 2. Raw bars - d=3mm, d=6mm and plate type sample (1x10x100 mm) for microstructure investigation (A) and metallographic orientation with respect to the specimen axis (B).

The metallographic cross sections were etched using etchant no. 22 according to ASTM E 407 for the grain size evaluation and Kalling's etchant 1 for the carbides content evaluation. The grain size evaluation was carried out using the ASTM E 112 Heyn intercept method. The microstructure investigation was performed for Inconel 718 after HT and HT0 heat treatment (Table 3) with Keyence VHX6000 microscope. For the same raw bars and plate type specimen the CT scans were generated (Fig. 3) with a GE v/tome/xs 240 tomograph.

Table 3. Test plan for microstructure investigation

Alloy	Heat treatment	Printing direction	Drawing type	SUM
1	2	3	3	**18**
Inconel 718	HT0 HT	00 degree 45 degrees 90 degrees	raw bar (d= 3mm) raw bar (d= 6 mm) plate type sample (1x10x100mm)	

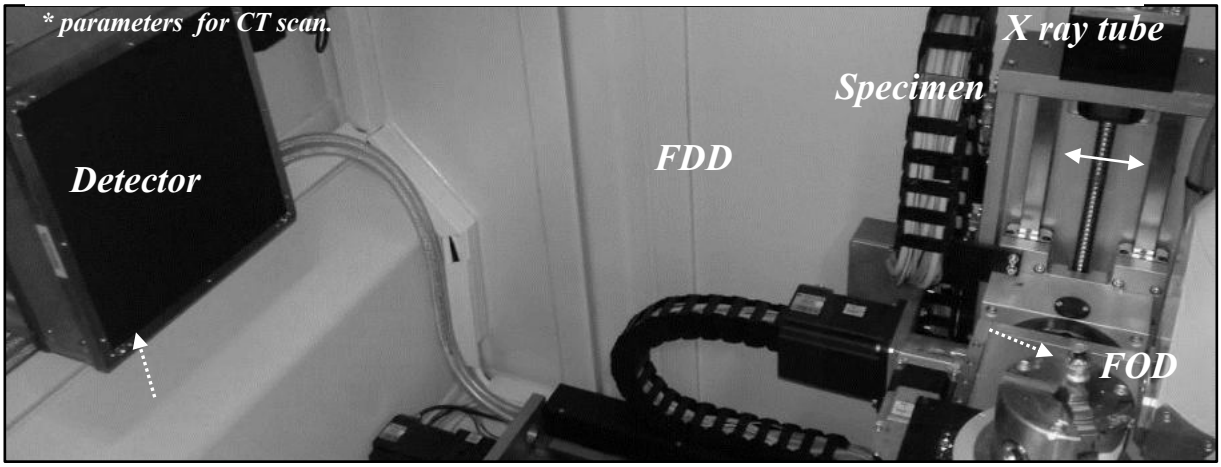

Fig. 3. CT System with parameters used for tested specimens.

RESULTS AND DISCUSSION

Mechanical tests – results

Different types of samples were built in order to determine the effect the surface roughness and the printing direction had on the mechanical properties (Fig. 4). The gage section of samples was not machined. The surface of the samples was therefore in the as-built state. This means that after printing, the samples were heat treated, the supports were hand-tool removed and the surface was only sandblasted in order to clean it after the supports had been removed.

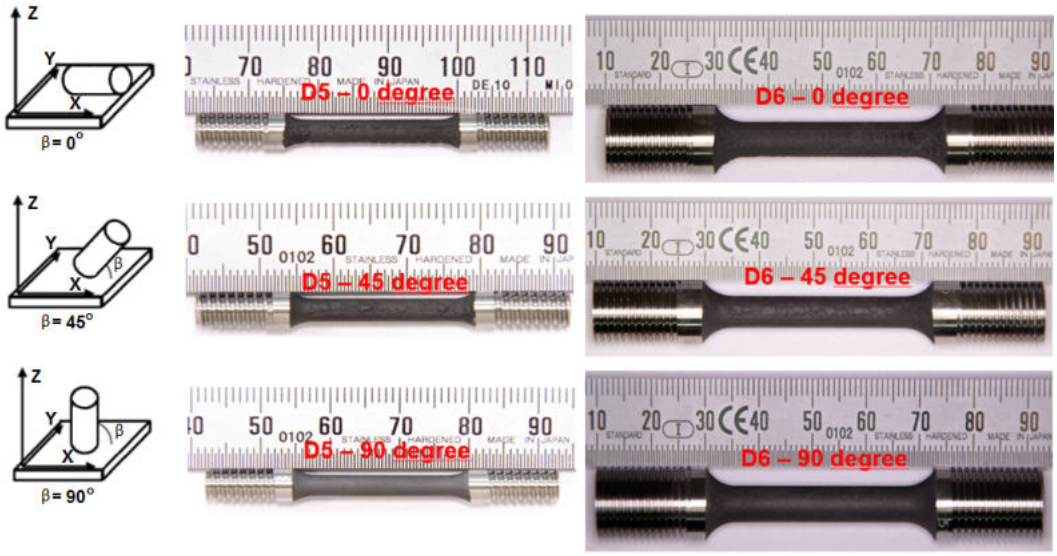

Fig. 4. Tensile tests, samples D5 and D6 (printing direction 0º, 45º and 90º).

The requirements for the mechanical properties for IN718 (additively manufactured) are included in the ASTM F3055-14 standard. For each tested specimen size (D5 and D6), the minimum requirements for elongation, ultimate tensile strength (UTS) and the yield strength (YS 0.2%) as specified in ASTM F3055-14 were obtained (Fig.5).

For some printing directions, it is necessary to use supports in order to manufacture samples without deformations. The samples manufactured in the direction of 90º (axis Z) do not have supports in the gage section, while the samples printed in the direction of 0º and 45º are characterized by a big number of supports with the biggest number of supports required for

the printing direction 0º. The number of supports affects the results of mechanical tests. The results for yield strength and ultimate tensile strength are more repeatable for samples without support (90º) compared to samples with supports (0º, 45º).

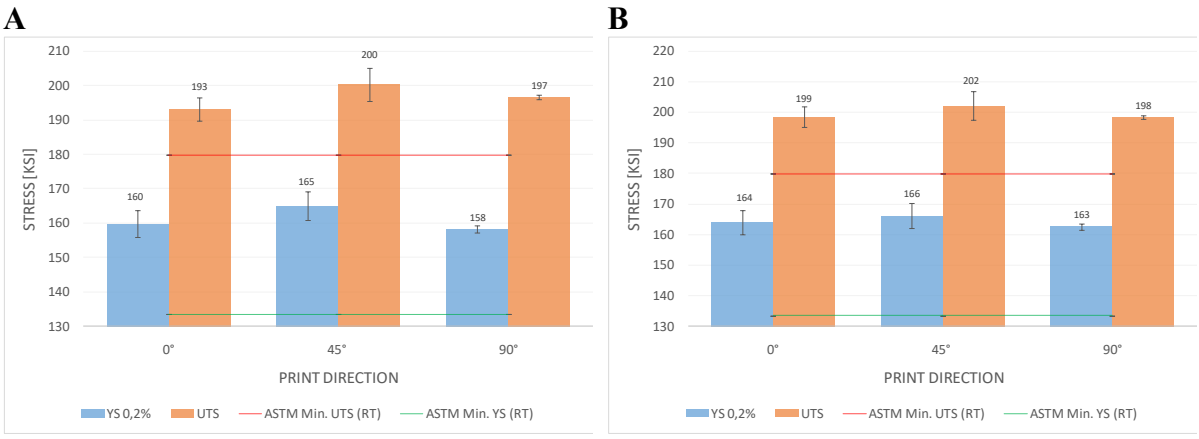

Fig. 5. Results for tensile tests for samples D5-A and D6-B (yield strength 0.2% - YS 0,2%, ultimate tensile strength - UTS).

As regards elongation and reduction of area (Fig. 6), it was observed that the printing direction impacted the results more significantly. The lowest elongation and reduction of area was observed for printing direction 0º while the highest result was obtained for 90º. The supports caused the occurrence of more cracks and pores at the support surface area, which reduced the ductility of the material.

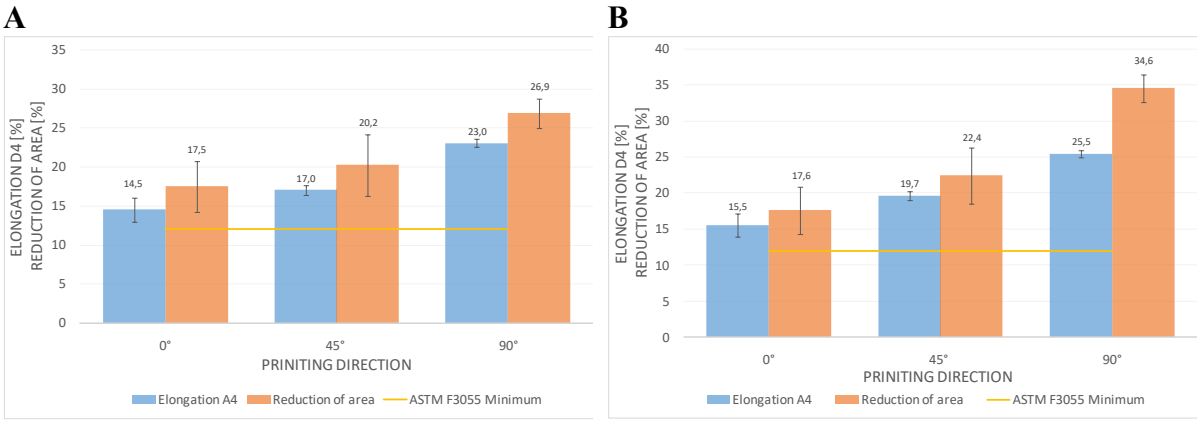

Fig. 6. Results for tensile tests for samples D5-A and D6-B (elongation A4, reduction of area).

The static tensile tests carried out for D6 samples allowed researchers to determine the effect of the size of printed bars on the mechanical properties. The gage section for D6 samples (d=6,35 mm) was also of an as-built type, however the diameter of this sample was higher than D5 sample (d=4,06mm). Comparing the results for samples D5 and D6 revealed that the mechanical properties (yield strength 0,2% and ultimate tensile strength) were about 1-4% higher for D6 samples. This was probably due to a higher percentage of active cross-section than for D5 samples. Defects such as a spherical shape of the gage section, higher roughness, and misalignment of the gage section with respect to the gripping part could affect the repeatability of the results.

Microstructural investigation – results

Typically, the primary structure of Inconel 718 after SLM, consists of epitaxial groaned columnar grains with a cellular substructure. Also, adverse segregations, Laves phases or MC carbides can be present. After HT and HT0 heat treatment epitaxial groaned grain structures were not observed (Fig. 7, 8, 9).

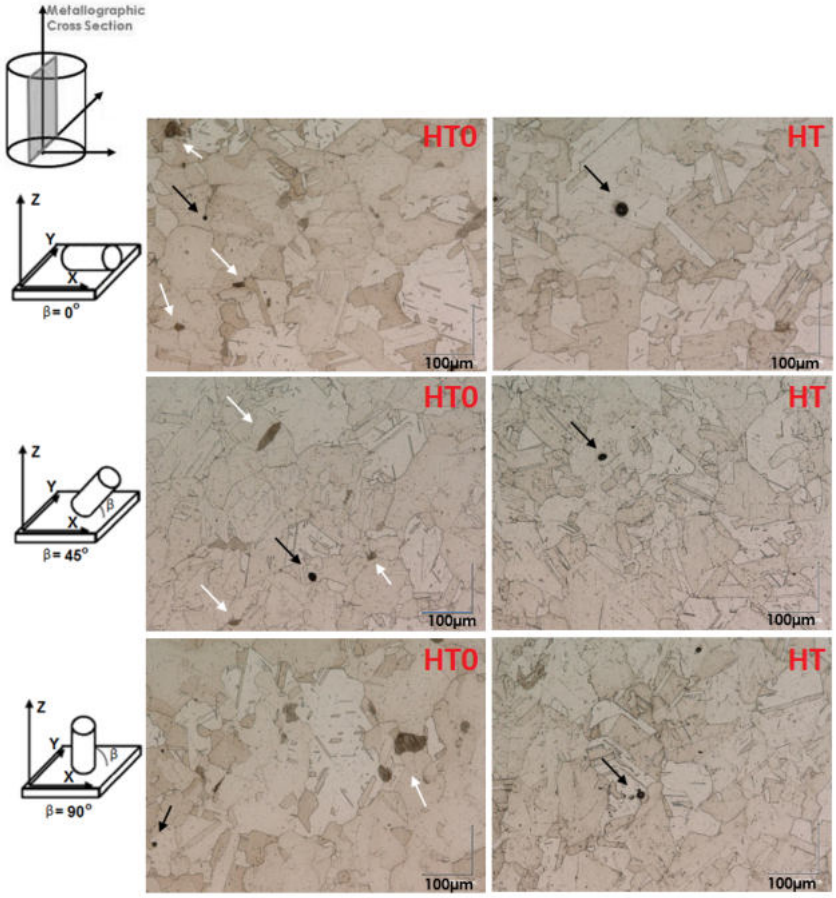

Fig. 7. Structure of Inconel 718 after HT0 and HT heat tratement in 3mm raw bars.

In general, there are no significant differences in the observed microstructure between HT and HT0 as well as between different printing directions. The structure after HT and HT0 consists of equiaxed grains with carbides (Fig. 10) in the form of small precipitates distributed in the grains as well as in grain boundaries. There are twin boundaries visible.

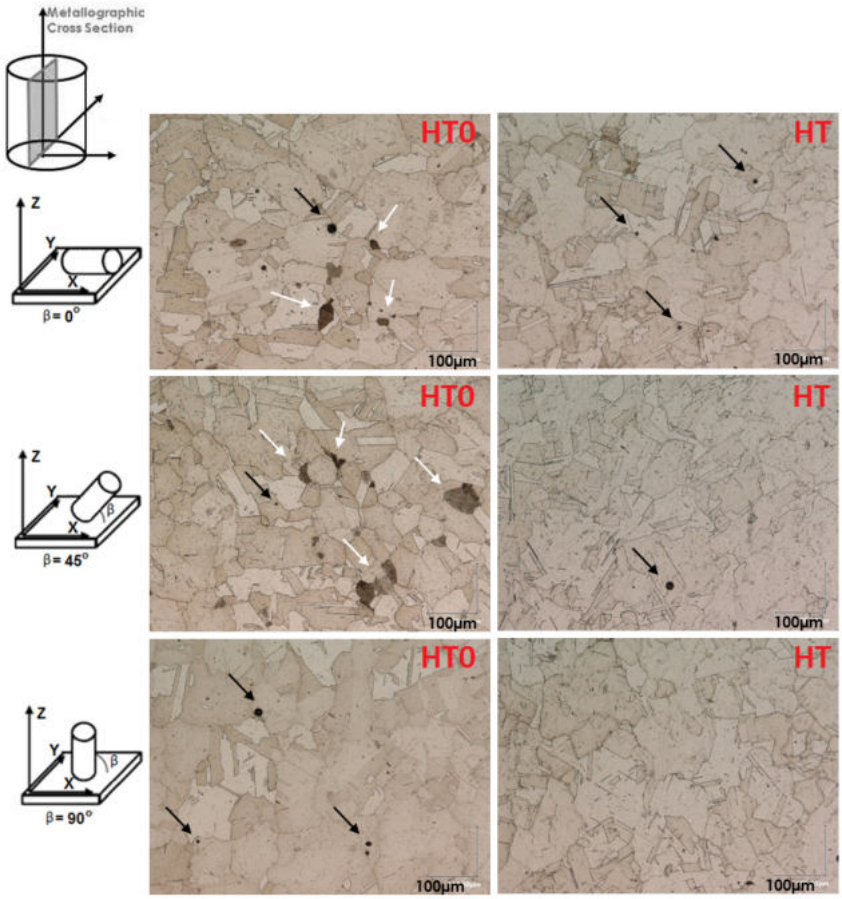

Fig. 8. Structure of Inconel 718 after HT0 and HT heat tratement in 6mm raw bars.

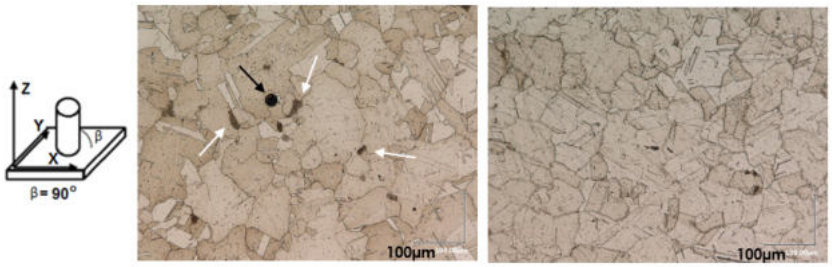

Fig. 9. Structure of Inconel 718 after HT0 and HT heat tratement in plate type specimens.

Some of the grains after HT0 were much darker than the rest of the grains. Such dark grains (white arrows in Fig 7, Fig. 8, Fig. 9) were observed in the stress relieved structure and the dark color is related to the element segregation or cellular substructure from epitaxial groaned grains. This may indicate that the recrystallization and homogenization of the material had not been achieved in full. After HT, those darker grains disappeared. Also, in the specimens after HT0 and HT some individual voids (pores) were found (black arrows on Fig. 7, Fig. 8, Fig 9).

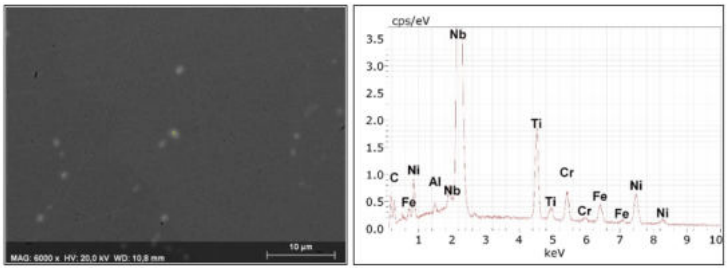

Fig. 10. EDX spectra for precipitations representing carbides in printed Inconel 718 in a bar rod 6mm printed in 45° direction after HT.

The grain size evaluation (Fig.11, Table 4) showed that after HT the grain size was slightly smaller, but the differences were within the general measurement error.

Table. 4. Numeric values of the grain size measurements for raw bars and plate type specimens.

Printing direction	Grain size [G±95%CI]					
	Specimen					
	ø3 mm		ø6 mm		plate	
	HT0	HT	HT0	HT	HT0	HT
0°	4,4±0,4	4,2±0,3	4,1±0,6	4,0±0,3	-	-
45°	4,3±0,4	4,1±0,3	4,5±0,3	3,7±0,3	-	-
90°	4,6±0,3	4,3±0,3	4,6±0,3	4,5±0,3	4,6±0,4	4,6±0,3

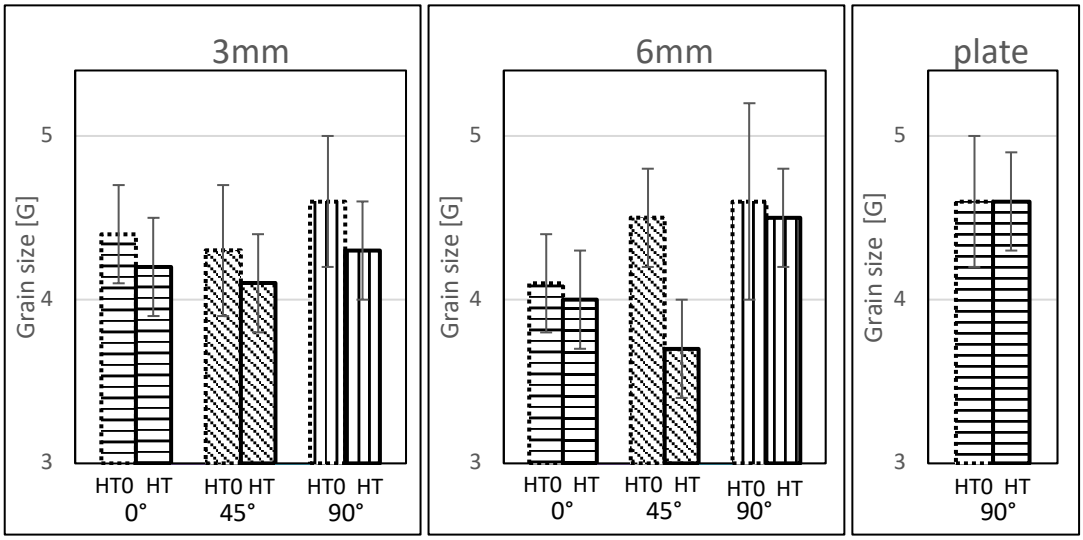

Fig. 11. Grain size evaluation for raw bars and plate type specimens.

It was found that in the surface area of all specimens there were places where the carbides content was much higher than in the volume area (Fig. 12). In general, there were no significant differences between carbide content in the specimens inspected (Fig. 13, Fig. 14). In the metallographic cross section from the raw bars printed in direction 0° and 45°, in the surface area there was a higher content of voids and presence of lack of fusion and micro cracks, which was most probably associated with the supports (Fig. 15).

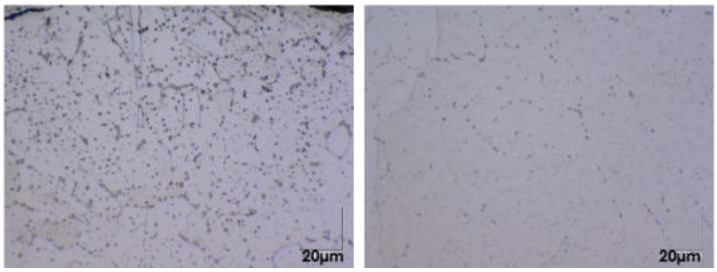

Fig. 12. Carbides in the surface area and in the material volume in one of the printed bar rod.

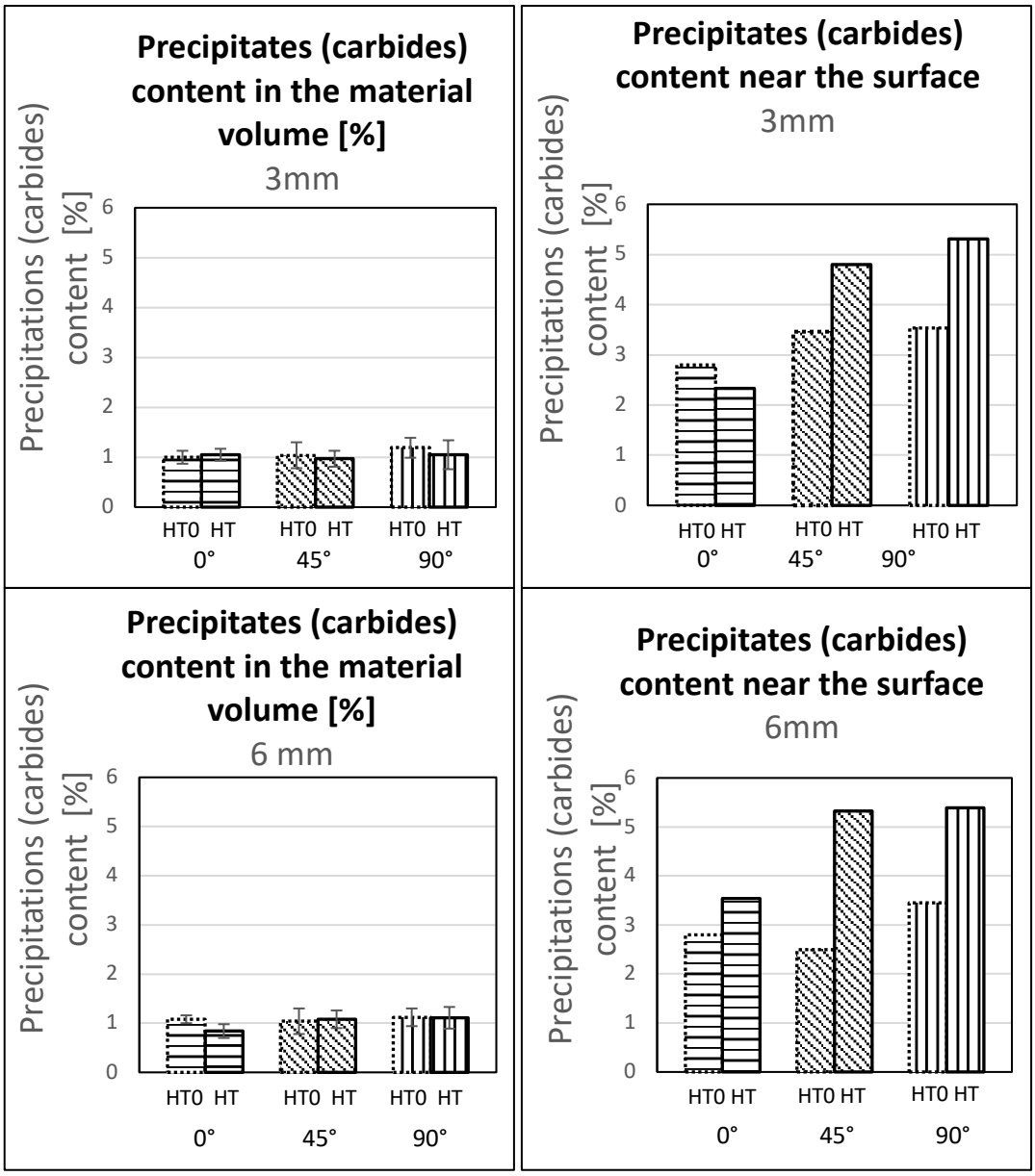

Fig. 13. Carbides content in printed bar rods.

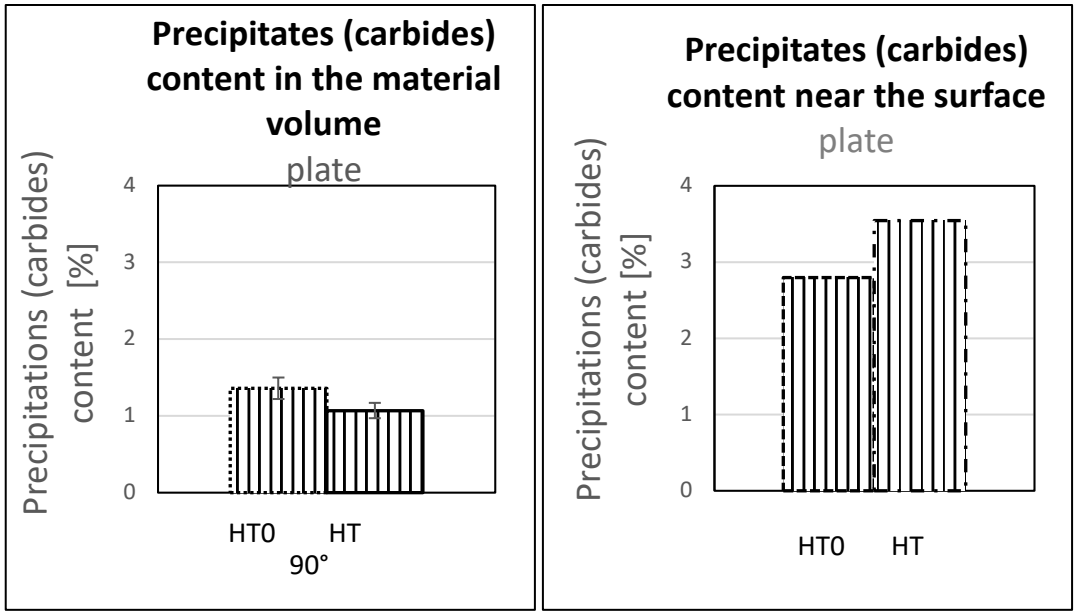

Fig. 14. Carbides content in plate type specimen.

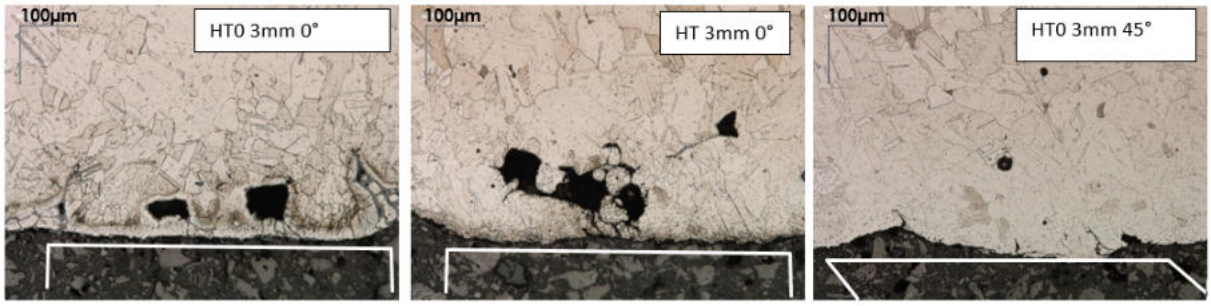

Fig. 15. Support surface area of raw bars printed in 45° and 0° direction.

The CT inspection revealed voids in all bars and plate specimens tested. The classification of materials as void or solid was done with VG STUDIO MAX 2.1 software. The solids and voids (air) are represented by two different peaks on the grey value distribution of the voxels in the volume scanned. Voids and solid were defined automatically based on statistical information about the voxels covered with a typical void (Darker) and solid (brighter) areas (Fig. 16). Void volume fraction in the inspected elements was measured by counting the relevant voxels. On metallographic cross section it was found that the voids with a diameter below 30µm could have significant share in the void volume fraction. Such small voids were not included in the void volume fraction (Table 5) estimated using the technique mentioned above. Among others it was most probably due to the geometric resolution of computed tomography being limited by the X-ray sources size (focal spot), detector pixel size and the magnification used (dependent FDD and FOD).

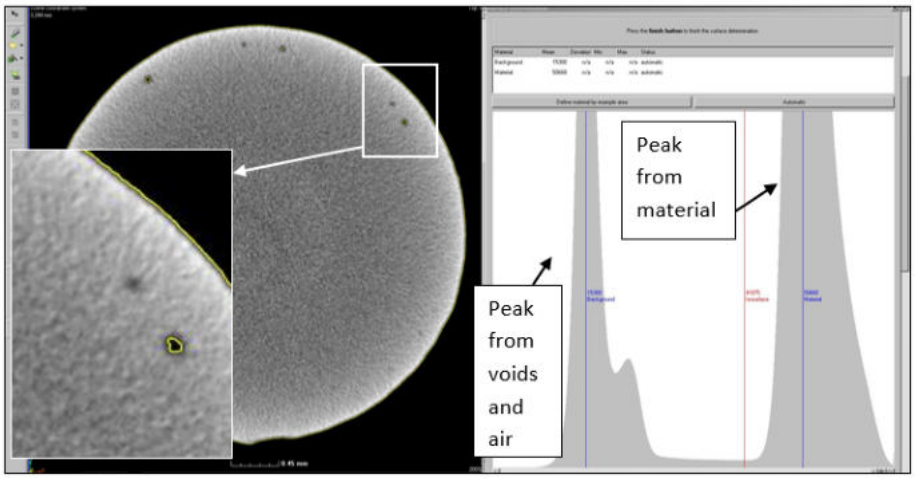

Fig. 16. Porosity evaluation technique of one of the raw bar using the surface analysis module available in the VG STUDIO MAX 21.

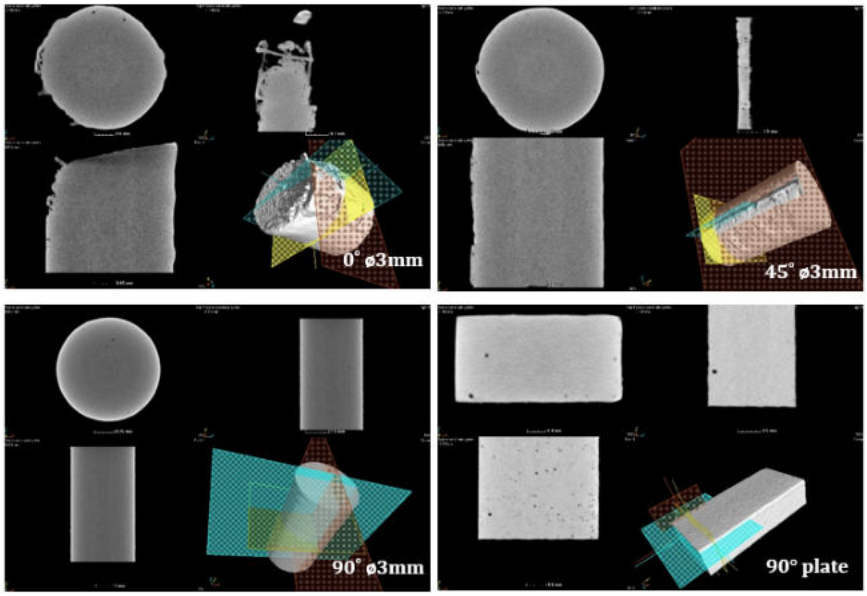

Fig. 17. CT of raw bars ø3mm and plate type specimen after HT.

Table 5. CT Estimation of the void volume fraction of the inspected bar rod and plate type specimens.

Printing orientation	Porosity [%]					
	Specimen					
	ø3 mm		ø6 mm		plate	
	H0	H2	H0	H2	H0	H2
0°	0,011	0,014	0,009	0,007	-	-
45°	0,005	0,003	0,011	0,002	-	-
90°	0,017	0,005	0,006	0,001	0,065	0,001

CONCLUSIONS

- Tensile tests (YS0,2%; UTS, elongation) yielded values higher are than the minimum values required by the ASTM F3055 standards.
- Mechanical properties (YS 0,2% and UTS) were higher for D6 specimens (d=6,35 mm) than for D5 specimens (d=4,06 mm) by about 1-4%.
- In some specimens, in the surface area the micro cracks, non-melted zones and porosity were present. The most of these discontinuities were related to the specimen's support structures and could be removed by machining or surface finishing.
- Micro cracks and voids in the support surface area that are present in the specimens built in 0^0 and 45^0 directions, were one of the reasons of lower elongation and other mechanical properties compared with the values received in the specimens built in direction 90^0.
- Carbides content in the specimens' surfaces was higher compared to the carbides content in the specimens' volume.

Contact:
Bartosz Madejski Bartosz.madejski@ilot.lukasiewicz.gov.pl

2.2. *Application of laboratory diffraction methods in characterization of elements made by additive SLM methods-state of the art* – E. Gadalińska, Ł. Pawliszak, G. Moneta [Ł-ILOT]

The greatest challenge of widely developed incremental manufacturing methods today is to obtain, as a result of the manufacturing process, such components that will have acceptable strength properties from the point of view of a given application. These properties are indirectly determined by three key characteristics: the level of surface residual stress, the roughness of the component and its porosity. Currently, the efforts of many research groups are focused on the problem of optimizing the parameters of incremental manufacturing so as to achieve the appropriate level of compressive residual stress, the lowest possible porosity and the lowest possible roughness of parts obtained by 3D methods. It is now recognized that determining the level of these three parameters is potentially possible using experimental X-ray diffraction methods. The use of this type of radiation, admittedly, is only used to characterize the surface layer of elements, but its undoubted advantage is its easy availability and relatively low cost compared to experiments carried out using synchrotron or neutron radiation.

Additive manufacturing technologies enable unprecedented freedom of design and fabrication of custom parts for economy sectors where mission-critical components are required. However, still many challenges lie ahead before 3D prototyping and production methods such as SLM (selective laser melting) can truly disrupt industrial scale manufacturing ways of operation known for the last decades. This in turn heavily underlines the necessity for fast, reliable, efficient and inexpensive methods aimed at AM components material properties characterization promoting for a substantially better understanding and even higher degree SLM fabrication process optimization. Non-destructive testing (NDTs) techniques e.g., diffraction methods fulfill those requirements especially if applied to residual stresses mapping and analysis in SLM produced parts, as it was demonstrated that a substantial body of work has been published to date on the topic. It is to note that although laboratory diffraction techniques are very versatile tool for material properties characterization and can be used for other tasks besides stresses investigation i.e., phase composition analysis they have their limitations. Nevertheless, several complementary measurement techniques exist that can be successfully

employed to gain a more thorough insight into the SLM process and the resulting components materials properties, which was briefly highlighted.

Contact
Elżbieta Gadalińska elzbieta.gadalinska@ilot.lukasiewicz.gov.pl

2.3. *Laser powder bed fusion and selective laser melted components investigated with highly penetrating radiation* – E. Gadalińska, Ł. Pawliszak, G. Moneta [Ł-ILOT]

Methods of incremental manufacturing, i.e. 3D printing, have been experiencing significant growth in recent years, both in terms of the development of modern technologies dedicated to various applications, and in terms of optimizing the parameters of the process itself so as to ensure the desired mechanical and strength properties of the parts produced in this way. High hopes are currently being pinned on the use of highly penetrating types of radiation, i.e. synchrotron and/or neutron radiation, for quantitative identification of parameters characterizing objects produced by means of 3D printing. Thanks to diffraction methodologies, it is feasible to obtain input information to optimize 3D printing procedures not only for finished prints but also to monitor in situ printing processes. Thanks to these methodologies, it is possible to obtain information on parameters that are critical from the perspective of application of such obtained elements as stresses generated during the printing procedure itself as well as residual stresses after printing. This parameter, from the point of view of tensile strength, compression strength as well as fatigue strength, is crucial and determines the possibility of introducing elements produced by incremental methods into widespread industrial use.

In conclusion it can be stated that additive manufacturing techniques changed the way components are being produced giving unprecedented freedom of design combined with reduced costs and faster time-to-market delivery. Although revolutionary in a way that complex geometry parts can be produced still challenges lie ahead in better understanding the processes taking place during manufacturing of components for various mission-critical applications. One of the main issues to be resolved is residual stress state formation due to high thermal gradients while metallic powders get solidified. Residual stresses formation can lead to shape distortion of the produced components that in turn can result in other defects formation, such as cracks and delamination therefore it is necessary to carefully tailor AM process parameters, which has been demonstrated to be a non-trivial task. Materials of interest under active study included the following: Ti6Al4V (Ti64), used mainly in aerospace due to its high fracture toughness and corrosion resistance but also in biomedical applications due superior biocompatibility, Inconel type alloys used in a wide range of high temperature applications due to excellent wear, fatigue and hot corrosion resistance combined with favorable weldability, stainless steels (SS316L), austenitic stainless steels (AlSi316L) due high tensile strength and low cost, but also studies on Ti553 could be found in the literature due to materials unprecedented tensile strength. It has been shown by numerous researchers that diffraction methods were a powerful tool for non-destructive testing of LPBF produced parts. Laboratory X-ray diffraction has been widely adopted for this purpose although it has some limitations, as only surface stress values could be studied. This of course could be potentially overcome by addition of electropolishing to map stresses layer, by layer. Fortunately, diffraction measurement applying highly penetrating radiation could be used to probe AM produced components material properties enabling both in-situ and ex-situ stress mapping capabilities at different sample depths. In-situ AM process parameters monitoring with synchrotron radiation also gained interest in recent years as it is shown by quite extensive body of work on the topic. Furthermore, synchrotron and neutron diffraction were employed to gather information later used in optimizing numerical simulations aimed at FE modelling of complex thermo-mechanics of the LPBF to reduce computational

costs and time. Several process parameters were observed to influence produced part quality. These included laser scanning speed, laser energy density and the scanning strategy itself. Some of the works on the other hand, were focused on the role of support structures and parts build direction in the investigation of residual stresses, as well as stresses evolution upon build platform removal. Post heat treatment and in-situ heat treatment influence on distribution of residual stresses were also studied.

Contact
Elżbieta Gadalińska elzbieta.gadalinska@ilot.lukasiewicz.gov.pl

2.4. *Laser powder bed fusion (LPBF) of NiTi alloy using elemental powders: the influence of remelting on printability and microstructure* – A. Chmielewska, B. A. Wysocki, E. Gadalińska, E. MacDonald, B. Adamczyk-Cieślak, D. Dean, W. Świeszkowski [Warsaw University of Technology, Cardinal Stefan Wyszyński University, Ł-ILOT, University of Texas at El Paso, The Ohio State University]

The purpose of this work was to investigate the effect of remelting each layer on the homogeneity of nickel-titanium (NiTi) parts fabricated from elemental nickel and titanium powders using laser powder bed fusion (LPBF).

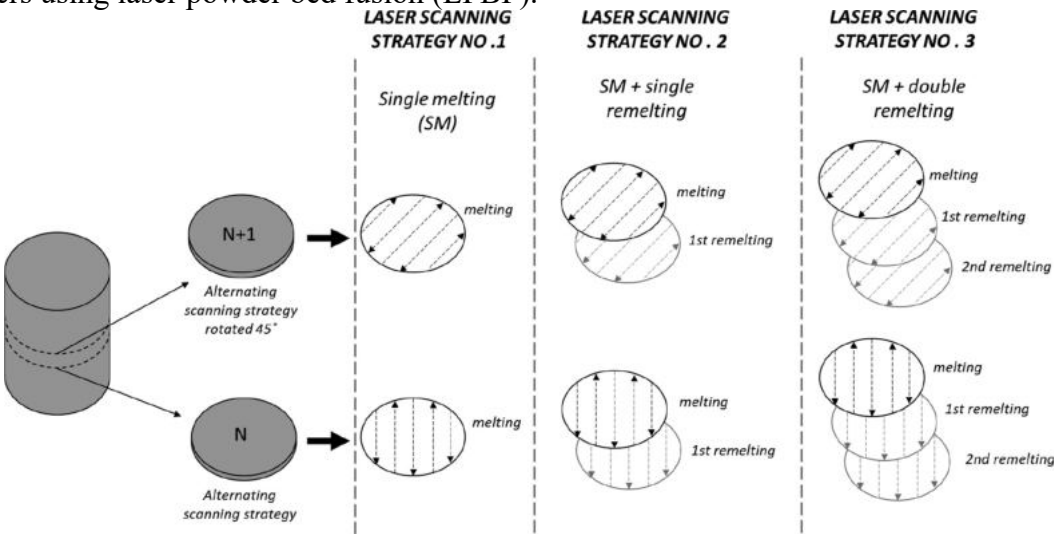

Fig. 1. LPBF process parameters and number of remelts used for processing of blended elemental Ni and Ti powders.

In addition, the influence of manufacturing parameters and different melting strategies, including multiple cycles of remelting, on printability and macro defects, such as pore and crack formation, have been investigated. The LPBF process was used to manufacture NiTi alloy from elementally blended powders and was evaluated with the use of a remelting scanning strategy to improve the homogeneity of fabricated specimens. Furthermore, both single melt and up to two remeltings were used.

The results obtained indicate that remelting can be beneficial for density improvement as well as chemical and phase composition homogenization. Backscattered electron mode in scanning electron microscope showed a reduction in the presence of unmixed Ni and Ti elemental powders in response to increasing the number of remelts. The microhardness values of NiTi parts for the different numbers of melts studied were similar and ranged from 487 to 495 HV. Nevertheless, it was observed that measurement error decreases as the number of remelts increases, suggesting an increase in chemical and phase composition homogeneity. However, X-ray diffraction analysis revealed the presence of multiple phases regardless of the

number of melt runs. For the first time, to the best of the authors' knowledge, elementally blended NiTi powders were fabricated via LPBF using remelting scanning strategies. The study showed that using remelting parameters with the same value of the energy density but resulting from different values of laser power (25 and 75 W) and scanning speed (1,000 and 3,000 mm/s) give radically different results. Remelting was observed to significantly reduce porosity. The relatively high density, revealed with mCT reconstruction estimated at the value at 99.17%, was observed for parts where remelting was applied. Additionally, remelting R1, with lower laser power and scanning speed, eliminated cracks, while remelting R2, with higher laser power and scanning speed, generated a high thermal gradient that is expected to promote the formation and growth of cracks. Increased NiTi homogeneity was observed to correlate with the increasing number of remelts. However, multiple phases were observed regardless of the number of remelts; thus, postprocessing heat treatment should be investigated in future research on LPBF remelting of Ni and Ti elemental powders. The microhardness of the parts remelted twice was more uniform than parts produced from a single melt or remelted once. XRD stress measurement suggested that residual stress and crack occurrence was reduced in LPBF processes that include remelting. WD-XRF chemical composition analysis showed that the highest amount of Ni evaporated during first melt run and subsequent tmelt runs did not influence Ni evaporation significantly. In conclusion, remelting was observed to significantly improve the blending of the Ni and Ti elemental powders during LPBF compared with single melt processes; however, it did not eliminate phase composition inhomogeneity entirely.

Contact
Agnieszka Chmielewska agnieszka.chmielewska.dokt@pw.edu.pl

2.5. *Microstructure-electrochemical behavior relationship in post processed AISI316L stainless steel parts fabricated by laser powder bed fusion* – A. Behjat, M. Shamanian, A. Taherizadeh, E. Lannunziata, S. Bagherifard, E. Gadalińska, A. Saboori, L. Iuliano

AISI316L stainless steel components produced via additive manufacturing techniques have quickly found new applications across several industrial sectors. However, parts manufactured through this method generally exhibit poor surface quality and performance in the as-built state. This work addresses the influence of laser polishing and water jet assisted recirculating shot peening on the surface quality, microstructure, and electrochemical properties of AISI316L samples produced by the laser powder bed fusion method. To do so, surface roughness analysis, residual stress measurement, scanning electron microscope and electron backscatter diffraction analysis were employed along with electrochemical tests, including cyclic potentiodynamic polarization, electrochemical impedance spectroscopy and Mott-Schottky analysis. Laser polished samples exhibited a smooth surface with high tensile residual stress on the surface, which led to the reduction of pitting potential and formation of passive layers, including more crystal defects. Microscopical analysis evidenced that the higher density of lattice defects and local microstrain on the surface of the shot peened samples promoted surface hardness and induced compressive residual stress. Therfore, the shot peened samples exhibited a wider passive range in cyclic potentiodynamic polarization measurements, higher polarization resistance in electrochemical impedance spectroscopy measurements, and less defective passive film in Mott-Schottky analysis. Moreover, it was calculated that the passive film thickness of the shot peened sample was slightly larger than the other samples. Low surface roughness, high crystal defect density, and compressive residual stresses.

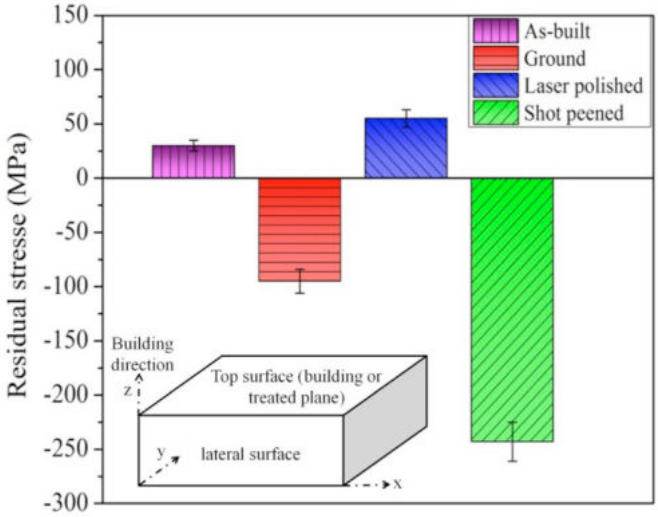

Fig. 1. Average top surface residual stress for the samples.

The main conclusions can be summarized as follows:

1. Based on the results obtained from EBSD analysis, grain boundary lengths and dislocation density on the surface of the shot peened samples were remarkably higher than the other series. This promoted surface hardness and induced compressive residual stresses on the surface. However, for the laser polished sample, the density of low angle grain boundaries was markedly reduced as a consequence of thermal input during the remelting process, where the dislocations were annihilated.

2. Electrochemical examinations demonstrated an increased pitting potential (mainly after shot peening) due to the high lattice defects density and large compressive stresses, which play an important role in reducing pit formation.

3. According to the EIS results, there was no significant difference in the electrochemical impedance and stability of the passive films formed on the as-printed, ground and laser polished samples. However, significant differences were observed in the polarization resistance of the oxide layer of the shot peened samples, suggesting that the crystal defects of passive alloys could affect the passivation process by changing the element's diffusion rate. Moreover, the film grown on the shot peened sample was slightly thicker than the other samples.

4. Based on the point defect model and Mott-Schottky analysis, it is hypothesized that induced compressive residual stress and increased crystal defect density on the sample surface induced by shot peening could increase the resistance of the passive layer against defect transport and pit initiation. The modifications of the surface properties with the peening-based mechanical treatment lowered the donor density and point defect concentration in the passive film.

Contact

Elżbieta Gadalińska elzbieta.gadalinska@ilot.lukasiewicz.gov.pl

2.6. *The effect of surface treatment and orientation on fatigue crack growth rate and residual stress distribution of wire arc additively manufactured low carbon steel components* – A. Ermakova, J. Razavi, S. Cabeza, E. Gadalińska, M. Reid, A. Paradowska, S. Ganguly, F. Berto, A. Mehmanparast [University of Strathclyde, NTNU, ILL, Ł-ILOT, Australian Centre for Neutron Scattering, The University of Sydney, Cranfield University)

The directed energy deposition (DED) processes, such as laser metal deposition or Wire Arc Additive Manufacturing (WAAM), are gradually becoming the preferred method for fabrication of large-scale components using metal additive manufacturing (AM) technology. In this work, the possibility of fatigue life enhancement in WAAM built low carbon steel components, by means of rolling and laser shock peening surface treatment techniques, was investigated. A series of fatigue crack propagation tests were performed on surface treated ER70S-6 and ER100S-1 WAAM built specimens, and the results were analysed and compared with the untreated materials tested under the same loading conditions. The obtained results were interpreted in terms of the sensitivity of the cracking behaviour to the specimen orientation and extraction location. Furthermore, the residual stress profiles were measured, before and after applying the surface treatment techniques, and the effects of locked-in residual stresses on the fatigue performance of WAAM built components were discussed. Finally, a detailed texture analysis was performed on the surface treated and untreated regions of both WAAM built materials considered in this work. The obtained results from this study provide an insight into the advantages and disadvantages of various surface treatment techniques for fatigue life enhancement of WAAM built components with the view to extend the application of this advanced manufacturing technology to a wider range of industrial applications.

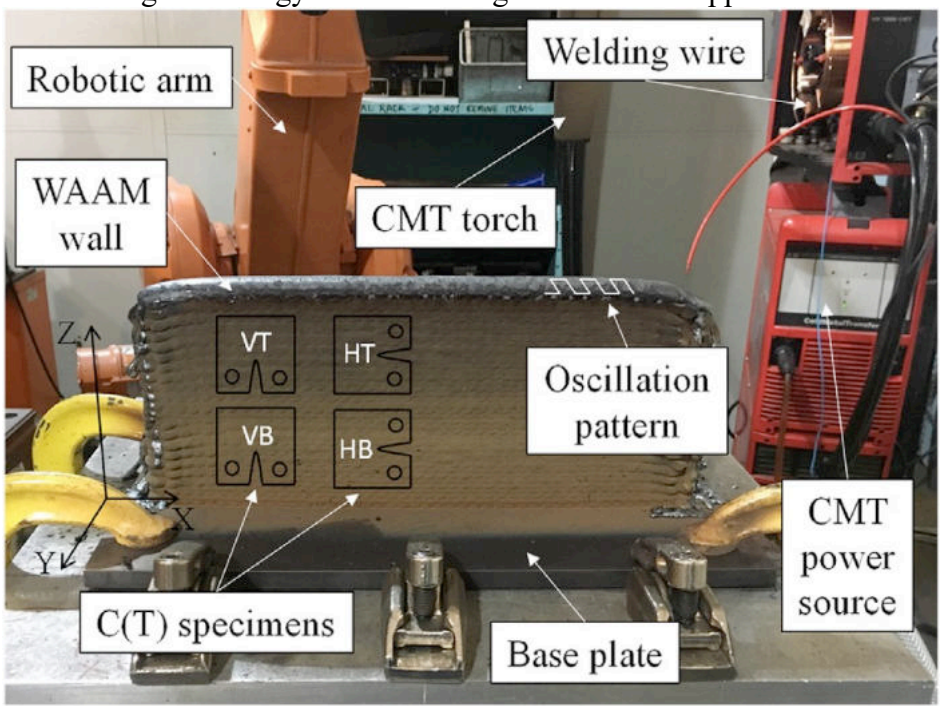

Fig. 1. WAAM-CMT system set up with schematic specimen extraction map.

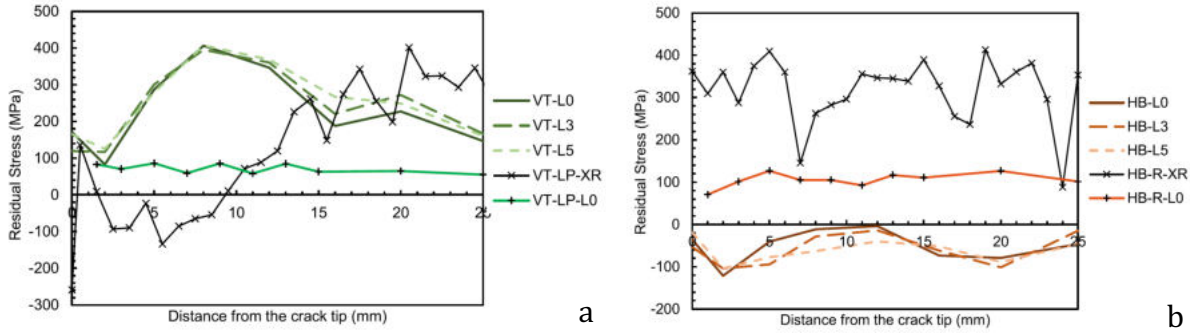

Fig. 2. Residual stress distribution in investigated specimens before and after surface treatment (a) 100-VT specimen before and after laser shock peening (LP), (b) 100-HB specimen before and after surface rolling (R). Measurements with neutron radiation were carried out at the mid-thickness L0 and the other two with 3mm(L3) and 5mm(L5) distance from the mid-thickness of the specimen. Surface measurements with X-ray are signed with XR.

In this study the effects of laser shock peening and surface rolling treatments on the fatigue crack growth (FCG) behaviour were comprehensively examined, along with the residual stress distribution and material texture of WAAM built low carbon steel components. The following conclusions can be drawn based on the obtained results from this work.

1. For ER70S-6 WAAM built components, both surface treatment techniques have been found to enhance the fatigue performance by reducing the FCG rates in the surface treated area compared to the untreated material.

2. For both materials, the laser shock peening technique resulted in the longest fatigue lives compared to the untreated samples. The longest test durations in laser peened specimens were observed in the vertical specimens extracted from the bottom of ER70S-6 and the top of ER100S-1 WAAM walls.

3. Application of rolling surface treatment, using the same parameters on both materials, was found to be inefficient for ER100S-1 specimens and resulting in a shorter fatigue life and higher FCG rates compared to the untreated material.

4. The surface rolling treatment introduces high residual stresses in the near surface region of ER100S-1 specimens, which resulted in deterioration of FCG performance, whereas laser shock peening induced significant level of compressive residual stresses which were beneficial for fatigue performance and results in lower FCG rates.

5. The residual stress measurements through-thickness of treated specimens showed small asymmetrical stress distribution with respect to the mid-thickness plane, which can be due to non-symmetrical application of surface treatment techniques.

6. The texture was found to increase by applying both surface treatment techniques; however, for laser shock peened specimens the texture index was found on average 2.7 times higher than the rolled specimens. Moreover, untreated specimens made of ER100S-1 material exhibited a higher texture compared to untreated ER70S-6 specimens.

7. ER100S-1 has finer grains compared to ER70S-6 specimens while the cracking mode in both materials was found to be transgranular under fatigue loading conditions.

8. A larger amount of residual strain was observed throughout ER100S-1 WAAM specimens, whereas in ER70S-6 specimens the highest residual strains were concentrated along the crack path.

9. Repeat tests are required in future work to evaluate the level of scatter for each surface treated specimen extraction location and orientation. Moreover, additional ND measurements need to be conducted to analyse the RS states in all surface treated specimens.

Acknowledgements
This work was supported by grant EP/L016303/1 for Cranfield, Oxford, and Strathclyde Universities Centre for Doctoral Training in Renewable Energy Marine Structures e REMS CDT (http://www.rems-cdt.ac.uk/) from the UK Engineering and Physical Sciences Research Council (EPSRC). The authors would like to thank ILL-France for provision of the neutron beamtime for residual stress measurements under https://doi.ill.fr/10.5291/ILL-DATA.1-02-292 and ANSTO (Proposal 13422).

Contact
Elżbieta Gadalińska elzbieta.gadalinska@ilot.lukasiewicz.gov.pl

3. STRESS IMAGING / SENSING

3.1. *Direct determination of phase stress evolution in duplex steel using synchrotron diffraction* – E. Gadalińska, A. Baczmański, S. Wroński, L. Le Joncour, C. Braham, M. François, B. Panicaud, K. Wierzbanowski [Ł-ILOT, AGH-University of Science and Technology, LASMIS-ICD Université de Technologie de Troyes (UTT), Laboratoire Procédés et Ingénierie en Mécanique et Matériaux]

The work deals with the investigation of the micromechanical behaviour of a duplex steel, which consists of two phases (austenite and ferrite) exhibiting significantly different mechanical properties. The stresses in both phases were experimentally determined in the elastic and plastic ranges of deformation using synchrotron radiation diffraction experiments.

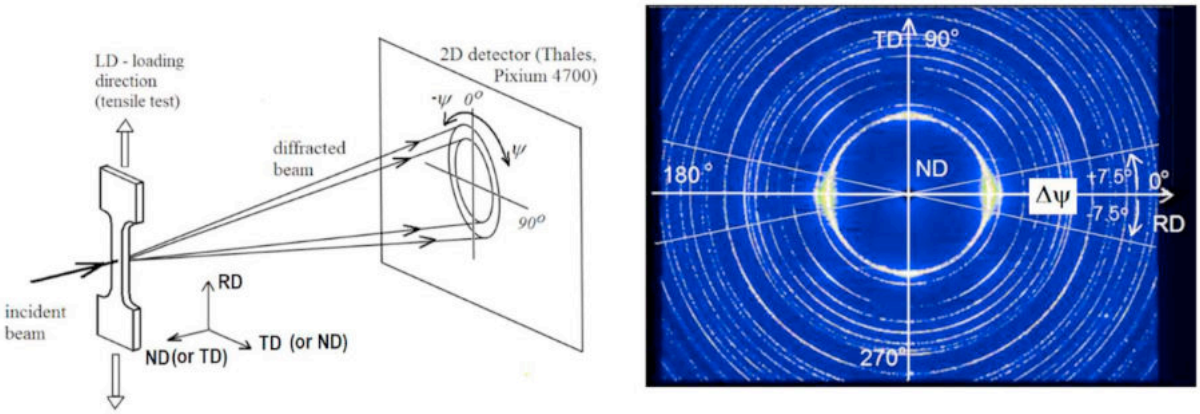

Fig. 1. The experimental setup used for lattice strain measurement at the ID15 synchrotron beamline (a) and the 2D image obtained for the studied duplex steel (b). The diffraction rings corresponding to reflections from ferrite and austenite and two "cake shape" sectors, with an angular size of Δψ *are shown.*

The used methodology enabled to determine the values of initial stresses and to study the evolutions of the principal phase stresses and the second order stresses during the elastic, as well as the plastic range of deformation. With the help of a self-consistent model, the critical resolved shear stresses and the work hardening parameters for slip systems, active in each phase, were also estimated. Comparison of the measured phase stresses and lattice strains evolutions with the model results showed a good agreement between prediction and experiment when the initial stress state in the sample and shape of grains approximated by ellipsoidal inclusions were taken into account. The overall outcome of the work is the determination of stress partitioning between the two phases of a polycrystalline material for all deformation

stages, determined directly from diffraction experiment. The results enabled analyses of von Mises, hydrostatic stresses as well as second order stresses evolutions in both phases during tensile deformation. Finally, the experimental data were successfully compared with predictions of the self-consistent deformation model.

Although previous works validated beforehand predictions of stress evolution in both phases of duplex steel by using self-consistent model, the direct comparison between measured and modelled stresses was not done yet. Models were usually validated by comparing the lattice strains measured for two directions of the scattering vector with the results of model prediction. In this work, the experimental determination of stress tensor in both phases of the studied steel allows us to perform a more detailed discussion of stress partitioning between phases without the help of the model. Moreover, the model calculations are eventually applied to find out the reasons of observed stress evolution, and the elasto-plastic self-consistent (EPSC) model is verified, comparing not only lattice strains, but also the phase stresses with the experimental data. The studies conducted here concern the investigation of stresses and lattice strains evolution during three stages of deformation, in which firstly both phases are elastic, next austenite undergoes plastic deformation when ferrite remains elastic, and finally both phases are plastically deformed.

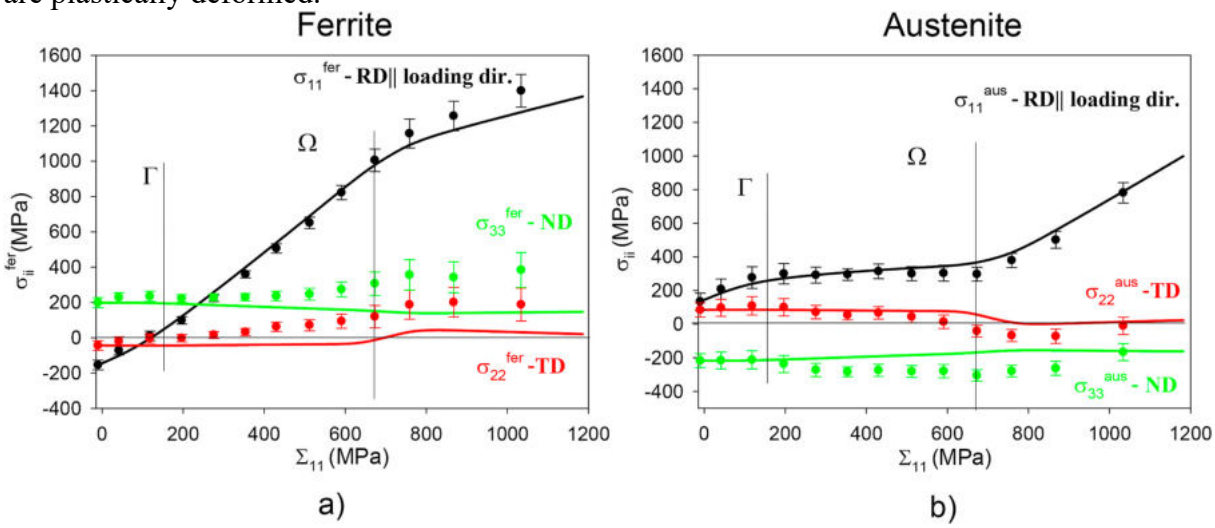

Fig. 2. Experimental phase stress evolution compared with self-consistent predictions for a) ferrite and b) austenite in the three chosen directions.

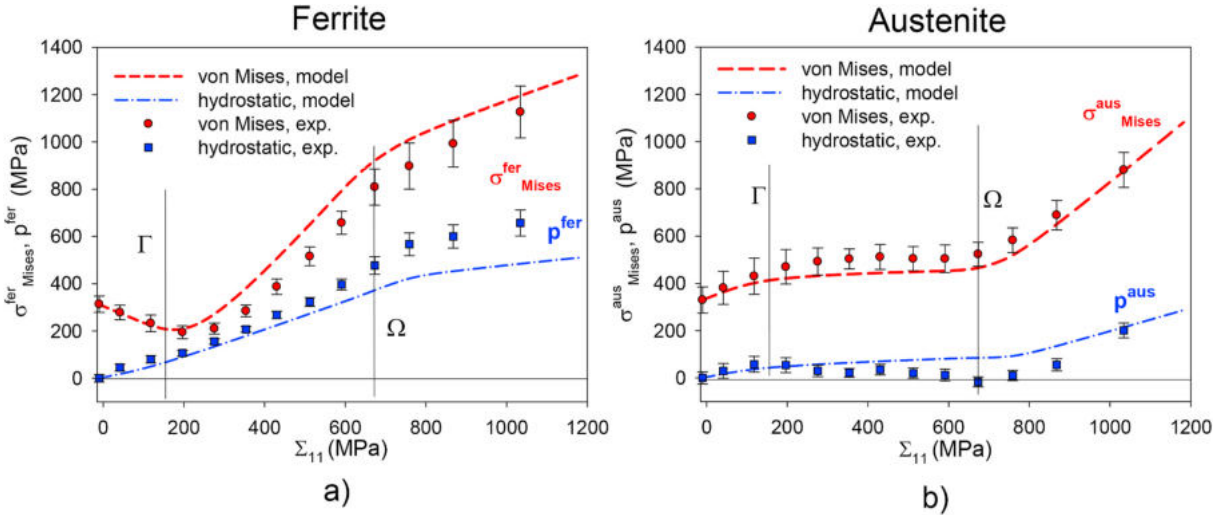

Fig. 3. Evolution of the von Mises and hydrostatic stresses determined from mean phases stresses for a) ferrite and b) austenite. The experimental values (points) are compared with model prediction (lines). Specimen with RD//loading direction.

The analysis of the diffraction results, obtained in in-situ during tensile test as well as theoretical predictions of EPSC model, show the partitioning and transition of the stresses between phases for the three stages of deformation (elasticity, plasticity in one phase, plasticity in both phases). The stress analysis is performed for principal components of the mean phase stress tensor, and also for the stresses at the scale of grains having different lattice orientations. The analysis of the von Mises stresses (calculated from the mean phase stresses) shows that the initial stress in the austenite is close to the yield stress; therefore, a small tensile load superimposed with the residual stresses leads to plasticity in this phase. During plastic deformation of austenitic phase, the stabilization of the von Mises stress vs. the applied stress occurs at the level of yield stress of austenite. In this case, the load is transferred to the elastic ferritic phase, until its yield. The transfer of the stress back to the austenite, when both phases undergo plastic deformation, is clearly seen on the evolution of the von Mises stress in function of the applied stress.
Furthermore, the dependence of the hydrostatic stress is analysed and compared with model predictions. It has been found that changes of these stresses are correlated with the elastic behaviour of the phases and that the hydrostatic stress increases significantly during elastic deformation of the ferrite, when the austenite is plastically deformed. In such a case, the hydrostatic stress does not change in the austenite. Again, when both phases are deformed plastically, the stress transfer to the austenitic phase is also clearly seen on the dependence of hydrostatic stress vs. applied stress. Using the data from in-situ diffraction measurements performed during tensile test, the mean phase stresses as well as the second order stresses are simultaneously determined and successfully compared with model predictions. It has been also found that the second order incompatibility stresses are generated in each phase when plastic deformation occurs in this phase (during elastic deformation this kind of stresses do not arise).This is one more effect due to the plastic process in a given phase. The EPSC modelling gives correct predictions of the evolution of lattice parameter for both phases and for all examined hkl reflections as well as the stress evolution in both phases of duplex steel. This model describes correctly the macroscopic, phase and the second order stresses. The mechanical behaviour of both phases is well predicted by the EPSC model and it allows identifying the parameters characterizing plastic deformation for both phases. Consequently, the evolution of lattice strains and phase stresses using diffraction enables to determine precisely the yield stresses and study the evolution of hardening process for both phases. The yield stresses can also be directly obtained from the dependence of von Mises stress as a function of the applied

stress, i.e. it is equal to the value of the von Mises stress at saturation. Using the model prediction, the values of critical resolved shear stress CRSS and hardening parameter H for austenite and ferrite are also obtained. It was found that the CRSS of austenite is much smaller compared to ferrite and this effect is expected due to precipitation process and spinodal decomposition occurring in ferrite during aging. It should be stated that, in the analysis of the plastic behaviour of individual phases, the influence of the initial stresses (in undeformed sample) as well as the ellipsoidal shape of inclusion are taken into account. It is found that these stresses and inclusion shape play an important role in deformation of the studied duplex steel. Based on the performed study an important conclusion concerning the applicability of the investigated duplex steel in structural components can be formulated. Analysing the macroscopic stress-strain plot, the yield strength of the duplex steel defined from the 0.2% deviation from linearity was estimated from experimental data (ca. 450 MPa) and from model results (ca. 600 MPa).

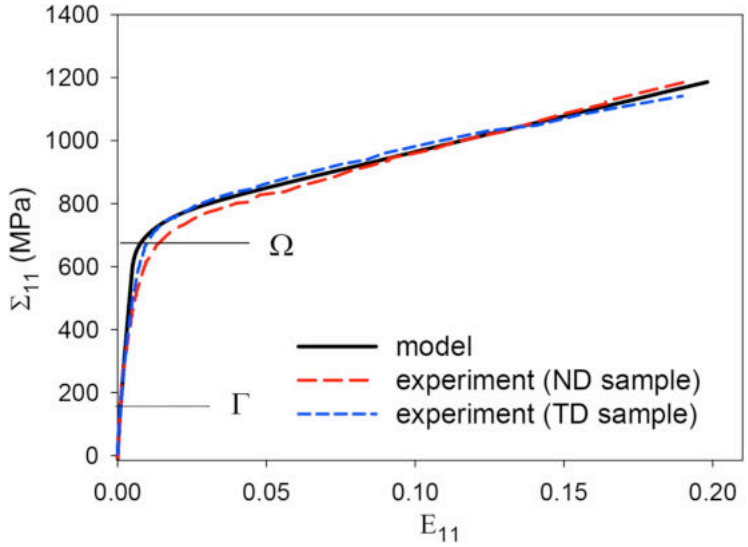

Fig. 4. Macroscopic experimental and model curves for tensile test performed for duplex steel.

It means that so defined yield stress of the steel is 2.7–3.7 times higher than the point where the yielding of austenite begins (ca. 160 MPa). This fact probably decreases high cycle fatigue properties of this steel due to significant accumulation of plasticity in the austenite at amplitudes significantly smaller than the 0.2% yield stress.

Acknowledgements
This work was supported by grant from the National Science Centre, Poland (NCN) No. UMO-2017/25/B/ST8/00134. We acknowledge the European Synchrotron Radiation Facility (ESRF) for the provision of synchrotron radiation facilities in the framework of the MA 1611.

Contact
Elżbieta Gadalińska elzbieta.gadalinska@ilot.lukasiewicz.gov.pl

3.2. *Experimental and numerical stress state assessment in refill friction stir spot welding joints* – E. Gadalińska, A. Kubit, T. Trzepieciński, G. Moneta [Ł-ILOT, Rzeszów University of Technology]

This work deals with the investigation Abstract Refill Friction Stir Spot Welding (RFSSW), a technology used for joining solid materials that was developed in Germany in 2002 by GKSS-GmbH as a variant of the conventional friction stir spot welding (FSSW). In the RFSSW technology, the welding tool consists of a fixed outer part and rotating inner parts, which are called a pin and a sleeve. The tool for RFSSW is designed to plasticize the material of the parts to be joined by means of a rotary movement. The design of the tool allows independent vertical movement of both elements of the welding tool. This allows obtaining spot welds without creating holes that could weaken the structure. The main advantage of RFSSW is the potential for replacing the technologies that add weight to the structure or create discontinuities, such as joining with screws or rivets. Thus, RFSSW has great potential in the automotive, shipbuilding and aviation industries. Furthermore, the technology can be used to join different materials that could not be connected using other joining methods. The main objective of this work was to understand the physical and mechanical aspects of the RFSSW method – including the residual stress state inside the weld and around the joint. The results of the investigations can help to determine optimal parameters that could increase the strength and fatigue performance of the joint and to prove the significant advantage of RFSSW connections over other types of joints. The work assumes the correlation of two mutually complementary investigation methods: numerical analyses and experimental studies carried out with diffraction methods. The comparison between numerical and experimental results makes potentially possible the determination of degree of fatigue degradation of the material by observing the macroscopic stress state and the broadening of the diffraction peak width (FWHM), which is an indicator of the existence of micro-stress related to the dislocation density and grain size.

Preliminary stress measurements along the axes of the welded specimens showed the possibility of obtaining reliable information on the stress distribution after a certain number of fatigue test cycles. When testing a welded specimen subjected to low-cycle fatigue, significant changes in the stress distribution were observed in the weld area starting from the weld centre point.

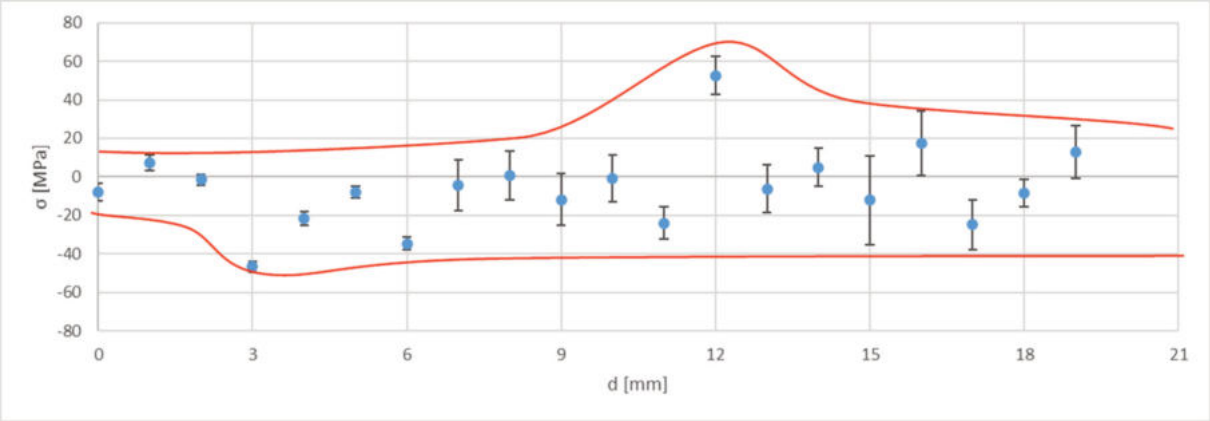

Fig. 1. Diffraction stress measurements for I3 specimen (initial state) for tangential direction.

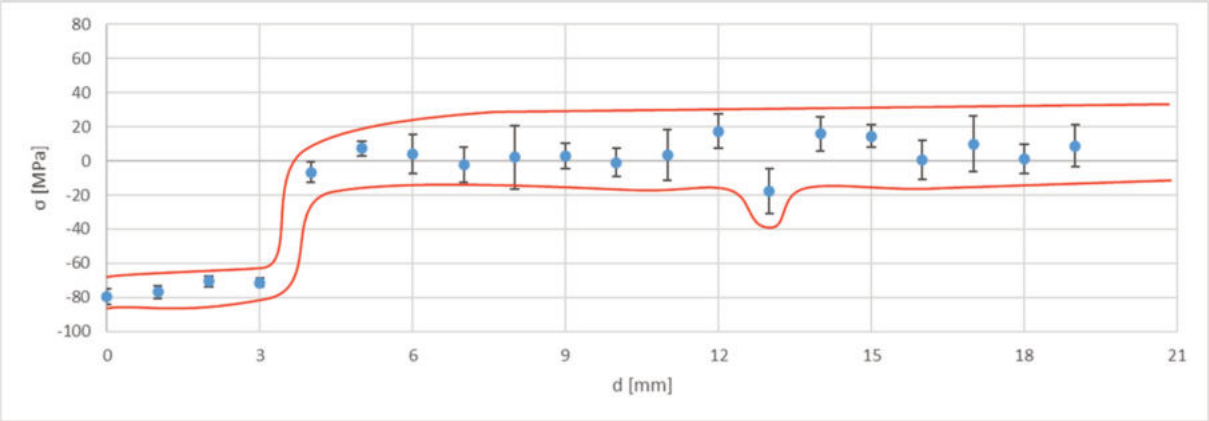

Fig. 2. Diffraction stress measurements for F2 specimen, after LCF testing, for tangential direction with respect to the weld geometry.

The measurements of the half-widths of diffraction peaks should, after further development of the methodology, allow researchers to determine the extent of fatigue processes in the weld and in the parent material of welded sheets.

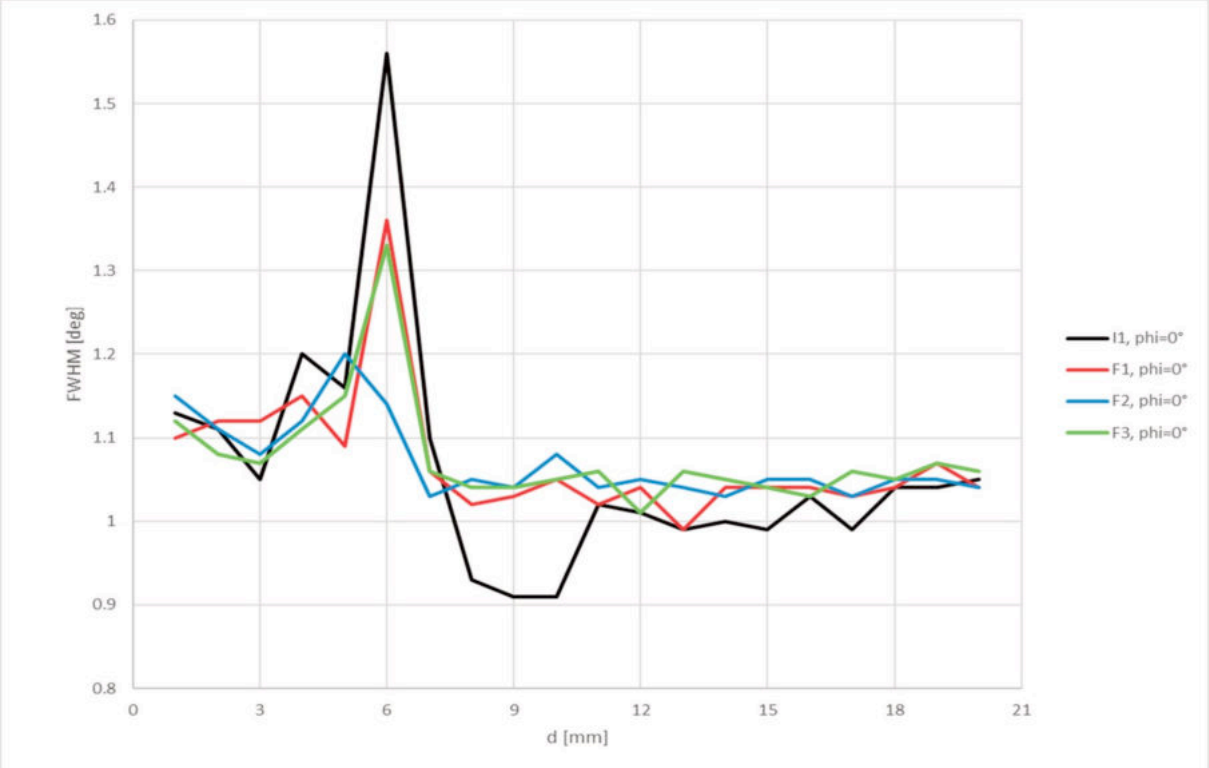

Fig. 3. The comparison of FWHM values for the specimen in the initial state (I1) and after the HCF (F1, F3) and LCF (F2) fatigue tests.

The preliminary FEA studies performed show good correlation of the peak stress location with the damage mechanisms observed. Considering the residual stress field in numerical simulations (which is planned for next studies) will contribute to a better understanding of damage phenomena that occur in RFSSW joints and will help in more accurate fatigue assessment and optimization of this joining technology for aviation structures.

Contact

Elżbieta Gadalińska elzbieta.gadalinska@ilot.lukasiewicz.gov.pl

4. MATERIALS TESTS

4.1. *Fatigue Life Evaluation and Prevention of Accelerated Degradation of Polymer Matrix Composites* – Andrzej Katunin [Silesian University of Technology]

The fatigue limit is often used as a quantitative measure of the fatigue lifetime of a structure, which is determined as a kind of material property. Traditionally, the fatigue limit can be estimated from the Wöhler curve, which requires performing numerous time-consuming fatigue tests. In recent decades, the new approach based on step fatigue tests and correlation of the applied stresses with the resulting temperature response allowed significantly accelerating testing procedure. The increase in temperature of a tested structure during fatigue loading, in the case of polymer matrix composites, is a result of the self-heating effect. In the study [1], it was shown that the fatigue limit is correlated with sudden changes in temperature response as well as acoustic emission, manifesting the beginning of the process of accelerated degradation of a structure. Moreover, the relationship between the fatigue limit and the critical self-heating temperature, both addressing the material properties, have been demonstrated in this study. The concept of criticality of self-heating temperature was broadly discussed in the paper [2], where the summary of tests using 15 different approaches to its estimation was presented, indicating the most sensitive ones. Further, the approach to determination of the fatigue limit of composites was combined with the developed self-heating based vibrothermography NDE technique, which was tested on CFRP and GFRP structures with impact damage [3]. The exemplary results of such an examination are presented in Fig. 1.

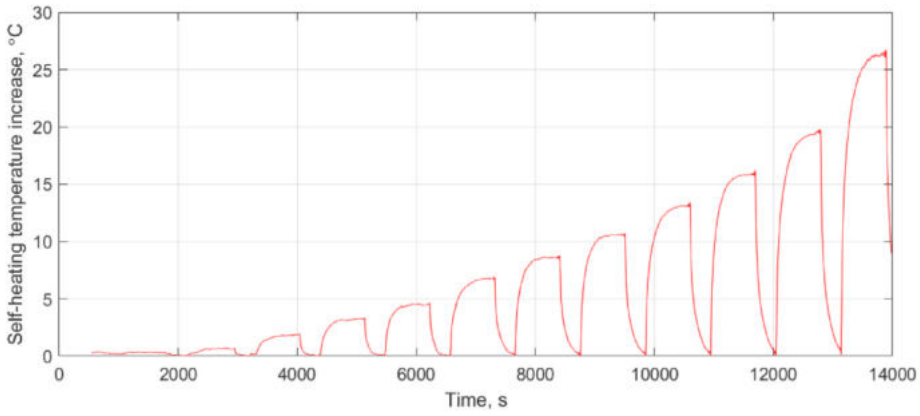

(a)

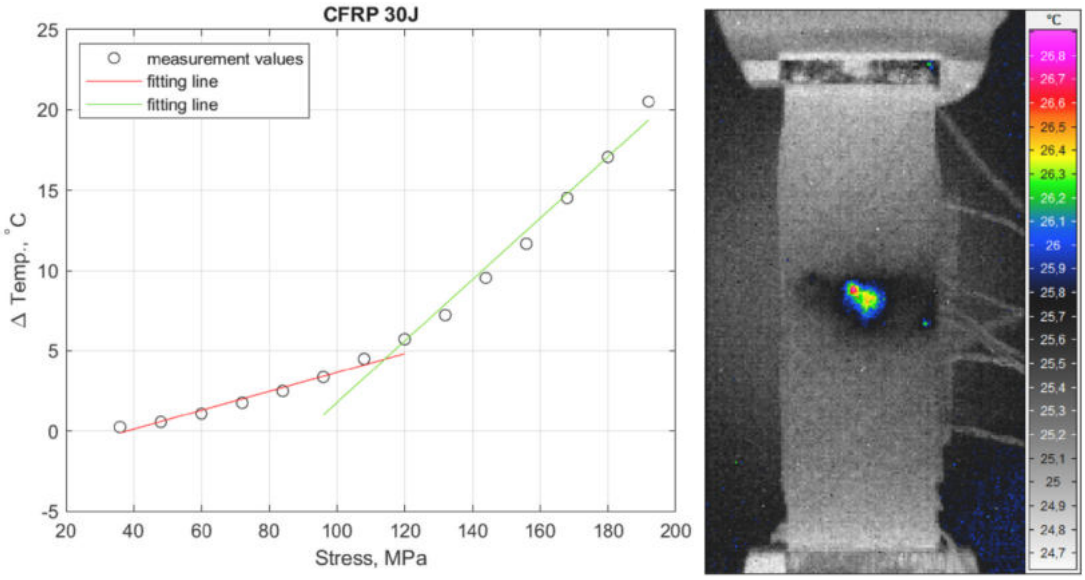

(b) (c)

Fig. 1. The results of testing: (a) temperature response during step testing, (b) the results of determination fatigue limit, and (c) the results of identification of damage [3].

The approach based on the evaluation of the critical self-heating temperature as an indicator of fatigue life was recently applied to estimate the durability of the new hybrid bio-composites reinforced both with natural and synthetic fibers [4].

Since self-heating is a dangerous phenomenon, in general, leading to accelerated degradation of composite structures, it is essential to limit its influence on the structural lifetime performance. First attempts were made using an air-cooling approach, described in detail in [5], where the GFRP specimen was cooled by air stream with a source located at various distances. The preliminary studies demonstrated that due to the application of surface cooling, the structural life of composite elements with the appearance of the self-heating effect can be significantly extended. Further deep studies on the cooling methods of composite structures during fatigue loading [6] allowed for the determination of influencing factors on the process, as well as the most appropriate cooling techniques depending on the loading conditions and a heating rate.

1. Katunin A., Wachla D., Determination of fatigue limit of polymeric composites in fully reversed bending loading mode using self-heating effect, Journal of Composite Materials 53(1), 2019, 83-91.
2. Katunin A., Criticality of the self-heating effect in polymers and polymer matrix composites during fatigue, and their application in non-destructive testing, Polymers 11(1), 2019, 19.
3. Katunin A., Pivdiablyk I., Gornet L., Rozycki P., A hybrid method for determination of fatigue limit and non-destructive evaluation of composite structures after low-velocity impact loading, Composites Part B: Engineering 238, 2022, 109898.
4. Katunin A., Wachla D., Santos P., Reis P.N.B., Fatigue life assessment of hybrid bio-composites based on self-heating temperature, Composite Structures 304, 2023, 116456.

5. Katunin A., Wachla D., Influence of air cooling on the fatigue of a polymer composite under self-heating, Mechanics of Composite Materials 56(1), 2020, 93-102.
6. Amraei J., Katunin A., Recent advances in limiting fatigue damage accumulation induced by self-heating in polymer-matrix composites, Polymers 14, 2022, 5384.

Contact:
Andrzej Katunin andrzej.katunin@polsl.pl

4.2. *Effect of Strain Range and Hold Time on High Temperature Fatigue Life of g17crmov5-10 CAST Alloy Steel* – Anna Polnik, Hubert Matysiak, Sławomir Czarnewicz, Zbigniew Pakieła [Baker Hughes, Warsaw University of Technology, Ł-ILOT]

In this work, cast steel G17CrMoV5-10 was investigated. The material subject to investigation as part of this study is commonly used to manufacture steam turbine casings. Modern steam turbines operate under elevated temperature and complex oscillated loads. Thus, the focus of this study was to investigate material under behavior during low cycle fatigue (LCF) test performance at 500 °C with and without hold time in tension. During all types of tests, cyclic softening of cast steel was noticed. Increasing of total strain rate and applying hold time significantly reduce fatigue life. During hold time, due to temperature and tension the material creep what is confirmed by increasing inelastic stain accommodation.

Material

G17CrMoV5-10 cast steel complying with EN 10213 (Steel Castings for Pressure Purposes, 2016) was tested. Chemical composition was measured using an optical emission spectrometer (OES) and a carbon and sulfur analyzer (quantitative technique), and the measurements are shown in Table 1. The test material was manufactured by sand casting in cylinders of 30-mm diameter. The material was subject to heat treatment as follows:

- hardening at 960°C/5 h/AC; and
- tempering 736°C/5 h/AC.

Table 1. Steel G17CrMoV5-10 chemical composition for cast

Element	**C**	**Si**	**Mn**	**P**	**S**	**Ni**	**Cr**	**Mo**	**V**	**Cu**	**Sn**
wt.%	0.19	0.4	0.9	0.014	0.011	0.08	1.44	1.04	0.2	0.30	0.001

Experimental Procedure

A full reverse stain-controlled fatigue test according to ASTM E606 (Standard Test Method for Strain-Controlled Fatigue Testing, 2008) was prepared. The test settings matrix used is presented in Table 2. Cylindrical samples with 8-mm diameter in the gauge section have been used. The tests were performed at 500 °C for a total of two strains—0.4% and 0.6%. Constant

triangular waveform of the load cycle was applied when no hold time was introduced, while trapezoidal waveform was applied with imposed hold times of 120 s.

Table 2. LCF fatigue test matrix

Temperature, T [°C]	500	Hold time, t_h (s)	Frequency, (Hz)	Total strain, Δε
Strain ratio, $R=\frac{\varepsilon_{max}}{\varepsilon_{min}}$	−1			
Cycle scheme				
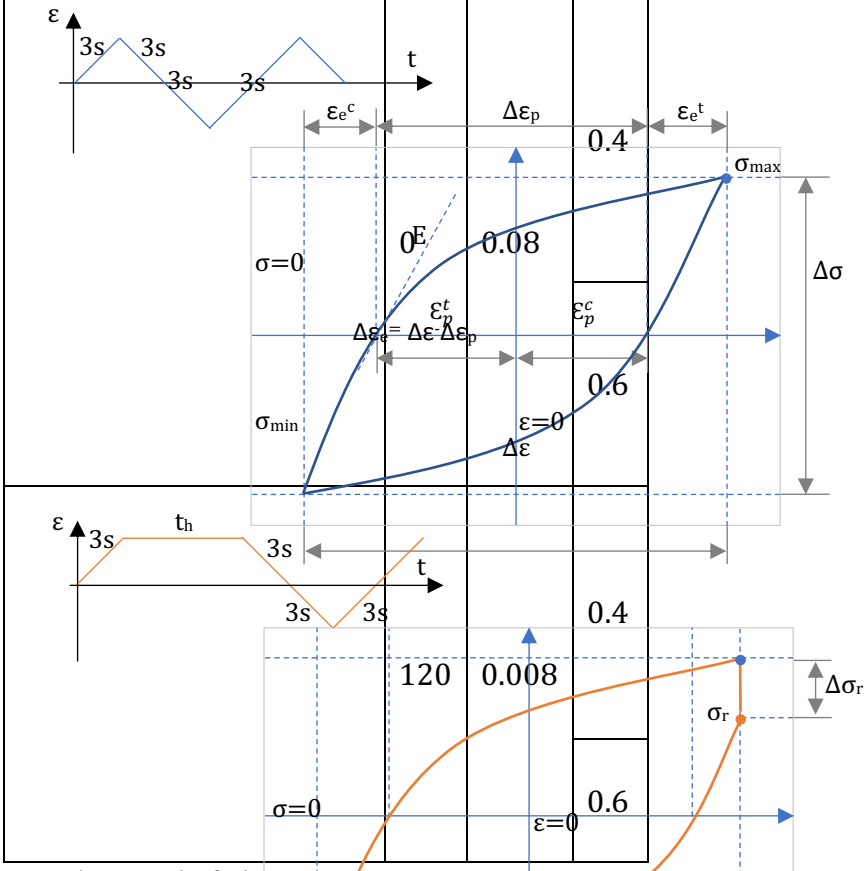				

LCF, low cycle fatigue.

Results and Discussion

Due to the large amount of test data, recorded throughout all LCF tests, three hysteresis loops for each case were analyzed, as shown in Figure 1. The curves show the stress–strain responses for selected cycles: beginning of life (100%), middle-life (50%), and end-of-life (0%). The envelope field of the loop is proportional to the energy irreversibly dispersed in the material (Kocańda, 1985; Carroll & Carroll, 2011; Alsmadi, Alomari, Kumar, & Murty, 2020).

For total strain 0.6%, the greater energy share is visible, observed with respect to the loops obtained for 0.4% of total strain. For added hold time 120 s, the behavior is similar: the area of the hysteresis loop field is increasing compared to loops without hold time. Introduction of hold time at tension causes a decline of maximum stresses during the lifetime of the cycle. The distribution of maximum stresses is presented in Figure 2. Cyclic softening of the material is noticed for all types of tests. Material softening is higher for curves with hold time.

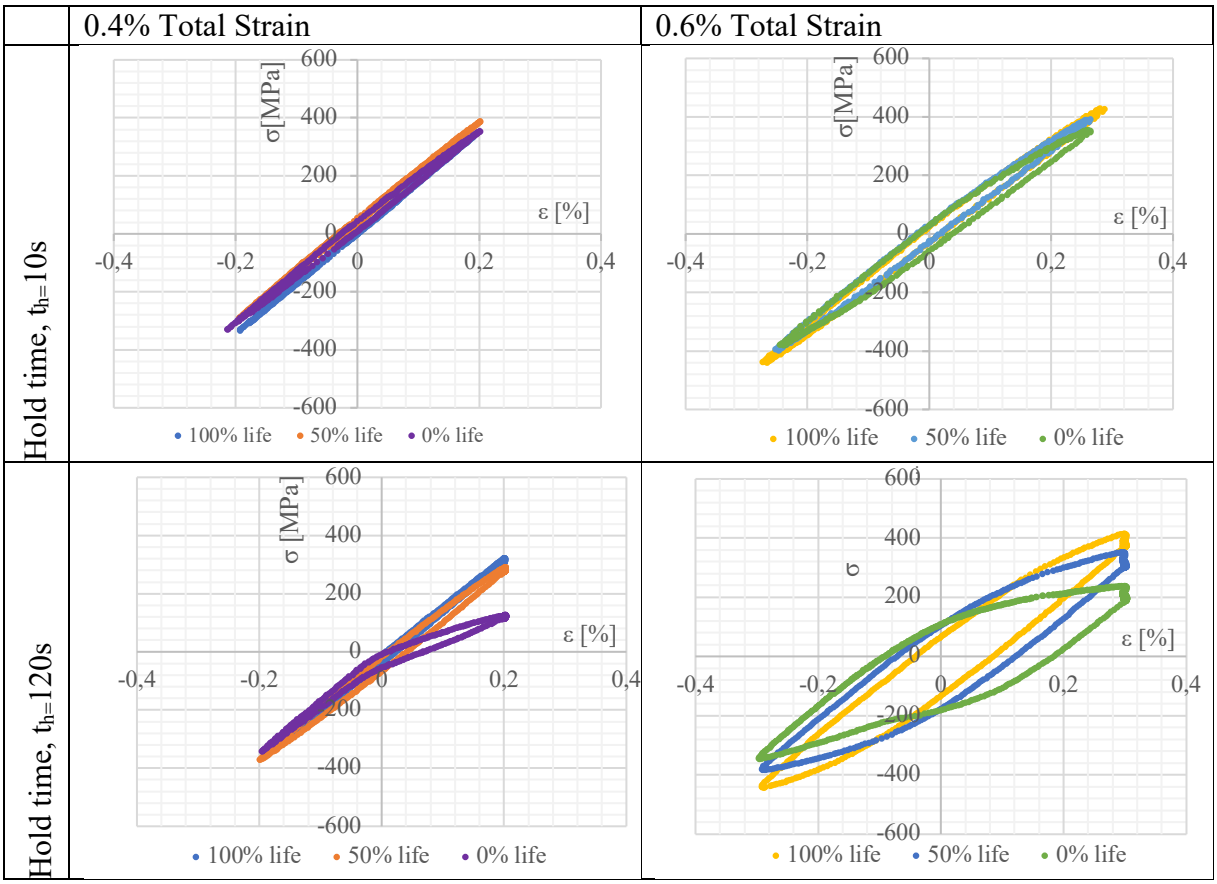

Figure 1. Hysteresis loop of the LCF test shown for 100%, 50%, and 0% of life. LCF, low cycle fatigue.

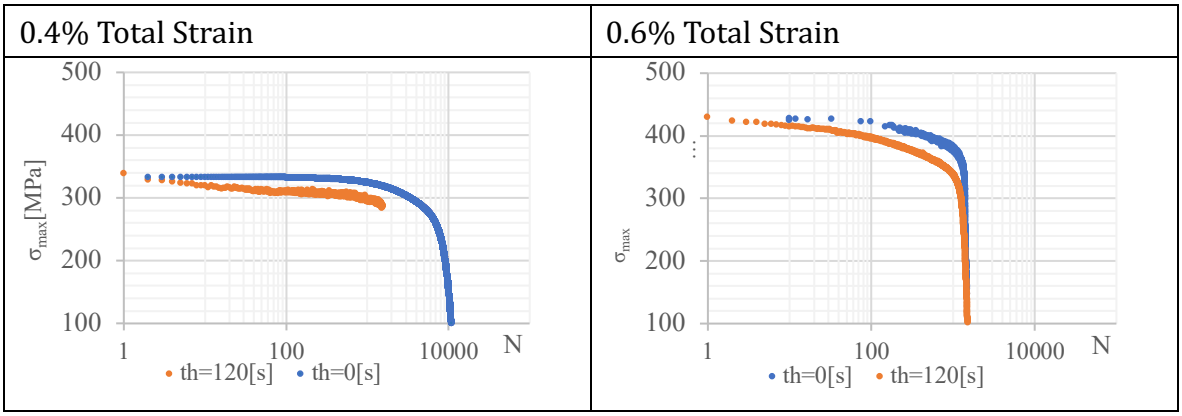

Figure 2. Maximum stresses.

The fatigue life—number of cycles to failure N_f—is shown in Figure 3. Both total strain range and hold time contribute to significant reduction of fatigue life. Increasing total strain range from 0.4% to 0.6% without hold time causes a drop of fatigue life to 85%, and with added hold, to 58%. Hold time reduces 70% of fatigue life for total stain 0.4% and 17% for 0.6%.

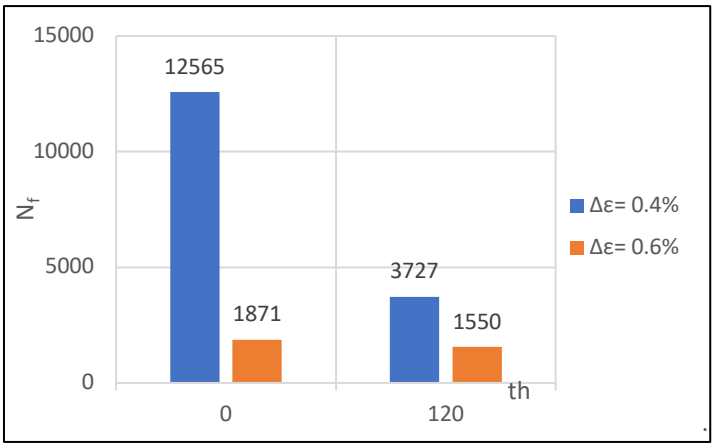

Figure 3. Fatigue life for 0.4% and 0.6% Δε total stain.

No impact of test condition on modulus of elasticity E was noticed. The average value was 169 GPa. Stress relaxation occurs during the tensile hold time presented in Figure 4. A similar drop ~60% was observed for both test conditions.

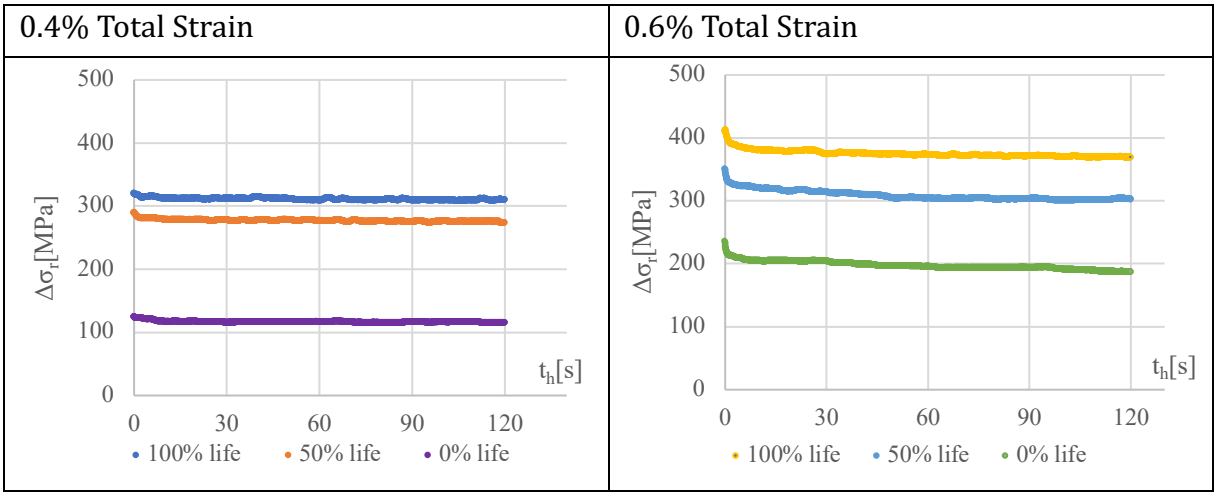

Figure 4. Stress relaxation during hold time, $t_h = 120s$.

The contribution of total inelastic stain $\Delta\varepsilon_p$ and elastic $\Delta\varepsilon_e$ (Kuhn & Medlin, 2000) has been calculated, as indicated in Figure 5. The value of $\Delta\varepsilon_p$ increases during material fatigue life, higher of 0.6% of total strain and with added hold time. This behavior suggests the occurrence of creep damage at test temperatures under relaxation stress on tension. Stresses were relaxed during the hold time under strain-controlled creep-fatigue tests, as presented in Figure 4, from σ_{max} to σ_r. Creep damage occurs, which is indicated by stress reduction. A similar observation is recorded in the literature (Takahashi, 2008; Carroll & Carroll, 2011; Alsmadi et al., 2020)

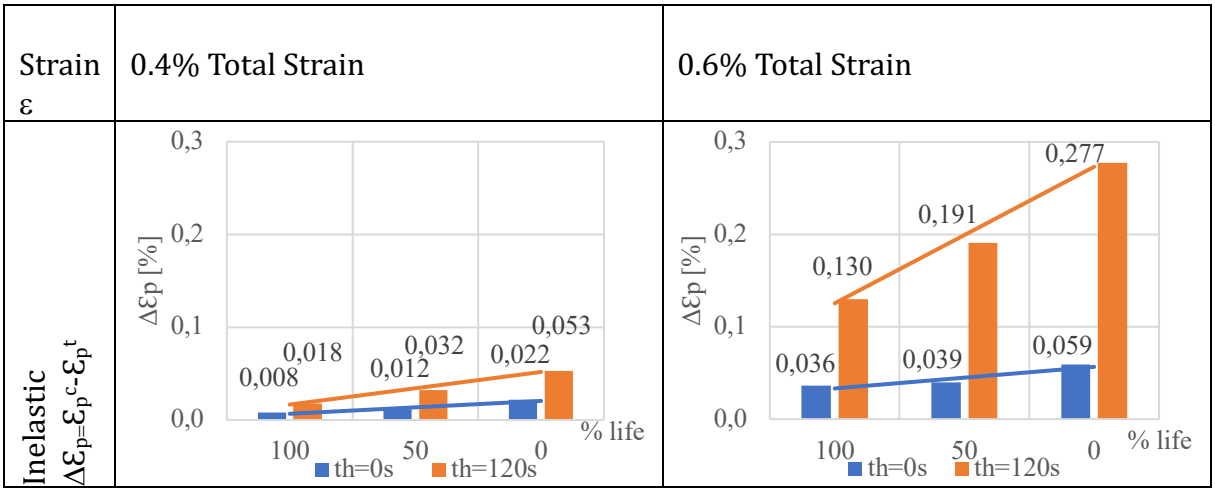

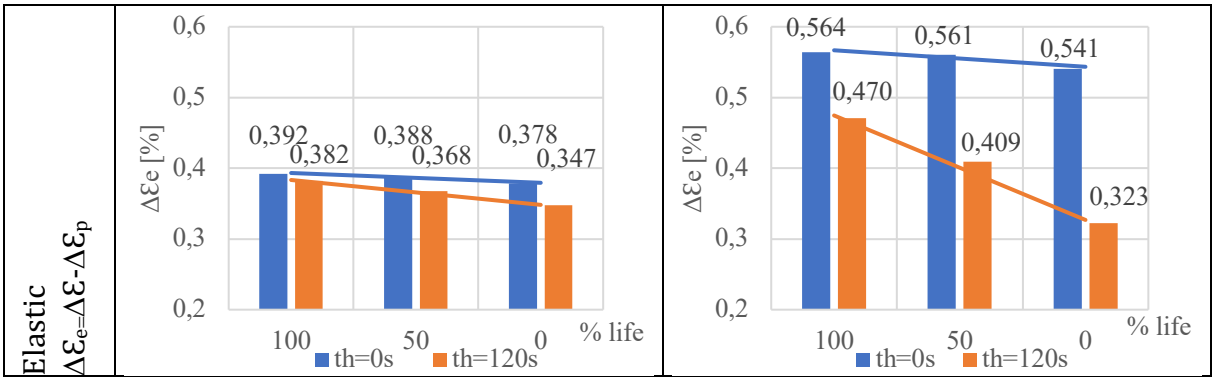

Figure 5. Strain during tests for 0.4% and 0.6% of total strain.

Additionally, as is shown in Figure 6, hold time causes increasing of the mean stress—it becomes compressive for the material (Takahashi, 2008). Compressive stresses can be considered as recovery of creep caused by tensile (Swindeman & Ren, 2018). Higher levels of compressive stresses were observed for 0.4% of total strain, which is another factor that explains the longer life in comparison with 0.6% of total strain.

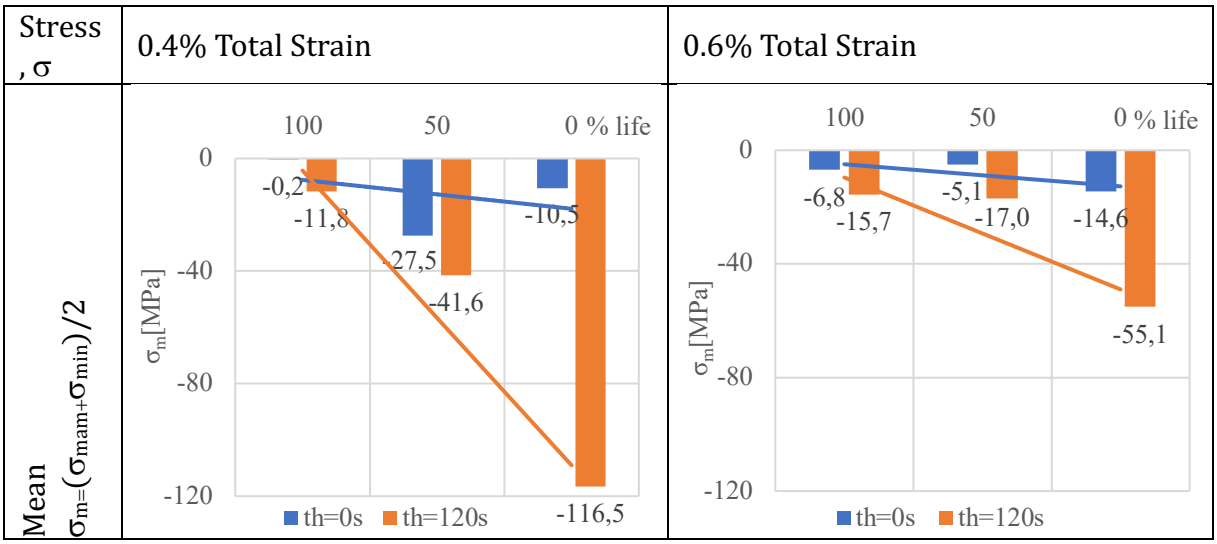

Figure 6. Alternating and mean stresses for 0.4% and 0.6% of total strain.

Conclusions

This study has led to the following conclusions:

1. Increasing total strain with application of hold time during tension resulted in a decrease of fatigue life of G17CrMoV5-10 cast steel.
2. Cyclic material softening behavior was noticed for all types of test conditions.

3. Fatigue tests with hold time showed occurrence of permanent deformations in the material during the life cycle, caused by cyclic creep.

Contact:

Anna Polnik anna.polnik@bakerhughes.com

4.3. *Unexpected crystallographic structure, phase transformation, and hardening behavior in the AlCoCrFeNiTi0.2 high-entropy alloy after high-dose nitrogen ion implantation* – P. Jenczyk, D. M. Jarząbek, Z. Lu, E. Gadalińska, N. Levintant-Zayonts, Y. Zhang [IPPT-PAN, University of Science and Technology Beijing, Ł-ILOT)

Harsh environments, such as nuclear power plants, require the development of materials with stable properties when exposed to radiation/bombardment conditions. In this work, a bulk high-entropy alloy (HEA) was implanted with nitrogen ions accelerated at 50 kV to induce and study crystal structural defects. X-ray powder diffraction (XRD) showed that the studies HEA consisted of two phases: σ and body-centered cubic (BCC) and underwent the σ to BCC phase transformation due to ion bombardment. Unexpectedly, XRD peaks of implanted samples could not be assigned to any known simple nitride, a finding that suggests the creation of new high- or medium-entropy ceramics. Studies of the mechanical and tribological properties with the use of nanoindentation and scratch tests revealed a hardening of both phases of the implanted surface and higher wear resistance. There were also surprising increases in the hardness-to-Young's modulus ratio and elastic recovery for both phases. The results are promising not only for the nuclear applications, but also for space applications, mechanical engineering, and tribology.

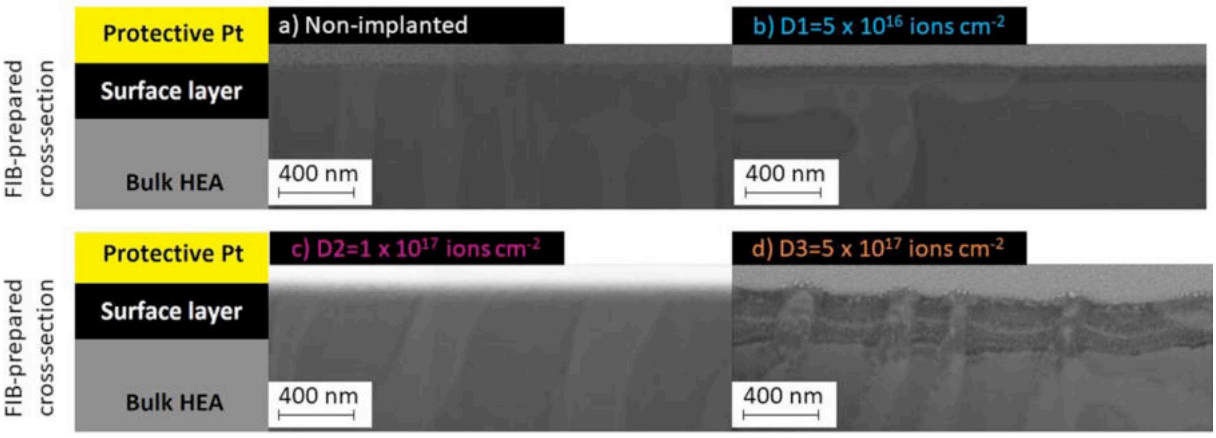

Fig. 1. Cross-sections through the sample surfaces. There are significant changes in the sample structure only for the D3 sample (exposed to the highest fluence). It should be noted that the protective platinum (Pt) layer has been deposited before FIB cutting to avoid implanting gallium (Ga) ions on the surface.

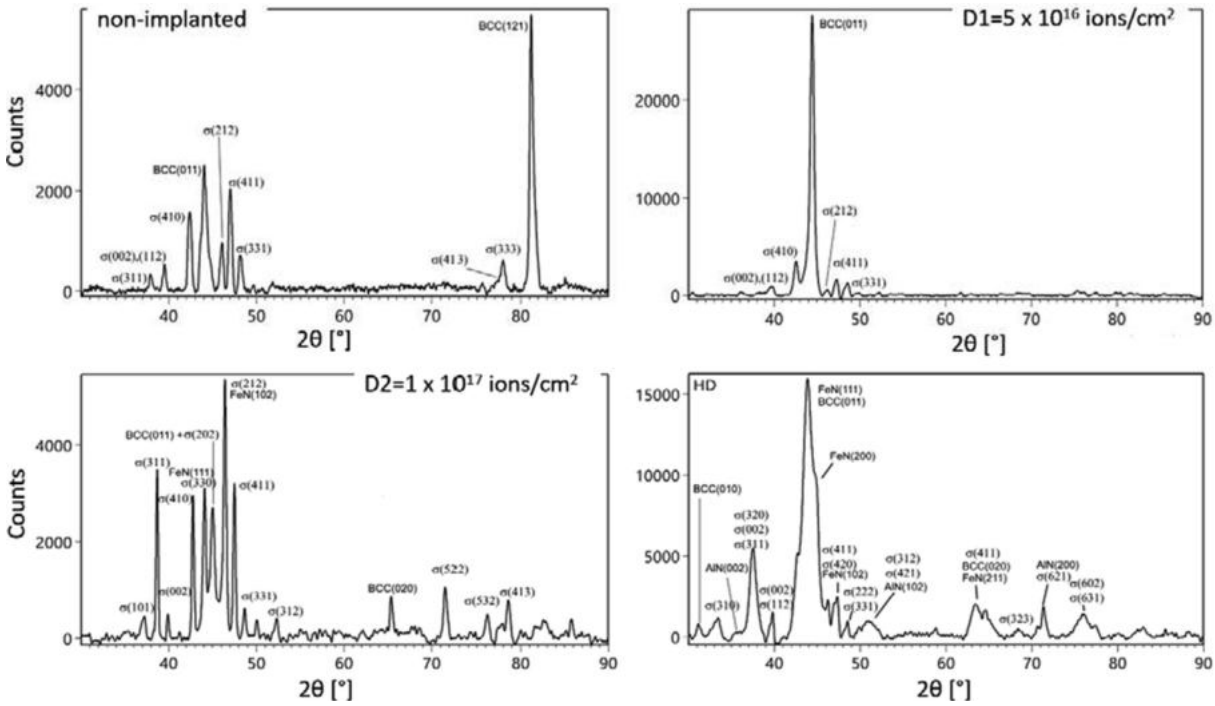

Fig. 2. X-Ray diffractograms for each sample.

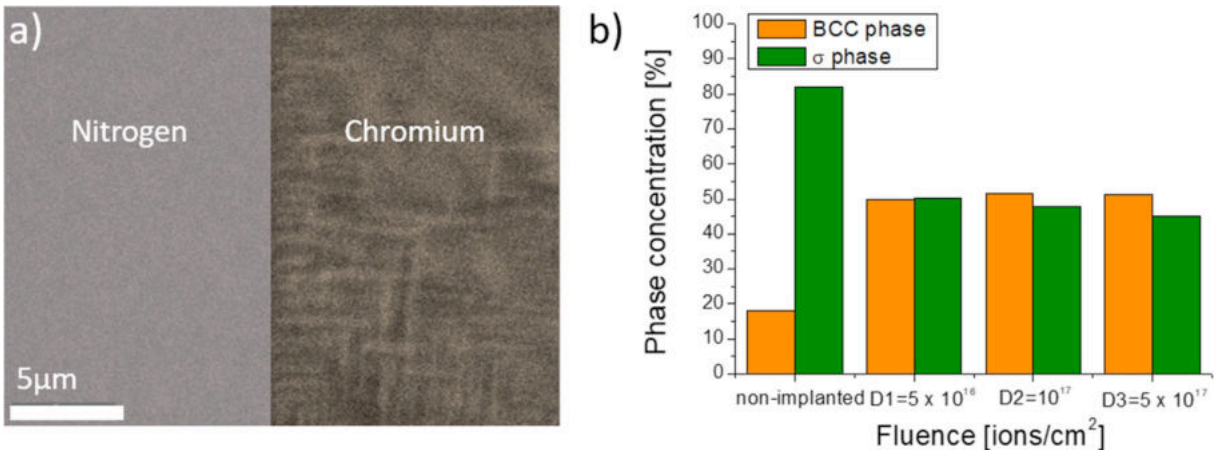

Fig. 3. (a) Representative nitrogen and chromium EDS signals of the same spot. (b) Phase concentrations for each sample calculated by using XRD.

It was shown that ion implantation of the AlCoCrFeNiTi0.2 HEA has led to unexpected XRD spectrum, phase transformation, and hardening of the surface layer. In contrast to thermal processes such as nitriding, nitrogen ion implantation does not lead to the creation of simple nitrides; rather, there are unidentified peaks. These peaks correspond to the BCC and σ phases, similarly to the bulk (virgin) specimen, but their ratio changes for the ion implanted samples. In general, the BCC phase stability was confirmed and the σ to BCC phase transformation was observed. Moreover, the hardening of the BCC and σ phases was observed. Simultaneously, there is a surprising increase in the H/E ratio and elastic recovery of both phases. Although the proposed criteria of possible composition of high-entropy materials have not been fulfilled, tentatively attribute the results to the creation of new high- or medium-entropy ceramics in the implanted samples. The new material also has promising and interesting properties, but the mechanism of its creation and its exact structure require additional, extensive research.

Contact
Dariusz Jarząbek djarz@ippt.pan.pl

5. OTHER WORKS

5.1. *Enhancement of NDE Techniques by Application of Advanced Signal and Image Processing Methods* – Andrzej Katunin [Silesian University of Technology]

Numerous attempts have been implemented to enhance the results of various NDE techniques potentially applicable for inspection of aircraft structures and components by using of the processing methods to raw results of inspection. The performed studies cover several NDE techniques, including shearography, self-heating based vibrothermography (the authored technique), modal analysis, ultrasonic testing, X-ray computed tomography, and D-Sight.
The studies focused on shearography aimed at improvement of the technique to make it possible to detect and identify small structural damage in composites were performed. For this purpose, the approaches based on wavelet transforms were used to filter out diagnostic information from the shearographic images containing fringe pattern and measurement noise. The developed algorithms within these studies are based on classical wavelet transforms, like non-decimated discrete wavelet transform [1,2], as well as some more advanced directional wavelet transforms [3]. The results of application of these processing algorithms show significant improvement of damage detectability based on shearographic testing (see Fig. 1), but also highlighted problems with application of classical wavelet transforms for such a class of problems, primarily the boundary effect, which may mask the presence of damage in the areas near edges and the dependency on the applied wavelet function, for which selection no strict rules exist.

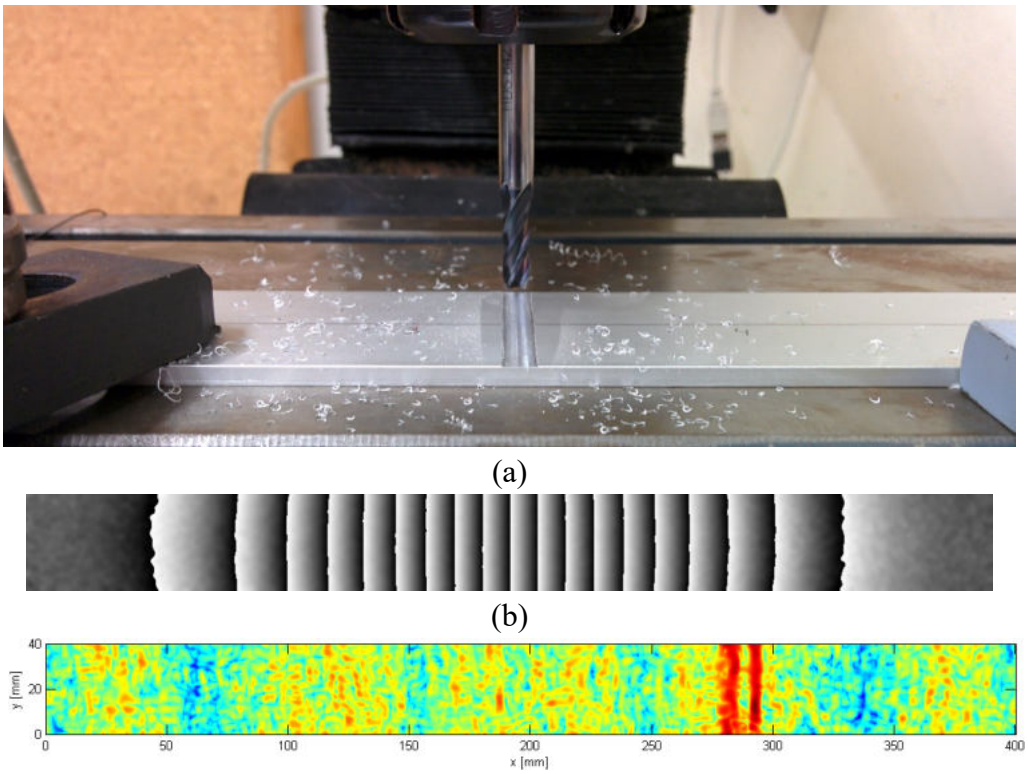

Fig. 1. Introduction of the artificial damage in a tested plate (a), filtered phase map for modal rotation field obtained from shearographic measurements and preprocessing (b), results of enhancement of the measured results with wavelet analysis (c) showing identified damage [1].

The above-mentioned problems were reduced by the developed algorithm based on S-transform [4]. The algorithm was tested on mode shapes of various composite structures with various damage types, and the achieved results confirmed lack or significant reduction of the boundary effect and easiness of application, since S-transform does not use basis functions (see Fig. 2, for instance). Similar approach was developed based on space-frequency distributions and tested on the shearographic NDE results [5], demonstrating limiting the mentioned deficiencies.

(a)

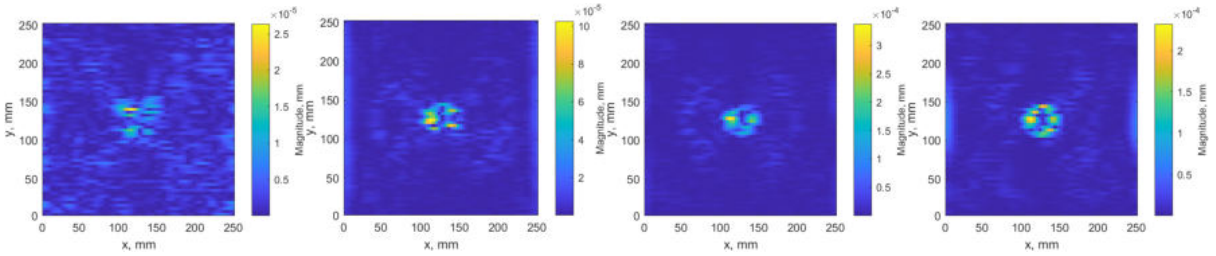

(b)

Fig. 2. The tested sandwich structure with debonding of a core (a) and the results of identification of damage for subsequent mode shapes considered in the study obtained using S-transform (b) [4].

The enhancement algorithms of raw NDE results were also developed for the authored NDE technique, the self-heating based vibrothermography. This technique eliminates the necessity of thermal excitation of the tested polymer matrix composite structures using external heat sources and substitutes it with mechanical cyclic loading by inducing vibrations at several resonant frequencies. The heat generated due to viscoelastic heat dissipation makes it possible to observe characteristic temperature distributions and, based on the local temperature differences, identification of damage. The example of temperature response obtained using this technique is presented in Fig. 3. Nevertheless, the observed differences, especially in the cases of small damage were barely recognizable or even undetectable (see Fig. 4(b)). The developed algorithms, which were based on estimation of statistical features as well as more advanced techniques, which include numerous dedicated processing methods for thermographic images, wavelet transforms, derivatives, and other, allowed improving the detectability of damage in tested composite structures significantly. The tests were performed on composite specimens with flat-bottom holes [6] as well as low-velocity impact damage (Fig. 4(c)) [7].

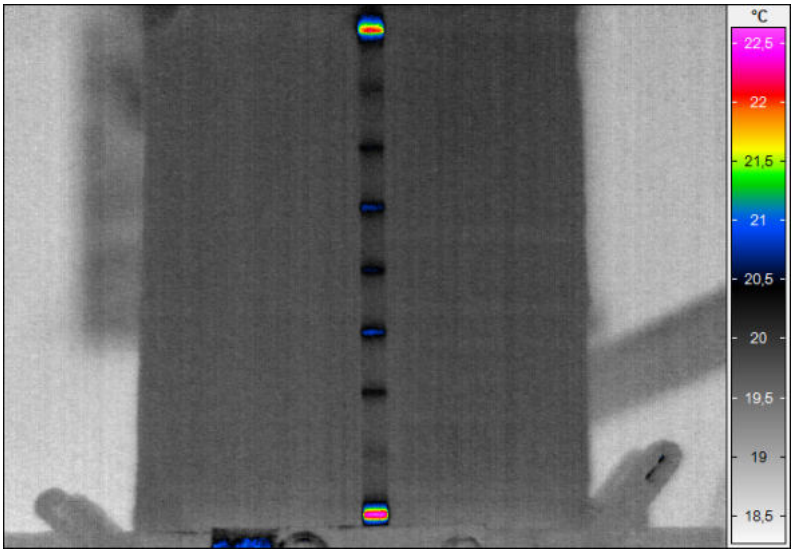

Fig. 3. The example of identification damage in GFRP structure using self-heating based vibrothermography.

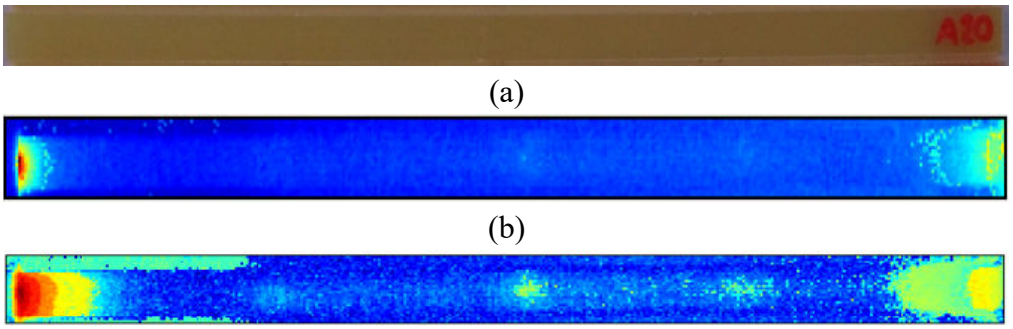

(a)

(b)

(c)

Fig. 4. The GFRP specimen with three barely visible impact damage sites (a), its thermographic response (b), and the enhanced thermogram with visible damage (c) [7].

Additionally, the studies on improvement of the D-Sight NDE technique were performed by introducing the method for image processing of raw D-Sight images. The D-Sight technique used for detection of hidden corrosion in aircraft structures is widely used in ground maintenance primarily as the qualitative technique. Recent advances allowed to make a step to quantification of hidden corrosion of aircraft structures appeared due to moisture ingress into riveted lap joints. The initial concept of this approach was reported in [8], while the next steps toward quantification consisted of development of the image processing algorithm to nivel the problems with variable angle of observation and inhomogeneous illumination of tested structures, and finally, identification of the spatial extent of hidden corrosion [9]. The example of identification of hidden corrosion is presented in Fig. 5. The sensitivity of the D-Sight technique as well as the accuracy in determination of spatial extent of hidden corrosion were performed on the specimens with simulated hidden corrosion using two reference techniques, namely laser metrology and digital image correlation, which allowed finding relationship between height of deformations and corrosion severity with its spatial extent [10].

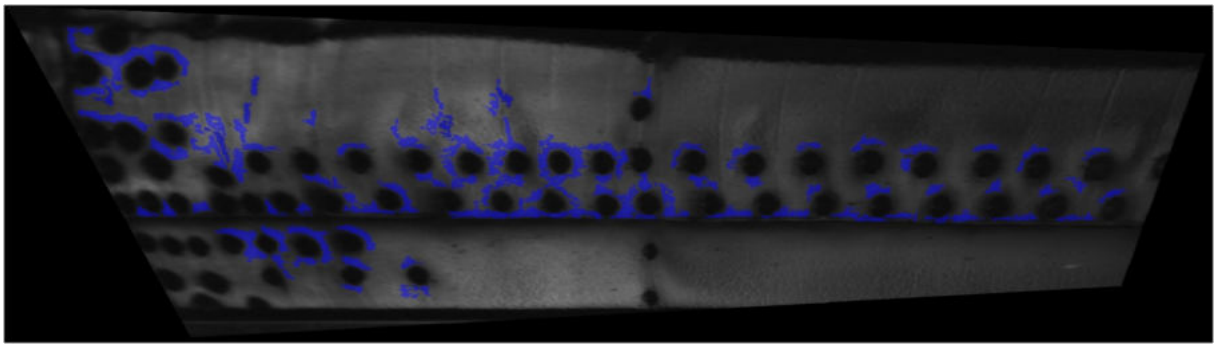

Fig. 5. The example of detection of hidden corrosion spots in aircraft panel based on processing of D-Sight images of a military helicopter.

The problem of evaluation residual life in damaged composite structures remain still open, primarily due to its high complexity. Recent attempts have been made to use NDE results of ultrasonic inspections, which is usually used in damage assessment for composite aircraft structures and elements. The idea behind this approach was to identify and classify barely visible impact damage (BVID), which is one of the most dangerous types of damage in composites, from ultrasonic scans and directly incorporate the obtained results to CAD/CAE models to make it possible predicting of structural residual life without necessity of performing CAI/TAI tests. The reconstruction algorithms for ultrasonic B- and C-scans of damaged CFRP and GFRP composite specimens have been proposed to acquire shapes and positions of cracks and delamination directly from the results of ultrasonic NDE results [11]. To assess the accuracy of identification of BVID the tests with reference techniques were necessary. Since X-ray computed tomography is the most sensitive and accurate in this case, it was selected to acquire reference data. The algorithms for classification of different types of damage (cracks, delamination) was developed based on segmentation and wavelet analysis of the 2D cross-sections of CFRP and GFRP composite specimens with BVID of various energy as well as fusion of the results of X-ray computed tomography and ultrasonic testing was performed for determining correction factors for overestimated dimensions usually obtained from ultrasonic testing for BVIDs [12,13]. The example of such fusion is presented in Fig. 6.

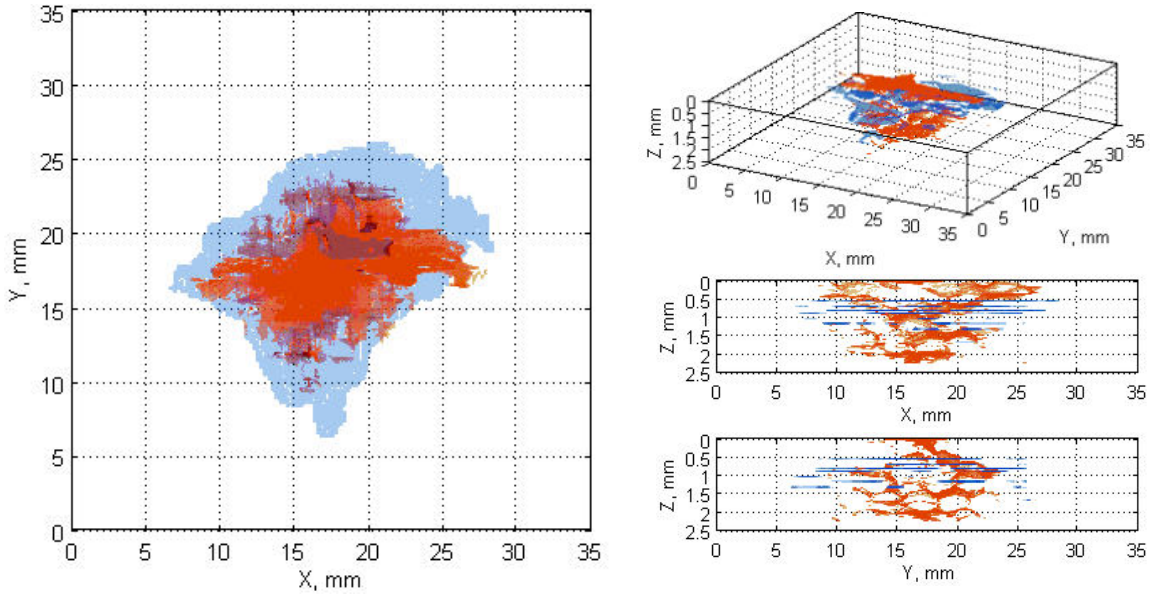

Fig. 6. Fused low-velocity impact damage detected in CFRP structure using the X-ray CT scans (red color) and the ultrasonic (blue color) C-Scan [12].

Based on these results, the methodology of modeling impact damage in composite structures based on the results of NDE inspection have been proposed based on the results of X-ray computed tomography, ultrasonic testing, and numerical models, where impact damage parameters were obtained through dynamics simulations [14]. The examples of such models are presented in Fig. 7.

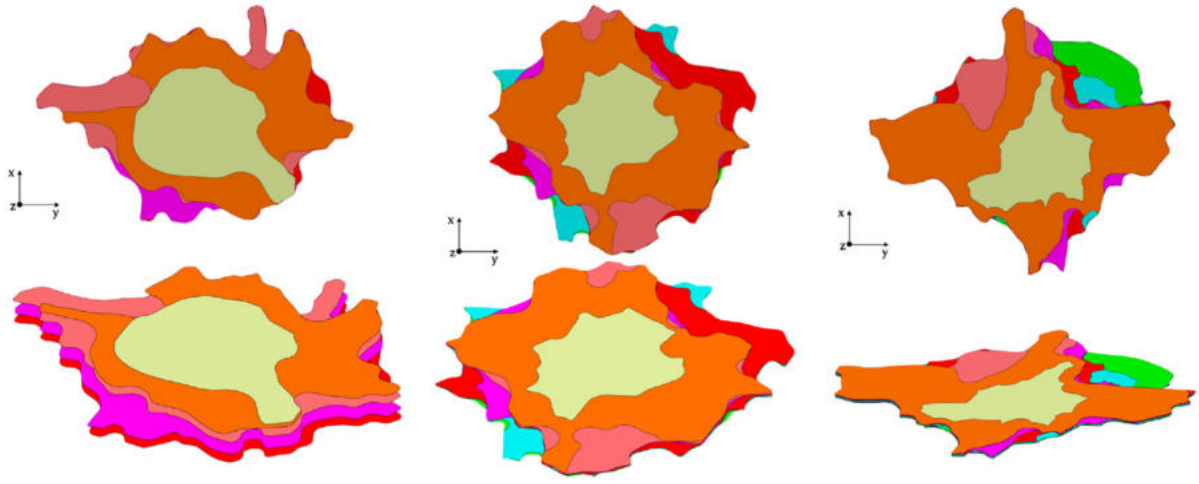

Fig. 7. The examples of CAD models of barely visible impact damage reconstructed from ultrasonic NDE results [14].

1. Katunin A., Lopes H., Araújo dos Santos J.V., Identification of multiple damage using modal rotation obtained with shearography and undecimated wavelet transform, Mechanical Systems and Signal Processing 116, 2019, 725-740.
2. Katunin A., Araújo dos Santos J.V., Lopes H., Damage identification by wavelet analysis of modal rotation differences, Structures 30, 2021, 1-10.

3. Katunin A., Performance of damage identification based on directional wavelet transforms and entopic weights using experimental shearographic testing results, Sensors 21(3), 2021, 714.
4. Katunin A., Identification of structural damage using S-transform from 1D and 2D mode shapes, Measurement 173, 2021, 108656.
5. Katunin A., Damage identification and quantification in beams using Wigner-Ville distribution, Sensors 20(22), 2020, 6638.
6. Wronkowicz A., Katunin A., Wachla D., Enhancement of damage identification in composite structures with self-heating based vibrothermography, Optik 181, 2019, 545-554.
7. Katunin A., Wronkowicz-Katunin A., Wachla D., Impact damage assessment in polymer matrix composites using self-heating based vibrothermography, Composite Structures 214, 2019, 214-226.
8. Katunin A., Dragan K., Qualitative to quantitative non-destructive evaluation: A concept for D-Sight inspections of aircraft structures, Applied Mechanics and Materials 909, 2022, 69-74.
9. Katunin A., Nagode M., Oman S., Cholewa A., Dragan K., Monitoring of hidden corrosion growth in aircraft structures based on D-Sight inspections and image processing, Sensors 22, 2022, 7616.
10. Katunin A., Lis K., Joszko K., Żak P., Dragan K., Quantification of hidden corrosion in aircraft structures using enhanced D-Sight NDT technique, Measurement 216, 2023, 112977.
11. Wronkowicz-Katunin A., Katunin A., Dragan K., Reconstruction of barely visible impact damage in composite structures based on non-destructive evaluation results, Sensors 19(21), 2019, 4629.
12. Katunin A., Wronkowicz-Katunin A., Dragan K., Impact damage evaluation in composite structures based on fusion of results of ultrasonic testing and X-ray computed tomography, Sensors 20(7), 2020, 1867.
13. Wronkowicz-Katunin A., Katunin A., Nagode M., Klemenc J., Classification of cracks in composite structures subjected to low-velocity impact using distribution-based segmentation and wavelet analysis of X-ray tomograms, Sensors 21(24), 2021, 8342.
14. Katunin A., Wronkowicz-Katunin A., Danek W., Wyleżoł M., Modeling of a realistic barely visible impact damage in composite structures based on NDT techniques and numerical simulations, Composite Structures 267, 2021, 113889.

Contact:

Andrzej Katunin andrzej.katunin@polsl.pl

5.2. *Works Concerning Fatigue Aspects Performed Under the MONICA Project* – Mirosław Rodzewicz [Warsaw University of Technology]

MONICA - is the acronym of the Polish-Norwegian project entitled: "Novel Approach to Monitoring of Impact of Climate Change on Antarctic Ecosystems" implemented in 2014-2015 by a consortium which included the Institute of Biochemistry and Biophysics of the Polish Academy of Sciences, Warsaw University of Technology - Faculty of Mechanical Power and Aeronautical Engineering and Northern Research Institute NORUT, Tromsø.

The main objective of the project was to monitor the Antarctic fauna, especially the number of sea mammals and birds belonging to the so-called indicator species. They include e.g. Penguins. Based on the data on the penguin population, it is possible to draw conclusions about the condition of marine ecosystems and support the rational management of Antarctic marine food resources by setting the so-called fishing quotas. This is the number of Antarctic krill that can be harvested without disturbing the ecological balance. Poland is a signatory to the Convention on the Conservation of Antarctic Marine Living Resources (CCAMLR) and since 1977 it has been conducting such monitoring in areas including two Antarctic Specially Protected Areas (ASPA 128 and ASPA 151), located in the vicinity of the Polish Antarctic Station – "Arctowski" on King George Island in South Shetland.

In order to achieve the goals of the project, the PW-ZOOM unmanned aerial vehicle was designed at the Faculty of Power and Aeronautical Engineering - specially adapted for photogrammetric missions. The main challenge for the designers of the aircraft and the implementers of these missions was not only the climate and the harshness of the terrain, but above all the sudden changes in the weather and gusty winds. An important aspect was the integration of the autopilot with the aircraft (i.e., tuning the dynamic characteristics of both systems), the strategy for planning photogrammetric routes, as well as the development of software supporting the operation of the ground control station.

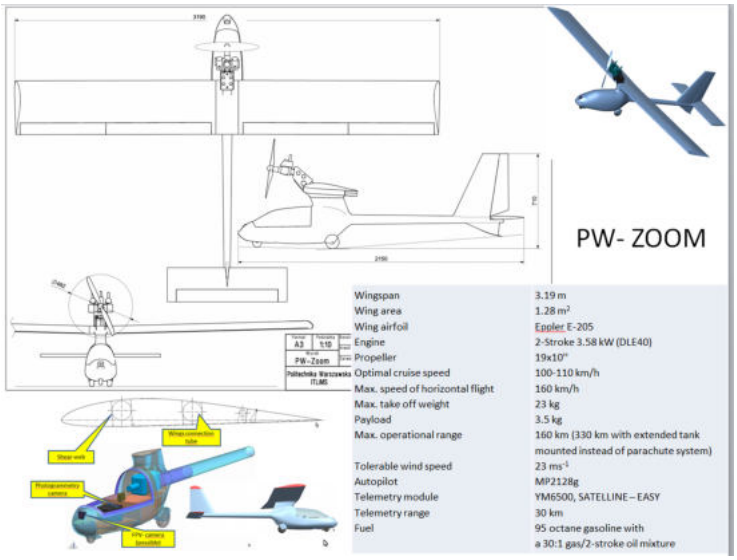

Fig. 1 The PW-ZOOM – the plane used in fotogrammetry missions in Antarctica

Three Antarctic expeditions were carried out during the project (2014, 2015 and 2016). During these expeditions, 26 task photogrammetric flights were made in the BVLOS (Beyond Visual Line of Sight) mode with a total length of over 3,640 km. About 24,000 aerial photographs were brought, which were used to develop detailed orthophotomaps of the ASPA-

128 and ASPA 151 areas. They were used for biological analyzes of flora and fauna as well as geomorphological and glaciological analyses. About 32,000 nests of different species of penguins were identified in the monitored areas. The culmination of the activities was the photogrammetric mission of PW-ZOOM over the volcanic Penguin Island, located in the eastern part of King George Bay. So far, no one has conducted a more extensive study of the ecosystems of this region of Antarctica using unmanned aerial vehicles.

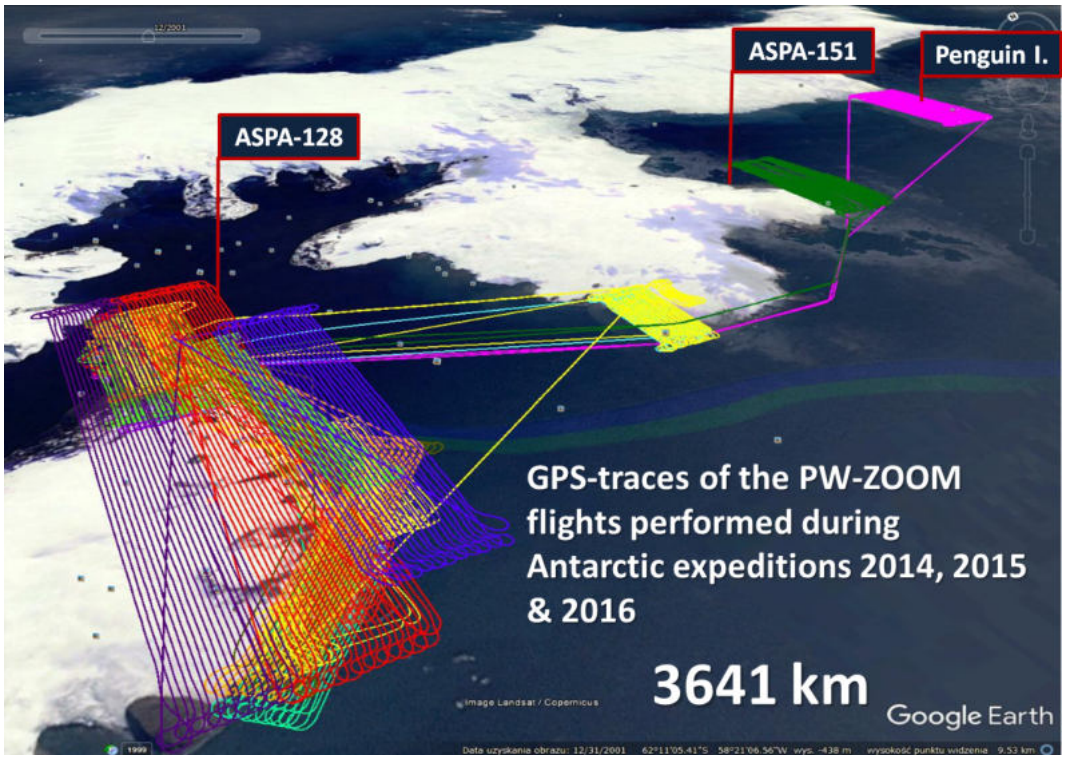

Fig. 2 Photogrammetrics flights of the PW-ZOOM over King Georg Island

During the project, in addition to the results related to the main goal of the project, a large collection of autopilot logs was also collected, which can be used for various analyzes of the dynamic behavior of aircraft during photogrammetric missions. In the autopilot log, not only the GPS route, but also the angles of the instantaneous values of spatial position of the airframe, accelerations and angular velocities, linear accelerations and aerodynamic and GPS speeds, servos control-signals and many other parameters are saved with a certain frequency. One of the important topics of the analyzes was the load spectrum of the PW-ZOOM aircraft in photogrammetric flights. The input signal for these analyzes is the acceleration relative to the z-axis (vertical design axis of the aircraft). By relating this acceleration to the g-acceleration, the load factor is calculated. The signal of load factor value is then scaled to a 32-steps scale of discrete load level and then transformed into a sequence of local extremes. This sequence is subjected to the Rainflow Counting algorithm and then the array of load half cycles (HC-array) is created. This array represents the load spectrum. Having the HC-arrays from many flights it is possible to manage different fatigue-oriented analyses. Such analyses were performed by the Authors-team involved in the MONICA Project. Below, there is the list of papers devoted to the problem of fatigue prepared by this Team.

A/ The papers presented on the fatigue conferences:

- Głowacki Dominik, Rodzewicz Mirosław, 2014: "Investigation into Load Spectra of UAVS Aircraft". *Fatigue of Aircraft Structures*. 2014. Vol. 2013, p. 40–52. DOI 10.2478/fas-2013-0004.

The conference took place 10-11 January 2013. The Authors presented all details of the algorithms developed by the authors for the load spectra derivation. Those algorithms were tested on the autopilot-logs database collected by the authors before the start of the MONICA project, and later were utilized to all analysis of the load spectra related to the MONICA project.

- Głowacki Dominik, Rodzewicz Mirosław, 2014: „Investigation into load spectrum of the UAV during Antarctic photogrammetric mission" - 9th Conference Fatigue of Aircraft Structures 14-15 January 2016

There was presented the aspect of influence of the turbulence generated by the wind on the load spectra.

- Głowacki Dominik, Rodzewicz Mirosław, 2019 "Influence of operational loads in the main phases of photogrammetry mission on fatigue life of a critical aircraft-frame element" - 12th Conference Fatigue of Aircraft Structures 10-11January 2019

The paper was focused on the aspect of influence of the methods of the aircraft control (manual or automatic) on the load spectrum.

- Głowacki Dominik, Rodzewicz Mirosław, 2019.. Study of Load Spectrum Occurring in the Course of Photogrammetric Missions of the UAV. In: Niepokólczycki, A., Komorowski, J., Proceedings of 30th Symposium of the International Committee on Aeronautical Fatigue - Structural Integrity in the Age of Additive Manufacturing. International Committee on Aeronautical Fatigue. 2019. p. 1112–1127. DOI 10.1007/978-3-030-21503-3_88.

This conference paper contains an analysis of the flight-logs, with a focus on investigation of load spectrum during photogrammetry missions. The analysis was based on flights having the same scenario and flight-track, but performed in different weather conditions, especially at different wind speeds. The load spectra were developed as half-cycle arrays of load factor signal (i.e. transfer arrays based on the rainflow counting algorithm), and as incremental load spectra. Calculation algorithms were prepared by the authors in the LabVIEW environment. The obtained results allow for assessing the influence of weather on the fatigue loads during flight. They can be useful as the basis necessary for load spectrum extrapolation and preparation of fatigue tests of the PW-ZOOM structure or similar planes.

B/ The articles:

Rodzewicz, Mirosław, Głowacki, Dominik i Hajduk, Jarosław, 2017. „Some dynamic aspects of photogrammetry missions performed by PW-ZOOM – the UAV of Warsaw University of

Technology". Archive of Mechanical Engineering. 2017. Vol. 64, p. 37–55. DOI 10.1515/meceng-2017-0003.

Abstract: The article presents the analyses of the flights carried out the by the Unmanned Aerial Vehicle (UAV) named PW-ZOOM used to perform a photogrammetric mission and monitoring of fauna in Antarctic areas. The analyses focus on the deviations of the optical axis of the photo-camera which occurred during photogrammetric flights carried out on the same route but during several Antarctic expeditions performed in subsequent years (2014 and 2015). The results were subjected to correlation tests with weather conditions (wind speed and variability). The basis for these analyses are the data from the onboard signal recorder integrated with an autopilot.

Rodzewicz, Mirosław, 2022. Close-proximity, conservative extrapolation of load spectra. Aircraft Engineering and Aerospace Technology. 2022. Vol. 95, p. 1–13. DOI 10.1108/AEAT-12-2021-0374.

The purpose of this paper is to present the author's method of conservative load spectrum (LS) derivation and close-proximity LS extrapolation applying a correction for measurement uncertainty caused by too low sampling frequency or signal noise, which may affect the load histories collected during the flying session and cause some recorded load increments to be lower than the actual values. Design/methodology/approach Having in mind that the recorded load signal is burdened with some measurement error, a conservative approach was applied during qualification of the recorded values into 32 discrete load-level intervals and derivation of 32 × 32 half-cycle arrays. A part of each cell value of the half-cycle array was dispersed into the neighboring cells placed above by using a random number generator. It resulted in an increase in the number of load increments, which were one or two intervals higher than those resulting from direct data processing. Such an array was termed a conservative clone of the actual LS. The close-proximity approximation consisted of multiplication of the LSs clones and their aggregation. This way, the LS for extended time of operation was obtained. The whole process was conducted in the MS Excel environment. Findings Fatigue life calculated for a chosen element of aircraft structure using conservative LS is about 20%–60% lower than for the actual LS (depending on the applied value of dispersion coefficients used in the procedure of LSs clones generation). It means that such a result gives a bigger safety margin when operational life of the aircraft is estimated or when the fatigue test for an extended operational period is programed based on a limited quantity of data from a flying session. Originality/value This paper presents a proposal for a novel, conservative approach to fatigue life estimation based on the short-term LS derived from the load signal recorded during the flying session.

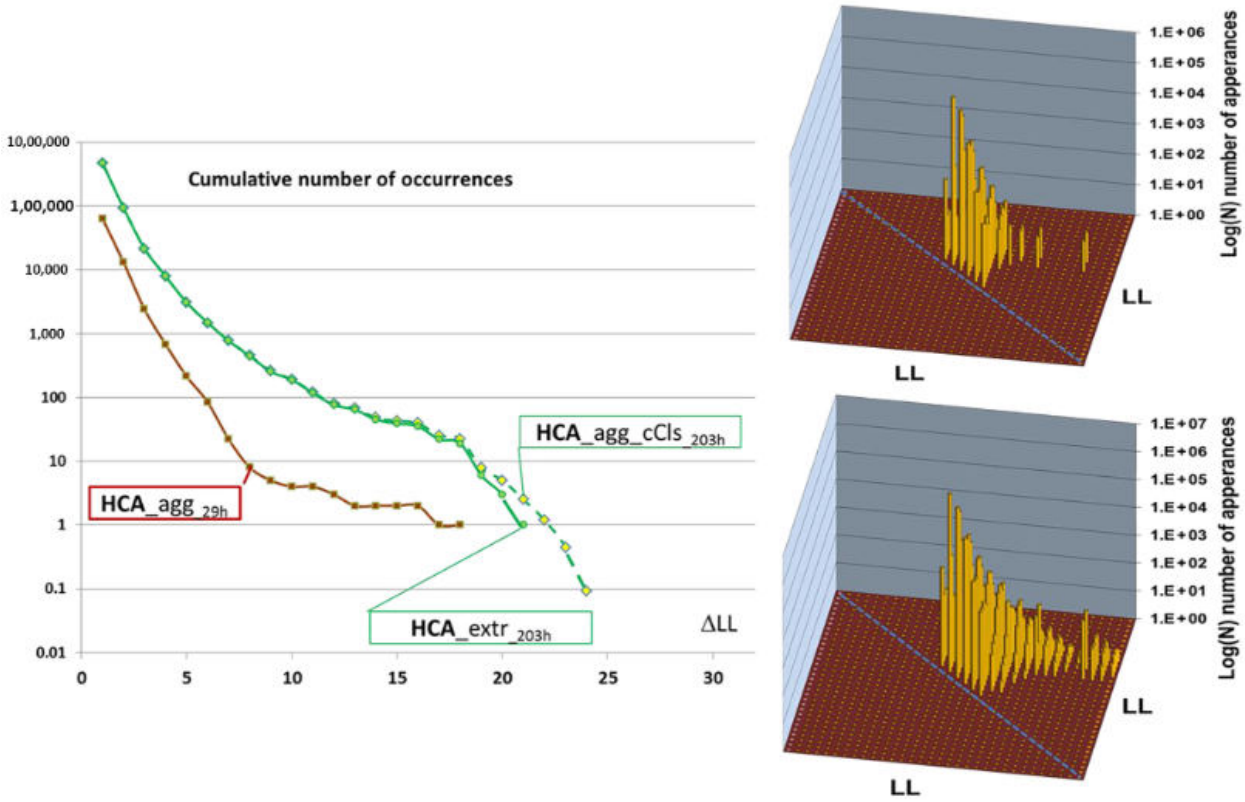

https://www.emerald.com/insight/content/doi/10.1108/AEAT-12-2021-0374/full/pdf

Fig. 3 The example of the PW-ZOOM load spectra analysis: the comparison of the incremental load spectra and the Full-Cycle arrays for the load spectrum collected during 29-hours flight session of the and the load spectrum extrapolated up to 203 hours.

Contact:

Mirosław Rodzewicz, miro@meil.pw.edu.pl

INVESTIGATIONS IN MILITARY AVIATION

1. *Service Life Extension Program of the Mi-24 Helicopter* - Marcin Kurdelski, Łukasz Piątkowski, Piotr Synaszko, Krzysztof Dragan [Air Force Institute of Technology]

Mi-24 helicopters were introduced to the Polish Armed Forces in the 1981. Helicopter deliveries were stretched over the decade. The last ones came to Poland in the early 1990's. Two versions of the Mi-24 helicopters are used in Poland (Mi-24D and Mi-24V). The first studies on the extension of the service life were undertaken in the years 2007 ÷ 2009. The research was carried out at Air Force Institute of Technology (ITWL) in Poland in cooperation with Military Aviation Works No. 1 JSC[1]. During the implementation of the project, financed by the Ministry of Science and Higher Education, the operation of the helicopters covered by the program was changed to condition based monitoring. The goals achieved allowed the helicopters to be used at least for the next 15 years with the limit of 4 000 flight hours.

Nowadays Polish Armed Forces request to achieve new goal for the Mi-24 helicopters. In 2019, Air Force Institute of Technology was tasked with checking the feasibility of operating the helicopters up to 4 500 flight hours. In view of the need to extend their service life and the planned modernization, the Ministry of National Defence ordered preparation and execution of the complex Service Life Extension Program for these helicopters. Based on the previous experience [2,3,4], the Institute proposed the Full Scale Fatigue Test (FSFT) concept of the Mi-24 helicopter structure as well as the implementation of the onboard Loads and Vibration Monitoring System in order to extend the service life and Structural Health Monitoring at the same time[5].

Mi-24 Helicopter Full Scale Fatigue Test

The main goal of the FSFT was to verify the total service life of the helicopter's structure beyond the range of 4 000 flight hours (up to minimum 4 500 flight hours) and up to 14 000 landings. The assumed safety factor of the test is 3, which means that the goal service life of the test structure was minimum 13 500 simulated flight hours and 42 000 simulated landings.

---

[1] Klimaszewski, S., Leski, A., Dragan, K., Kurdelski, M., & Wrona, M. (2009). Helicopter structural integrity program of Polish Mi-24 Hind helicopters. In *ICAF 2009, Bridging the Gap between Theory and Operational Practice: Proceedings of the 25th Symposium of the International Committee on Aeronautical Fatigue, Rotterdam, The Netherlands, 27–29 May 2009* (pp. 263-277). Springer Netherlands.

[2] Leski A., Reymer P., Kurdelski M. (2011). Development of Load Spectrum for Full Scale Fatigue Test of a Trainer Aircraft. In: Komorowski J. (eds) ICAF 2011 Structural Integrity: Influence of Efficiency and Green Imperatives. Springer, Dordrecht.

[3] Reymer, P., Leski, A. and Dragan, K., (2012). Recent Progress in Full Scale Fatigue Test of PZL-130 "Orlik" TC-II Structure, Fatigue of Aircraft Structures, Vol. 1, pp. 76-81.

[4] Reymer, P., Leski, A., Zieliński, W. and Jankowski, K., (2015). Full Scale Fatigue Test concept of a Su-22 fighter bomber, Fatigue of Aircraft Structures, Warsaw, 2015, vol. 6, pp. 79-87.

[5] Reymer, P., Zieliński, W., Kurnyta, A., Cichocki, T., Leski, A., Kurdelski, M., & Dragan, K. (2019). Mi-24 Helicopter Full Scale Fatigue Test Concept. Fatigue of Aircraft Structures, 2019(11), 11-18.

The tested structure has been taken out of service as Mi-24 helicopter which has accomplished 3 250 flight hours and 6 500 landings.

Other specific objectives expected to be achieved during the test were:

- detection of critical places of the structure, susceptible to fatigue damage;
- determination of fatigue life until cracking and failure;
- determination of the propagation rate of the fatigue cracks;
- providing data for the development of appropriate methods for inspecting the condition of the structure during operation;
- verifying the technology of possible repairs that would extend the service life of the helicopters.

The tested structure has been composed of the fuselage, tail boom, wings, landing gear and the main gearbox, which were used as the fixture for the whole structure. In order to monitor the reaction forces in the fixture, a special adapter has been designed. The adapter allowed researchers to transfer all these six loads (pitch, roll and yaw moments as well as vertical, longitudinal, and transverse forces) and to monitor them throughout the test in order to avoid the overloading of the tested structure.

The tests assumed mapping the following types of loads occurring in flights:

- loads from the tail rotor and vertical stabilizer;
- loads from main rotor;
- inertial loads;
- aerodynamic loads on the fuselage, wings and tail fins;
- loads carried by the landing gear during take-offs and landings.

The source for determining the loads sequence for the fatigue test was the history of operation of all Polish Mi-24 helicopters from 2012 ÷ 2018. At the same time, an analysis of flight documentation and records from on-board flight data recorders was performed. An additional test system for measuring loads during flight was installed on the selected helicopter. Records from flight tests has been used to create and control load sequence.

Load sequence block, which was repeated periodically in the fatigue test, consist of 500 flight hours. Each one consists of four parts covering:

- flight loads during hover maneuvers, circles and en-route flights;
- flight loads occurring during simple and medium pilotage;
- flight loads with armament and cargo;
- ground loads, take-offs, and landings, starting and stopping engines.

For each part above, load sequence was created and performed proportionally during the test as a part of sequence block.

The Full Scale Fatigue Test has been carried out in the facility of WSK PZL-Świdnik S.A. (a Leonardo Helicopters company). The test rig prepared for research is shown on the figure below. Simulation of the flights and ground sequence was performed separately which required changing the configuration of the test rig.

Figure 1. Mi-24 helicopter installed on the test rig

During the test, weekly visual inspections of the structure were carried out by WSK PZL-Świdnik S.A. specialists. The methodology, prepared by ITWL, lists 14 areas to be inspected during the fatigue test. In the case of changes in the recorded signals from strain gauges or in order to register crack propagation, additional inspections of individual areas were performed.

In addition, specialists from the ITWL NDT team performed several inspections using the eddy current method and the ultrasonic method. ITWL inspections were aimed at:

- confirmation of the cracks indicated within weekly reports;
- confirmation of the quality of composite repairs;
- precise determination of crack tops (for drilling purposes);
- measurement of the crack length to determine their propagation rate.

Detailed inspection results were included in reports. On their basis, non-destructive testing methodologies are being prepared. It will be used during the further operation of the helicopters.

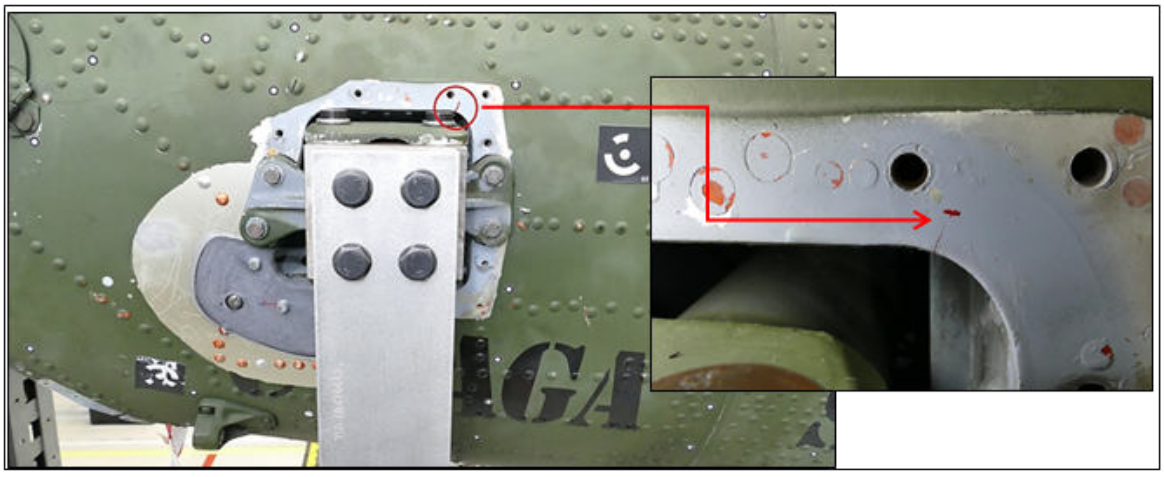

Figure 2. Skin crack and composite repair over the horizontal stabilizer mounting

Conclusions

As a result of the Full Scale Fatigue Test, a confirmation of the fatigue life of the Mi-24 helicopter structure with a value of 4 500 flight hours was obtained. The result obtained is for a safety factor SF=3 and a load sequence consistent with the operation profile in the Polish Armed Forces.

Currently, activities are underway to implement the results of the fatigue test. The last significant tasks remain to be performed during the current service life extension program are:

- teardown inspection (TI) of the fuselage;
- non-destructive inspection program;
- selected repair methodologies.

Further use and the scope of possible modifications to the structure depend on the needs and requirements of the user. The dynamic geopolitical situation may significantly affect the future use of Mi-24 helicopters in Poland.

Contact:

Marcin Kurdelski Marcin.kurdelski@itwl.pl

2. *SHM Application to Remotely Piloted Aircraft Systems – SAMAS Project* - Michał Dziendzikowski, Krzysztof Dragan [Air Force Institute of Technology]

Impact damage detection monitoring in SAMAS project

One of the major issues which could increase safety of aircraft operation is automated early detection of different damage modes of composite structures[6,7]. There exists certain type of damage which can affect the performance and durability of composite structures: disbonds, delamination, foreign object inclusion and porosity[8]. Furthermore, composites are vulnerable to impacts, which can introduce in the structure the so called Barely Visible Impact Damage (BVID)[9]. BVID can be formed even for impacts of low energies, and they decrease the stiffness and durability of a composite due to multiple delaminations and transverse cracks of composite layers.

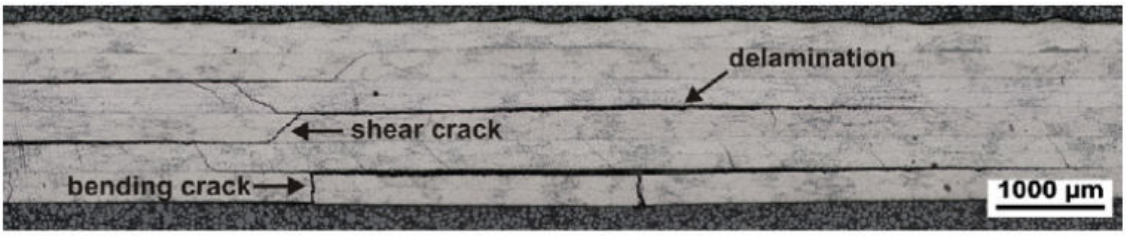

Figure 1. An example of BVID of a composite structure[10]

For BVID visual structure evaluation is not possible, therefore other non-destructive techniques needs to be applied. The most commonly used non-destructive method for BVID detection and evaluation is ultrasonic testing. This method, with use of dedicated automated scanners, allows for precise damage localization and sizing, however the inspection is time consuming and can be only performed during aircraft maintenance on the ground. Maintenance procedures related to preserving integrity of platform structures may soon be highly inefficient, both in terms of costs as well as the safety. Increasing usage of modern materials in the aerospace, composites in particular, will require development of new approach to structure maintenance. Non-destructive inspection of such materials is a burden with significant costs, related to time consumption as well as advanced equipment and skilled workforce requirements. Development

[6] M. Sohn, X. Hu, J. Kim, L. Walker, Impact damage characterisation of carbon fibre/epoxy composites with multi-layer reinforcement, Composites Part B: Engineering 31 (8) (2000) 681–691.
[7] S.-X. Wang, L.-Z. Wu, L. Ma, Low-velocity impact and residual tensile strength analysis to carbon fiber composite laminates, Materials & Design 31 (1) (2010) 118–125.
[8] R. Adams, P. Cawley, A review of defect types and nondestructive testing techniques for composites and bonded joints, NDT international 21 (4) (1988) 208–222.
[9] C. Poon, T. Benak, R. Gould, Assessment of impact damage in toughened resin composites, Theoretical and Applied Fracture Mechanics 13 (2) (1990) 81–97.
[10] J. Bieniaś, P. Jakubczak, B. Surowska, K. Dragan, Low-energy impact behaviour and damage characterization of carbon fibre reinforced polymer and aluminium hybrid laminates, Archives of Civil and Mechanical Engineering, Volume 15, Issue 4, 2015, pp. 925-932.

of new approaches for structure integrity assurance is in particularly important for the UAV market in order to grow to its full potential, otherwise it will be constrained by overwhelming maintenance cost needed for assuring safety of UAV platforms operation.

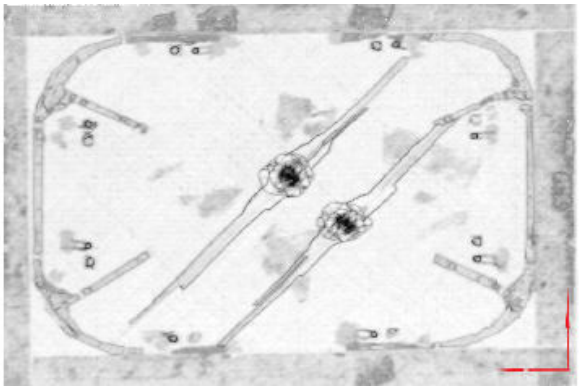

Figure 2. An example of BVID mapping with use of automated ultrasonic scanner

Therefore, it is highly desirable to complement non-destructive testing techniques with application of the so-called Structural Health Monitoring (SHM) systems. SHM systems are based on networks of sensors, permanently integrated with aircraft structure allowing for continuous aircraft integrity monitoring. Application of such methods would improve the safety and reduce maintenance costs, especially when considering hard to access “hot-spots”.

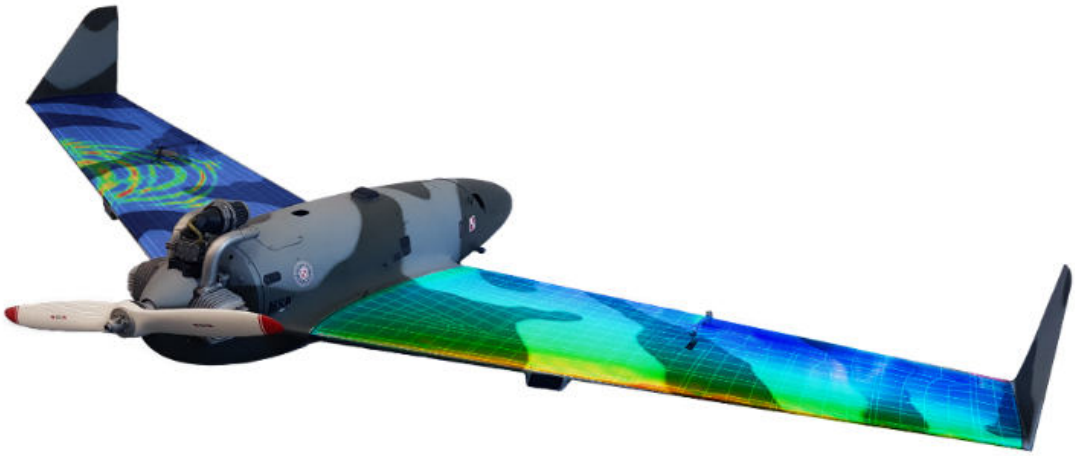

Figure 3. Digital visualization of SHM system data on UAV structure

One of the approaches for Structural Health Monitoring systems development is based on PZT piezoelectric transducers (Figure) application. In this approach elastic waves in a monitored element are generated by a network of PZT transducers. At ultrasonic frequencies, PZT transducers can excite and receive elastic waves traveling long distances along the thin-walled aircraft structures. Piezoelectric transducers, when permanently integrated with a monitored

structure, provide bidirectional energy transduction from the electronics into the structure and from the structure back into the electronic component of the system, allowing for their multimode application for SHM. Elastic waves propagating between PZT actuator and PZT sensor can be distorted during their transmission through the encountered damage. Due to these phenomena, the signal acquired by the PZT sensor can be changed.

Figure *4*. Different type of PZT transducers11

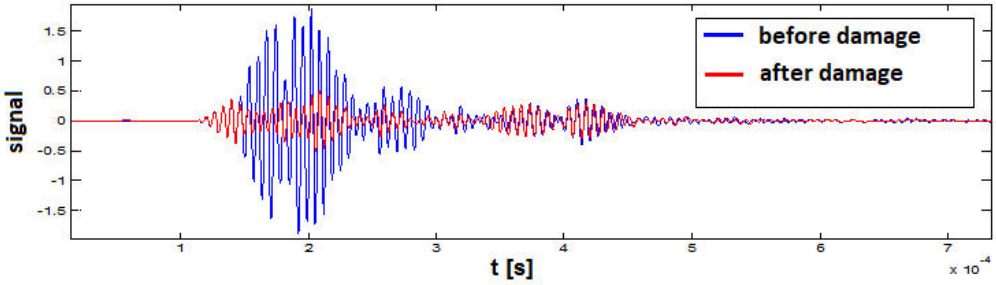

Figure *5*. Example of distortion of signal acquired by PZT sensor in the presence of damage

PZT transducers technology was applied in the SAMAS project for SHM system development. For automated analysis of signals and inference about damage presence several techniques were developed within the project. The developed techniques can be used regardless of the complexity of the structure being monitored or the type of damage and without necessity to perform additional system calibration activities in addition to obtaining a database of reference signal, which is of particular important for applicability of SHM system in operational practice. Efficiency of PZT techniques for impact damage detection of composite structures has been evaluated in the SAMAS project for:

– low velocity impact damage of energies in the range 20 ÷ 70 J;
– ballistic impact damage (Figure).

[11] Pi Piezo Technology - https://www.piceramic.com

Numerous test of SHM system performance have been delivered within the project, including impact damage detection on full scale composite component of MALE class UAV (Figure).

Figure 6. Ballistic impact test bed

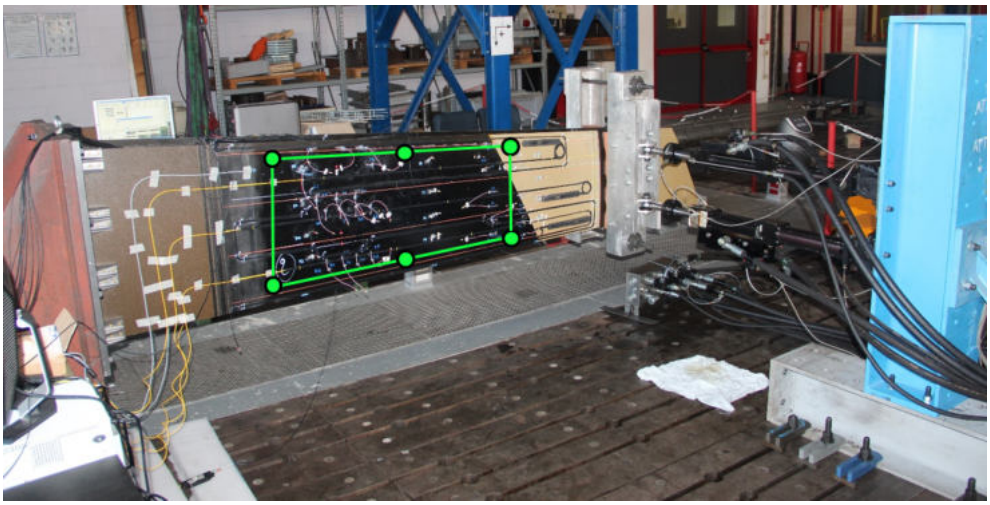

Figure 7. Full scale composite component with installed PZT sensors

Based on the data acquired during ballistic tests as well as for low velocity impacts including tests performed in varying environmental conditions, capability of SHM system towards impact damage detection at TRL 5/6 was confirmed within the SAMAS project. The highest indications of SHM system are obtained within the area of a monitored structure where it is affected by the impact (Figure, Figure). The system maintains its operational damage detection capability also under the damaged state of the structure. Subsequent impacts of the monitored structures can be correctly identified by the system as well which proves its applicability to entire lifecycle of a monitored structure, i.e., when impact damage does not require monitored part replacement. Also, it can be observed that the obtained damage intensity depends on energy of impact and therefore on its size.

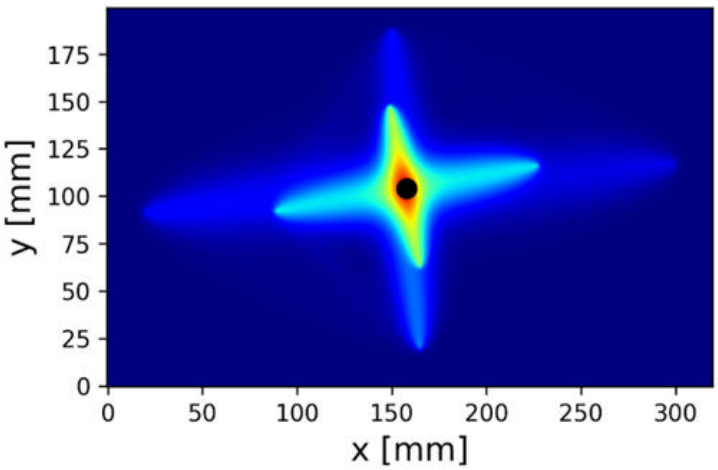

Figure 8. SHM system data visualization after impact damage

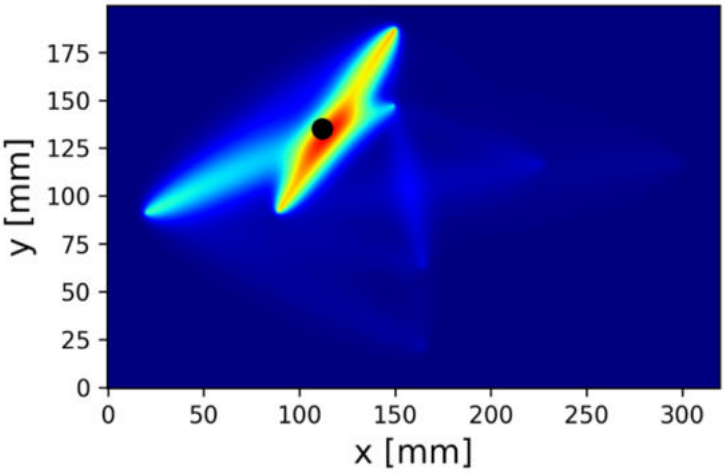

Figure 9. SHM system data visualization after subsequent impact damage

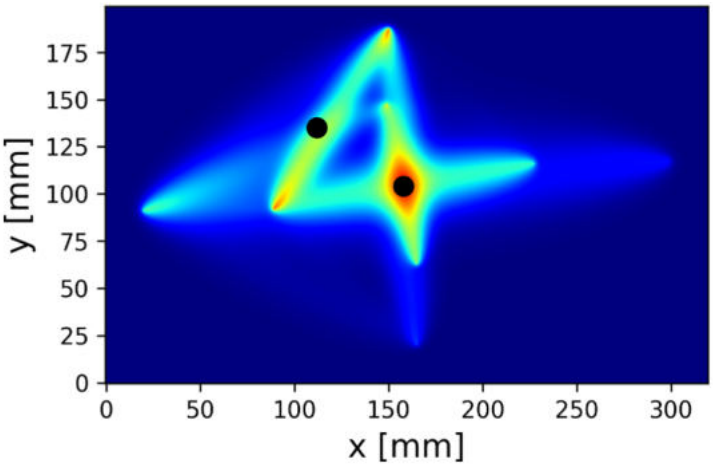

Figure 10. Smoothened data visualization map for aggregated impact damage

Conclusions

The growing demand for improving the reliability and survivability of aerospace systems has led to the development of Prognostics and Health Management (PHM), Structural Health Monitoring (SHM) and Fault-Tolerant Control (FTC) systems. This project deals with those technologies that enable the determination of the status of the flight - and mission critical systems and parameters automatically. In this context, status determination means to identify if there are any conditions in the on-board systems or in the platform structure which prevent the system to fulfill its functions as intended. Such conditions might be the result of wear or sudden damage, such as battle damage or other accidental events, to name two examples. The knowledge about the system status enables decision making regarding further action to be taken with regard to the ongoing mission, but also feeds into smart maintenance planning and supply chain optimization. Foreseen breakthroughs in the aerospace - above all, the anticipated common and widespread use of Unmanned Aerial Vehicles (UAV) both in civil as well as military applications - will require a new approach to structure and subsystems maintenance. This is due to the necessity of increase the safety of aircraft operation in the perspective of a massively growing aerial objects usage, potentially counted in hundreds of thousands of vehicles. In short- to mid-term perspective, the current approach to maintain safety cannot be sustained without radical change of its foundations. The cost of manual, fixed-schedule platform inspections, personnel training and certification, will be no longer a cornerstone of safety assurance, both in civil and military context. Non-destructive inspection of new type materials (e.g., composites or 3D printed components) is a burden with significant costs, related to time consumption, as well as advanced equipment and skilled workforce requirements. Cost-efficiency of aerial systems is a crucial factor to maintain EU-leadership in the aerospace domain and prevail over its competitors, following the spirit of past EU-funded calls (e.g., MG-1.3-2017 - Maintaining industrial leadership in aeronautics). Results obtained within the SAMAS project is one of the contributed to the process of provision to the EU full autonomy in the development and application of Structural Health Monitoring in civil and military applications. The results are only be limited to the aerospace industry but can be transferred to other industries of strategic importance for the EU, including, but not limited to renewable energy (wind turbines), automotive (autonomous and zero-emission vehicles), oil and gas, shipbuilding and chemical industry.

The scope of the SAMAS project agrees with the agenda of strategic and modernization plan for the EU as well as Partner Member States, in particular:

- European Defence Funds priorities list: Priority *Materials and components*, topic 7A – Advanced materials for enhanced performance of defence systems, Priority 11 *Key cross-domain enablers*, topic 11E – Sustainment and life-cycle management, including technologies that reduce logistic and maintenance dependency;
- Priority research directions of Ministry of National Defence of Poland for the period 2017 – 2026, Priority 3.6 *Modern materials, including smart materials*, Priority 3.7 *Breakthrough technologies*.

Contact:
Marcin Kurdelski Marcin.Kurdelski@itwl.pl

3. *Structural Health and Ballistic Impact Monitoring and Prognosis on a Military Helicopter – SAMAS2 Project* - Artur Kurnyta, Krzysztof Dragan, Marcin Kurdelski [Air Force Institute of Technology]

The aim of SAMAS 2 project is to develop a Structural Health Monitoring and Prognosis (SHMP) tool for corrosion degradation, bullet impact damages, that can be even possibly exploited for airframe load monitoring and generic damage development. These have been identified as critical factors for the structural integrity of the helicopter, since they can compromise the whole structural assessment and be a safety concern for the crew. The project is realized in a Polish – Italy consortium (

Table 1).

The project includes two main streams of activities:

1. Development of a corrosion monitoring system, with two goals:
   - verify the possibility to extend the fault-tolerant design to corrosion, answering the question whether the corrosion pit is equivalent to a standard notch in the definition of the fatigue endurance limit;
   - defining how to monitor corrosion and its progression rate.
2. Development of a ballistic impact and damage monitoring system, with three goals:
   - impact detection;
   - damage detection and quantification;
   - load monitoring and damage progression estimate.

The project is addressing the following topics:

4. The realization of an efficient corrosion monitoring system that will be tested both on a ground laboratory environment and a flight test. The system will include empirical models and a database of different scenarios for a real-time corrosion degradation assessment and prognosis.
5. The realization of an efficient impact monitoring system that will be tested both on a ground laboratory environment and a flight test. The system will include a Digital-Twin and a database of different scenarios for a real-time structural assessment and prognosis.
6. The realization of a load and damage monitoring system for aircraft and shafts of a real helicopter, which must be tested in flight. This monitoring system will be based on the knowhow acquired during the previous projects, with the main objective to assess its effectiveness in flight.
7. Based on the industrial partners experience, particular attention will be placed on the economic advantages derived from the SHM tool application on the helicopter. A Digital-Twin that includes Cost and Benefit Analysis and an evaluation of the Life Cycle Cost in different scenarios will be developed to support the decisions of the operators (maintenance, overhaul schedule, service life, flight preparation, etc.).

Specifically for ground tests for corrosion, a large number of coupon specimens is exposed to corrosion environment (Fig. 1) and used:

- to understand the criticality of corrosion damage in relation to similar mechanical damage;
- to find a correlation between the corrosion level and the measurements of environmental sensors and active sensors.

Different materials will be selected according to the critical regions identified by the manufacturer and users. For each material, a realistic component will be designed, exposed to corrosion and in most cases tested under fatigue load cycles.

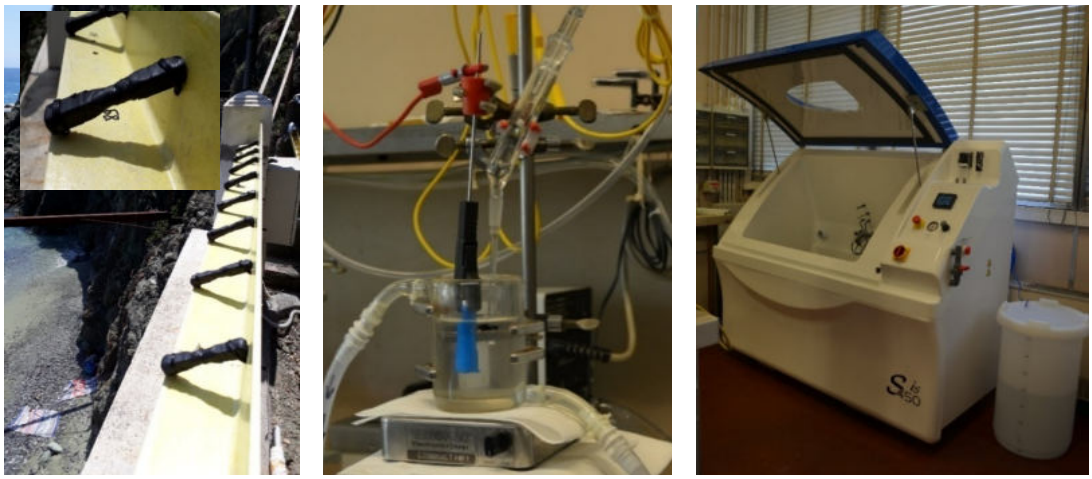

Figure 1. Methods of corrosion damage creation: natural environment, electro dissolution, salt chamber

Specifically for the ground test of the impact monitoring, a full-scale test rig of the tail boom of a helicopter including transmission and tail rotor (Fig. 2) is used for:

- analysis of the dynamic behaviour of the undamaged system;
- analysis of post-impact dynamic behaviour and damage identification.

Impact damage will be induced on the transmission shafts in a selected shooting range. It is proposed to create a motorized bench with supports in replication of the real ones (in the full-scale rig) on which bullet impact tests will be carried out in the shooting range. Sensor's signals will be acquired before, during and after the impact. Experimental performances and results will be compared with the prediction from simulations and the accomplishment of a set of previously defined performance requirements will be verified.

Figure 2. Ground test stand for impact detection and the region of interest

Table 1. SAMAS 2 Partners

Partner Name	**Acronym**	**Type**	**Nation**
Politecnico di Milano Dipartimento di Meccanica (leader)	POLIMI	University	Italy
Leonardo S.p.A. Helicopter Division	LND	Industry	Italy
Consiglio Nazionale delle Ricerche	CNR	Research Center	Italy
Air Force Institute of Technology	AFIT	Research Center	Poland
Military Aviation Works No. 1	WZL1	Industry	Poland
Łukasiewicz – Institute of Aviation	ILOT	Research Center	Poland
Military University of Technology	MUT	University	Poland

Contact:
Marcin Kurdelski Marcin.Kurdelski@itwl.pl

4. *MiG-29 Composite Bonded Repair Building Block Approach* - Piotr Synaszko, Michał Sałaciński, Krzysztof Dragan, Marcin Kurdelski, Andrzej Leski, Armen Jaworski [Air Force Institute of Technology, Ł-ILOT, CIM-MES Project]

The MiG-29 aircraft have been introduced into Polish Air Force into late 80's and early 90's. After a change in the operating philosophy of these aircraft in Poland from safe life to condition-based maintenance, additional inspections of the composite and honeycomb structures were introduced. During these inspections over the years have recorded damage to both structures composite as well as sandwich structures[12]. According to the damage tolerance philosophy commonly used today, the damaged component should be replaced or repaired[13]. The available documentation from the aircraft's manufacturer contained only guidelines for minor repairs, while some of the damage found was beyond the specified dimensions. This necessitated taking action. Typically, when damage exceeds the limit specified in the SRM, manufacturer support is required. The situation is slightly different for military aircraft. In some cases, technical support is carried out in the user's country by maintenance organizations or the research centers[14,15]. Guided by this approach, the development of a dedicated repair technology for MiG-29 aircraft composite structures was undertaken, including modeling methods, calculations as well as repair manuals. As part of the same project, repair technology was also developed for sandwich components.

Composite structures in aviation are commonly used nowadays. Important advantages include the ability to manufacture large monolithic components with complex geometries, low density and high strength. From the designer's point of view, they are much more demanding than traditional metal structures. The calculation methods used for composites are more complex[16]. A problem that is difficult to ignore is the susceptibility of composites to damage caused by low-energy impacts that can significantly reduce the strength of the component[17]. This damage can usually only be detected using non-destructive testing techniques[18,19,20] which affects the

[12] K. Dragan, and S. Klimaszewski, "In-service flaw detection and quantification of the MiG-29 composite vertical tail skin," Proc. of European Conference of Non- Destructive Testing, Berlin, 2006
[13] AC 20-107B Change 1. DoT FAA, 2010
[14] W. Baker, I. McKenzie and R. Jones, Composite Structures, Vol. 66 I. 1-4, p. 133-143 (2004)
[15] A. Baker, L. R. F. Rose and K. F. Walker, Applied Composite Materials Vol.6, p. 251–267(1999)
[16] Kelly, J.; Cyr, E.; Mohammadi, M. Finite Element Analysis and Experimental Characterisation of SMC Composite Car Hood Specimens under Complex Loadings. J. Compos. Sci. 2018, 2, 53. https://doi.org/10.3390/jcs2030053
[17] Ratwani MM. Effect of damage on strength and durability, RTO-EN-AVT-156-05
[18] Katunin, A.; Wronkowicz-Katunin, A.; Dragan, K. Impact Damage Evaluation in Composite Structures Based on Fusion of Results of Ultrasonic Testing and X-ray Computed Tomography. Sensors 2020, 20, 1867. https://doi.org/10.3390/s20071867
[19] Klepka, L. Pieczonka, W.J. Staszewski, F. Aymerich, Impact damage detection in laminated composites by non-linear vibro-acoustic wave modulations, Composites Part B: Engineering, Volume 65, 2014, Pages 99-108, ISSN 1359-8368, https://doi.org/10.1016/j.compositesb.2013.11.003
[20] Roach, Dennis Patrick, et al. Inspection Options for Detecting Various Types of Impact Damage in Composite Structures. No. SAND2013-7877C. Sandia National Lab.(SNL-NM), Albuquerque, NM (United States), 2013

range and intervals of inspections[21,22]. The introduction of composite components therefore requires the development of a somewhat broader program of testing and analysis than for metal structures to confirm their applicability and safe use. Such a program must be developed both for whole aircraft and for the significant structural modifications being introduced[23]. The case described in the article concerns the development of the repair technology using composites for selected components of the MiG-29 aircraft. Repair according to the proposed approach requires removing the damaged section of the structure and replacing it with an autoclave made patch made of a material with similar properties. This is a significant modification of the structure due to the introduction of new materials and adhesive joints. In this case, a program of testing and analysis is absolutely required.

Development of a research program

Based on the certification requirements of the documents mentioned above, a test program was selected. The programme in accordance with the recommendations of the documents and best practices[23] was composed in the form of a pyramid of tests. An important role was played by previous experience[24,25]. The first level, which included material characterization testing, was expanded to include thermomechanical testing. This extension was dictated by the need to verify if elevated temperatures during repairs would not reduce the performance of the materials used in the aircraft structure. Other test results from this level were intended to confirm the strength properties of the materials and provide input data for engineering calculations. In the pyramid of tests developed for the repairs of the MiG-29 aircraft, the second somewhat unusual level of the pyramid played an important role. At this level, tests and numerical analyses were carried out on specimens reproducing characteristic parts of the structure but made of similar materials. Most of these materials were repair materials. The use of equivalent components was primarily due to limited access to aircraft parts that could be used to make specimens. Due to the complexity of the components being repaired as part of the project, it was anticipated that the pre-selected test and simulation methods could produce results that differed from those expected. Therefore, the approach used was to train the test and simulation methods on an equivalent structure until the expected level of convergence of test methods with numerical simulations results was developed. The next level of the pyramid is the study of subcomponents. By this term are qualified sections taken from the actual structure (fragments of vertical stabilizer skin, etc.). As mentioned, their number was very limited, and the research served primarily to confirm conformity of the numerical simulation models developed at the previous

[21] Vilhena, B.S., Lourenço, G., Parracho, F.J., & Pereira, R. (2010). Damage Tolerance Design Damage Tolerance Design for Wing Components – Procedure Standardization

[22] Bos, Marcel J. "Fielding a Structural Health Monitoring System on Legacy Military Aircraft: A Business Perspective." Journal of the Korean Society for Nondestructive Testing. The Korean Society of Nondestructive Testing, December 30, 2015. doi:10.7779/jksnt.2015.35.6.421

[23] Military Handbook - MIL-HDBK-17-3F, U.S. Department of Defense, 2002, E-ISBN 978-1-59124-508-7

[24] 15. P. Synaszko, NDT ACTIVITIES DURING COMPOSITE BONDED
REPAIR OF PL C-130E WING BOTTOM SKIN, Chapter in Continuing Airworthiness of Aging Systems, AC/323(AVT-275)TP/930, 2020

[25] 16. Sałaciński, M., Stefaniuk, M., Synaszko, P., & Lisiecki, J. (2017). Use of a composite repair patches to repair the upper air intake flap for the MIG-29 aircraft engine. Aviation Advances & Maintenance, 40.

level of the pyramid. The fourth level of the pyramid involved fatigue testing of whole components with repairs. Within the fourth level, two fatigue tests were conducted. The first involved a composite repair. A vertical stabilizer with two repairs was tested. The second concerned repairs to the sandwich structure and was performed on the rudder with three repairs performed for three material variants. Positive results from all laboratory tests carried out in the project allowed to move to the highest level of testing, that is, flight testing. Flight tests are carried out according to developed by Air Force Institute of Technology and approved by military aviation authorities' programs that covered the full range of aircraft use.

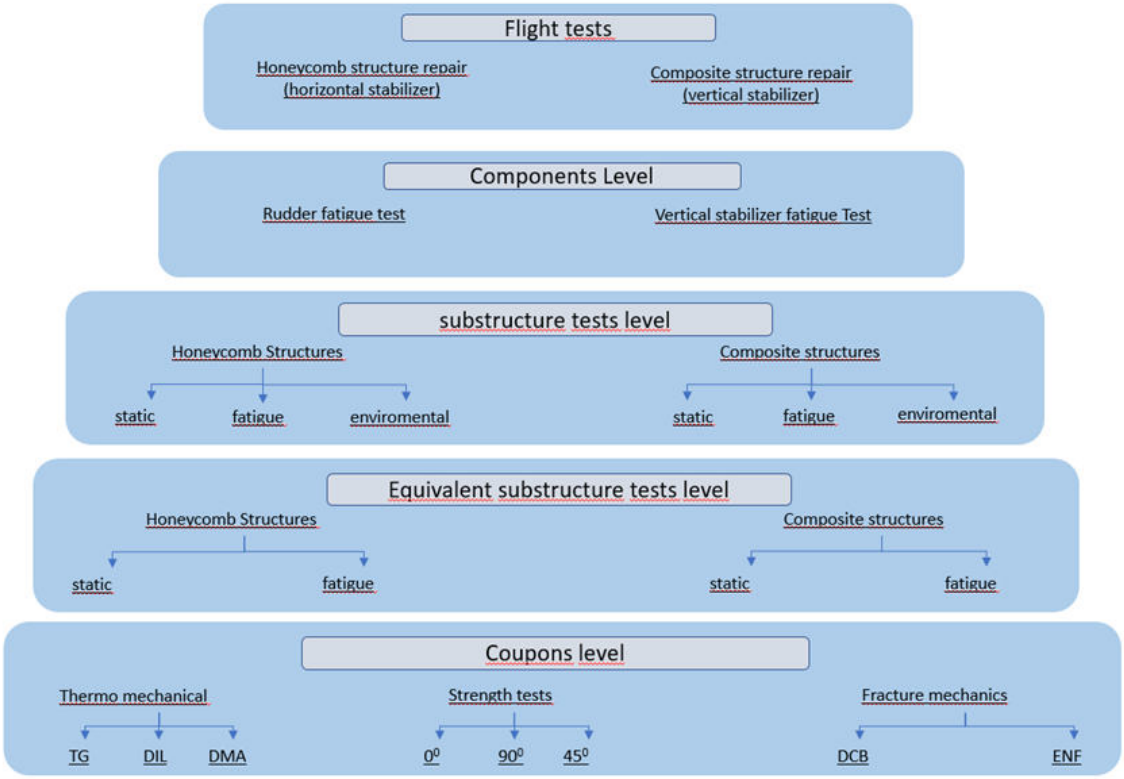

Figure 1. Test pyramid

Implementation

Due to time constraints, it was not acceptable to enter the next levels of the pyramid only after work on the previous level was completed. Some work had to be done in parallel. therefore, it was necessary to determine which results determine the performance of further research.

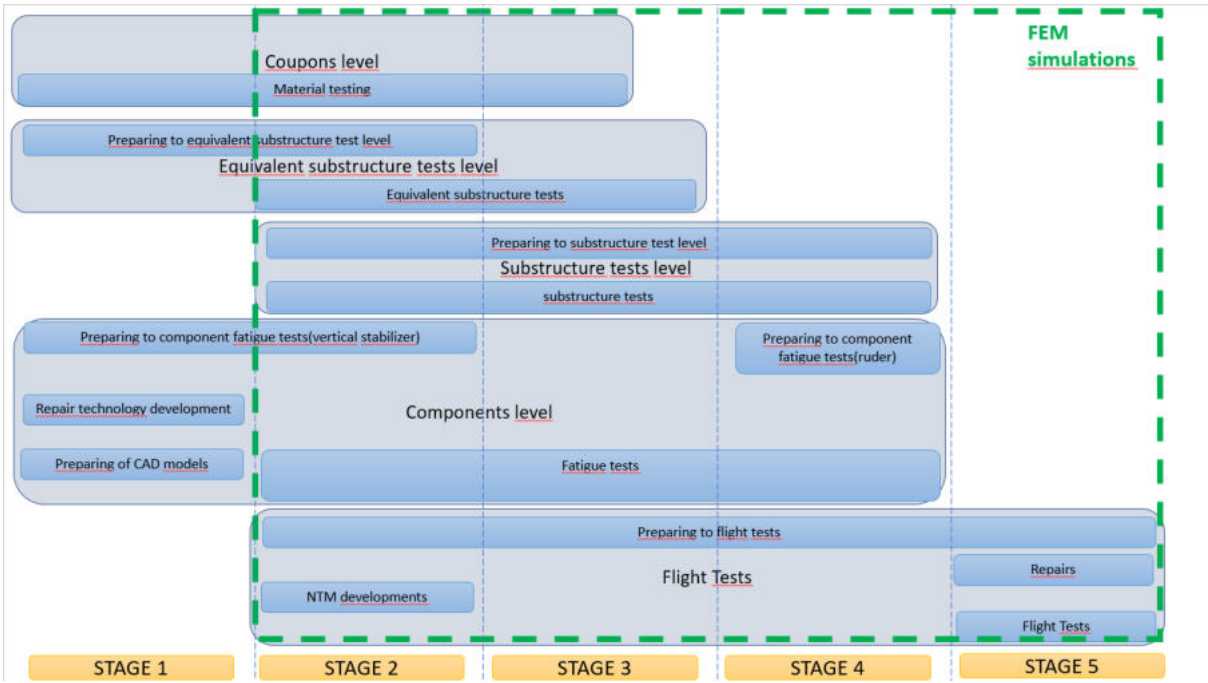

Figure 2. Test pyramid - impementation

In our case, moving further from the first to the second level of the pyramid was conditioned primarily by confirming the strength of the selected materials. Other studies were also significant. It was important to exclude the possibility of damage to the repaired elements as a result of the thermal cycle during the repair. The transition from the second to the third level required ensuring that the selected test and simulation methods would allow to obtain reliable results on a much smaller number of samples taken from the aircraft structure. The fourth level - tests of entire components with repairs was conditioned primarily by positive results from the first level. Thanks to this, the fatigue tests of the components could start quite early. The last fifth level of the pyramid - flight tests required the completion of a full research program and the development and approval of a set of documents regulating the issues of flight tests and further in-service inspections. A certain difficulty was the lack of knowledge at the beginning of the project about what damage cases will be subjected to prototype repairs. According to the assumptions of the project, aircraft for repairs were to be selected during the project implementation depending on the current operational needs of the air force. In the case of repairs to the honeycomb element, everything went according to the assumed scenario. Complications arose during the repair of the composite vertical stabilizer skin. During the preparations after removing the antenna cover, it turned out that we are dealing with several damages at small distances, which resulted in a significant increase in the repair area. A choice had to be made between performing the repair in accordance with the technology but with the risk of damaging the internal elements of the fin or shortening the length of the bonding below the limit. Finally, the option minimizing the risk of damage to the stabilizer was selected. The problem of too short bondline was solved by designing and making two repair packages. The first one was made in autoclave technology and bonded in place of the removed damaged structure. A second also prepreg made using a vacuum bag was applied to the enlarged area

covering the first packet and reinforcing the weakened area. The computational approach developed in the course of the project confirmed the effectiveness of the adopted solution.

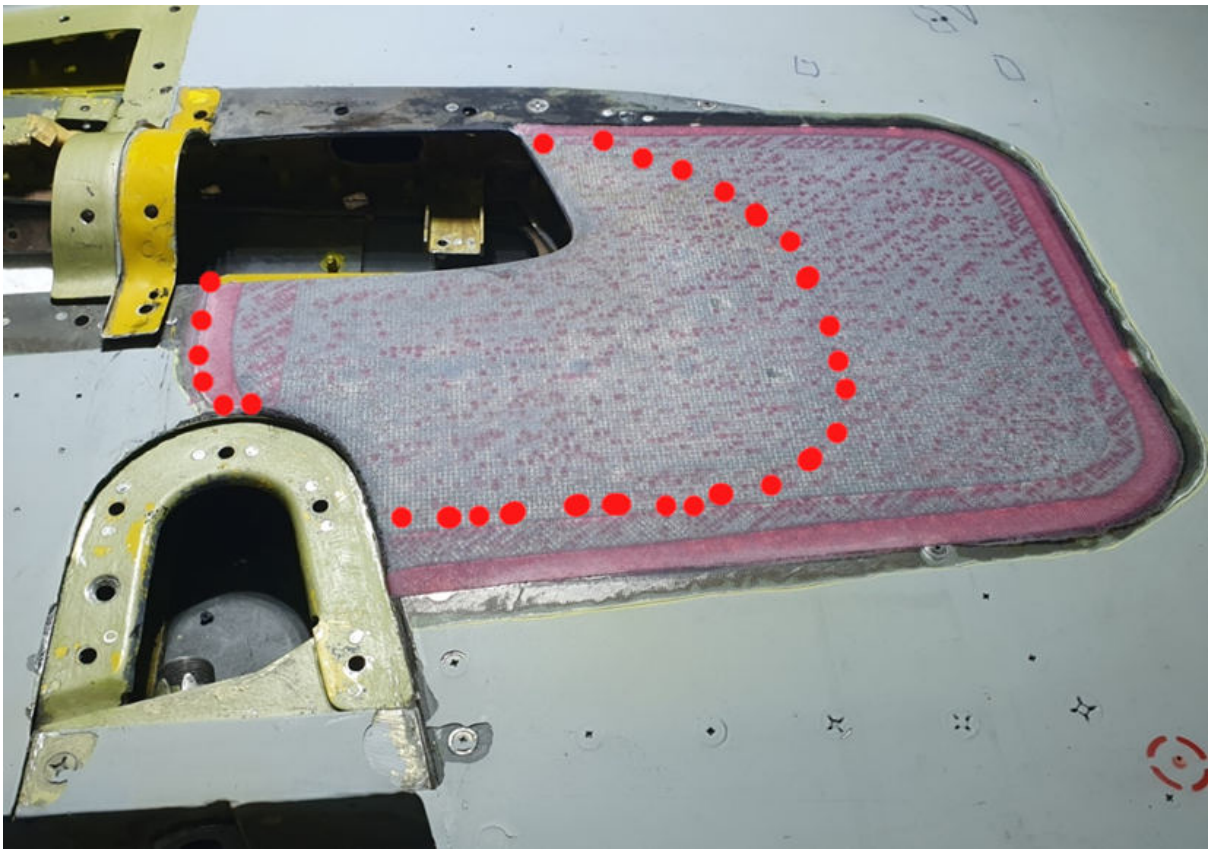

Figure 3. Repair of the vertical stabilizer skin. First patch is marked by red dots. Photography was made after curing second patch, before painting.

The end result of the research was sets of formal instruction documents describing the design and repair process. Due to the wide range of applications, the developed technology requires an individual project for each repair. Methodologies for performing calculations in the project are defined. In addition, operational bulletins and Non-destructive manuals have been developed specifying inspection intervals and maximum acceptable damage.

Summary

Some of the mitigation measures taken to minimize project risk have proven to be significant. This was the case with several repair material configurations. Finally, due to the too high risk of introducing manufacturing defects, one of the considered configurations was abandoned. Similarly, some of the assumptions made turned out to be inappropriate. This was the case with the use of technological core filling. During the aging tests, it was revealed that the use of a material that required rinsing with water caused the possibility of closing a small amount of water in the repaired structure and led to corrosion damage to the cell core. In the end, the applied approach turned out to be effective. The adopted methods of risk minimization were

sufficient. Calculation methodologies and numerical models supported by data obtained from research were developed. A set of formal instruction documents in the form of repair bulletins and service bulletins together with non-destructive testing methodologies was prepared. The whole process was verified by flight tests, after which the aircraft with repairs was sent to service. The inspections carried out so far confirm the durability of the repair.

Contact:
Marcin Kurdelski Marcin.Kurdelski@itwl.pl

5. *Corrosion Health Monitoring System (CHMS)* - Patryk Ciężak, Piotr Synaszko, Artur Kurnyta, Krzysztof Dragan [Air Force Institute of Technology]

In response to the demand from the defense sector and awareness of issues related to the problems of an aging aircraft fleet, such as increased maintenance costs. It must be done more and more NDT tests and costs related to repairs caused by corrosion phenomena increase. AFIT researches the development of the Corrosion Health Monitoring System (CHMS). Which will complement in terms of corrosion the Structural Health Monitoring (SHM) system already used on the platform of the aircraft Su-22 and the helicopter Mi-8 in the Polish Armed Forces. In 2019 SHM and CHMS were installed on the attack helicopter Mi-24.

CHMS as a system

There are many different approaches to Corrosion Health Monitoring System (CHMS). The most common approaches are:

1. CHMS is an integral part of a larger system, i.e. it is inextricably linked with Health and Usage Monitoring (HUMS) and together they form the Structural Health Monitoring (SHM) system. An example of a platform on which this type of solution has been applied is the F-35 aircraft (all aircraft users)[26].
2. CHMS is a standalone system that functions without cooperation with SHM because SHM has not been implemented on the aircraft. An example of a platform where only the CHMS system has been installed and research is ongoing is NH90 (the Netherlands).[27]
3. CHMS is an SHM subsystem, which functions in cooperation with SHM, but at the same time can function independently. An example of a platform on which this type of solution exists is the Mi-24 helicopter (Poland).

[26] Ludmila 't Hoen-Velterop, "Assessing the corrosion environment severity helicopters encouter using environmental sensors," Department of Defense – Allied Nations Technical Corrosion Conference, Paper No. 2017-400177 (Birmingham, AL, USA).

[27] Ludmila 't Hoen-Velterop, J.J.H.M. van Es, G.A. Bosma, K. Boeije, Assessment of the corrosivity of the operational environment of helicopters using sensors and modelling," Department of Defense – Allied Nations Technical Corrosion Conference, Paper No. 2019 (Oklahoma City, OK, USA).

Structure of Corrosion Health Monitoring System (CHMS)

BAE Systems has developed a CHMS system called Environmental Degradation Monitoring and Prognostics (EDMAP)[28]. EDMAP uses data from onboard sensors (Witness Plate, surface temperature sensor, surface wetness, RH, and air temperature), off-board databases, and corrosion prognostics to determine the current and future corrosion status of a platform. This status is referenced to maintenance opportunities to determine inspection deferrals and optimization of maintenance planning. EDMAP is the equivalent to corrosion as Health and Usage Monitoring (HUMS) is to the management of aircraft fatigue. EDMAP can also bring clarity and rigor to special servicing activities, such as those based on saline or hot/humid exposure and wash/rinse scheduling by forecasting the need for these activities based on individual aircraft conditions. EDMAP generates corrosion and environmental degradation reports, which are tailored to the specific needs of the maintainer.

Another approach to the CHMS structure is the application Passive SHM System for Corrosion Detection by Guided Wave Tomography use of the PZT transducers reduces the complexity of the system. In this case, it is possible to use noise cross-correlation techniques that have been conducted to do passive guided wave tomography of extended defects (such as corrosion) using an array of piezoelectric (PZT) transducers.[29]

The AFIT developed its own CHMS structure based on the experience in maintenance processes, overhauls of aircraft that are in the state of the Polish military, and the knowledge obtained from other global research centers. It contains 4 main system cores, a database, and algorithms that enable the analysis of data obtained from the operation.

The structure of the CHMS developed at AFIT:

- CORE 1 data on the use of the helicopter;
- CORE 2 flight parameter data;
- CORE 3 data from corrosive sensors placed on the helicopter KOR1, KOR2, KOR3;
- CORE 4 data from corrosion test side, NOAA and KOR4.

[28] Aaron Sudholz, “A corrosion prognostic health management system”, https://www.baesystems.com/en-aus/blog/a-corrosion-prognostic-health-management-system, (19 April 2018).

[29] Chris Loader, Darren Gerrard, James Waldie, Joel Smithard, Andrew Butler, Aaron Sudholz, “Corrosion Prognostic Health Management Principles Applied to Deployment of Environmental Sensors on Australian Defence Force Helicopters,” STO-MP-AVT-303 (2018).

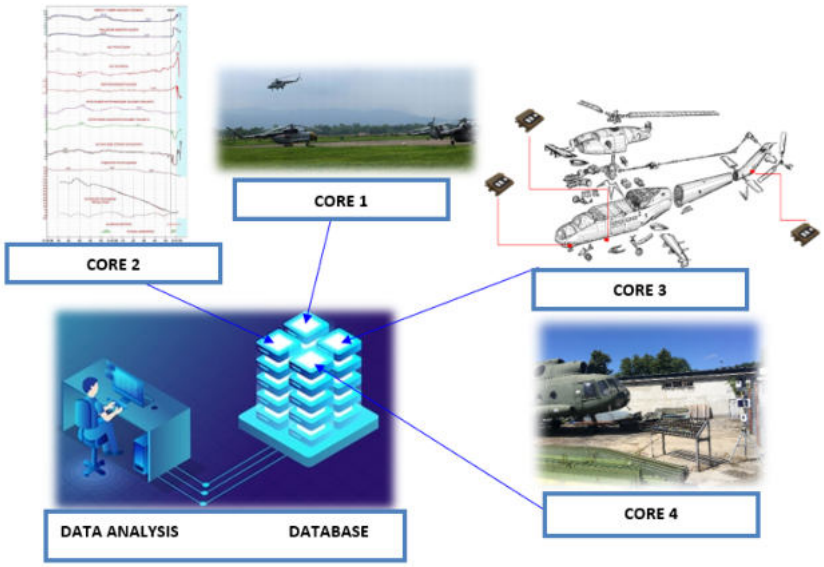

Figure 1. Diagram of CHMS as all maintenance system

Corrosion Health Monitoring System (CHMS) will be performed in 4 stages:

STAGE I:

- selecting corrosion sensors for testing;
- selection of places to place corrosion sensors;
- placing a set of corrosion sensors KOR1, KOR2 KOR3 in the structure of the Mi-24 helicopter;
- placing the KOR4 sensor in a closed space located at a permanent corrosion station;
- assembly of the weather station on a permanent corrosion station;
- commissioning of a corrosion station enabling environmental tests to be carried out, thanks to which the corrosivity criteria of the microclimate will be determined;
- development of a database enabling the compilation and analysis of data from corrosion sensors installed on the helicopter and from a permanent corrosion station.

STAGE II:

- development of a database collected by corrosion sensors (KOR1, KOR2 KOR3, KOR4), tests carried out at permanent corrosion stations, NDT tests in the field of corrosion detection (UT, ET, IRT, RT, D-SIGHT), test results obtained at fixed stations corrosive in the years 2004-2006, models for estimating the susceptibility to corrosion of aviation alloys obtained during the development of the corrosion prevention and control program for the PZL-130 TC-II Orlik aircraft in 2014;
- development of a database containing the history of the use of the helicopter during its operation.

STAGE III:

- compilation of data and development of an algorithm for their processing and interpretation;
- development of criteria for assessing the corrosion state of the aircraft structure (i.e. full parameterization of corrosion sensors).

STAGE IV:

- qualification of the CHMS (verification of criteria and development of the final form of system functioning).

Location of corrosion sensors on the helicopter

The CHMS system is based on a minimum number of sensors located in closed spaces that are distant from each other. It will enable the collection of data on the parameters of microclimate occurring in the aircraft. The location of the sensors was selected based on the analysis of available documentation, consultations with maintenance shops, and also manufacturers and users of airframe structure condition monitoring systems. 3 areas have been designated reflecting the microclimate in various zones of the helicopter Mi-24. It is shown in Figure 2. The first zone is the front part of the fuselage (the helicopter's gun hatch - non-hermetic zone), the second zone is the middle part of the fuselage (under the floor of the transport cabin, near the fuel pump - non-hermetic zone), the third zone is the rear part of the helicopter, vertical stabilizer (near the intermediate gear). The sensors make it possible to collect parameters that will allow determining the corrosion models of the aircraft structure. The fourth sensor will perform a validation function for corrosion measurements and will help in building a computational model for determining the probability of corrosion in all 3 zones of the helicopter. The sensor will be placed in a closed zone on a corrosion test site where validation samples will be also located. The fourth sensor will also provide service protection for those sensors who are mounted on the helicopter.
Sensors were installed by Military Aviation Works No. 1 in Łódź. The company has knowledge and experience in the field of maintenance and repair of Mil family helicopters. The sensor mounts enable their disassembly, replacement of the power battery and the panel with corrosion sensors. Also, have access to the port with the possibility of downloading data.

Figure 2. Location of sensors on the airframe of the Mi-24 helicopter

Sensors used in the CHMS used on the Mi-24 helicopter.

The selection of a type of sensor and selection of recorded parameters was a key element in the process of developing the concept of the entire CHMS. Under consideration were taken such parameters as pH, air temp., surface temp., humidity, RH (relative humidity), surface contamination, free corrosion, and galvanic corrosion. The sensor would have to pass the tests before installing it on the aircraft.

Environmental Specifications.

Fulfilling the Environmental Requirements is necessary to ensure that the equipment mounted on aircraft is safe for aircraft and users (pilots, maintenance crew, and passengers). Depending on the region of the world, country, and aviation authority: military or civil, various documents confirm the reliability of the equipment. Often, but not always, certification documents issued by one aviation authority are accepted by another aviation authority. The main aviation authorities are the Federal Aviation Administration (FAA - USA) and the European Union Aviation Safety Agency (EASA - Europe), which does not mean that they are the only ones. In Poland, there are two aviation authorities responsible for a type of aircraft: civil and military. Civil aircraft are managed by the Civil Aviation Authority (CAA), which is under the jurisdiction of EASA. Military aviation has its own aviation authority in Poland. Regardless of the aircraft belonging to the aviation authority, flight by plane or helicopter must be safe. Because AFIT installed corrosion sensors on military helicopter Mi-24 it needed approval from the military aviation authority. Polish Air Force Authority must give the type certificate to all equipment which is installed on any aircraft or helicopter. The type certificate is a document by which the authority states that an applicant has demonstrated the compliance of a type design to all applicable requirements. [30]

[30] Jeff Demo, Fritz Friedersdorf (2015), Aircraft corrosion monitoring and data visualization techniques for condition based maintenance, IEEE Aerospace Conference Proceedings, 2015(Big Sky, MT, USA)

AFIT Environmental Specifications which the sensor must fulfill before mounting on a helicopter:

- Operating Temperature: Mil-STD-810F Methods 501.4 and 502.4 Procedure;
- Storage Temperature: Mil-STD-810F Methods 501.4 and 502.4 Procedure I;
- Altitude: Mil-STD-810F Method 500.4 Procedure II;
- Rapid Decompression: MIL STD-810F Method 500.4 Procedure III;
- Explosive Decompression MIL-STD-810F Method 500.4 Procedure IV;
- Shock: MIL-STD-810F Method 516.5 Procedure V;
- Sinusoidal Vibration: MIL-STD-810F Method 514.5 Procedure I;
- Random Vibration: MIL-STD-810F Method 514.5 Procedure I;
- Acceleration Operational: MIL-STD-810F Method 513.5 Procedure II;
- MIL-STD-810G, Method 513.6, Procedure I;
- Water Ingress (Drip Test) Mil-STD-810F Methods 506.4 Procedure III;
- Humidity: Mil-STD-810F Method 507.4;
- EMI/EMC (at least 2 of these): MIL-STD-461E, CE101 (30Hz to 10kHz), CE102 (10kHz to 10MHz) CS101 (30Hz to 150kHz), CS114 (30Hz to 150kHz), CS115, CS116 (10kHz to 100MHz), RE102 (10kHz to 18GHz), RS103 (10kHz to 1GHz, 70V/m), RS103 (400MHz to 18GHz 200V/m), BS3G100 Part 2, Section 2 Magnetic influence, compass safe distance;
- Salt Fog Testing: MIL-STD-810F Method 509.4.

Data obtained from sensors of the CHMS located on helicopters Mi-24

To assess the differences in the corrosivity of environments between what is in the air base and inside the helicopter structure, sensors were placed on the aircraft and in the air base. The diagrams below show the corrosivity of the atmosphere in different parts of the helicopter.[31]

In Figure 3, you can see the relationship between Relative Humidity and Conductance High Frequency. These relationships determine the degree of salt contamination of the surface. This information can be used to determine the degree of air salinity in which the helicopter operates. Knowing the RH and temperature, we can determine the amount of water contained in the air. This will allow us to determine the type of environment in which the aircraft is located. When the atmosphere is saltier, we can conclude at which distance from the sea (knowing of course the salinity of the water reservoir) the helicopter flies.

[31] Bastien Chapuis, Eric Sjerve, Sensors, Algorithms and Applications for Structural Health Monitoring, IIW Seminar on SHM, 2015 (Paris, IIW Seminar on SHM, 2015).

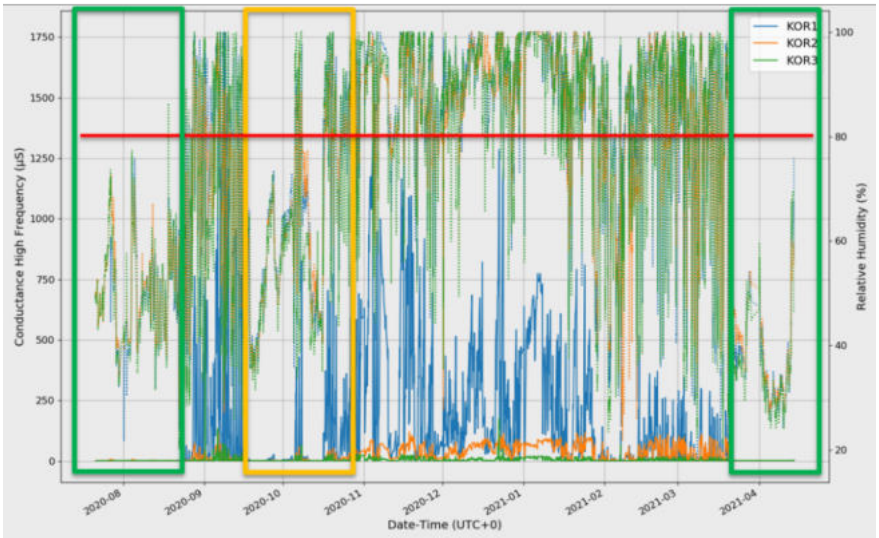

Figure 3. Relationship between Relative Humidity and Conductance High Frequency

The sensors were placed in 3 locations with the highest occurrence probability of corrosion. It has been observed that the vicinity of the automatic gun to corrosion sensor in front of the helicopter has the most prone to corrosion. On the other hand, the likelihood of corrosion under the helicopter fuselage floor is small, unless there are additional factors, such as e.g., strong air humidity due to the infiltration of a large amount of liquid into a closed space, such as fuel leakage from the fuel pump (the KOR2 sensor is in the immediate vicinity of fuel pump).

Conclusions

As can be seen, there is a problem with the aging aircraft fleet. This prompts a large-scale action. The Polish Armed Forces, trying to fight the problems of maintaining their fleet in the best condition, are taking measures to prevent long-term stops of aircraft on service. According to the DoD reports, the costs related to the fight against corrosion constitute 25% of all maintenance costs, which is a huge value[32]. Corrosion damage also causes that the aircraft must stay in the hangar for waiting for a long-time repair. The introduction of a CHMS can significantly reduce maintenance time by keeping the operator informed about the current corrosion condition of the structure.

As shown by the research results of tests carried out on the Mi-24 helicopter, it is possible to determine the corrosivity of the atmosphere in areas to which there is no access, e.g., under the floor (a zone where the fuel system with tanks is quite often located). There is a high probability that corrosion will occur underneath the floor. After consulting the maintenance bases that support cruise airplanes and emergency medical helicopters, it was discovered that the area under the floor was most vulnerable to liquids such as coffee, sweet drinks in the case of airlines, and blood and other fluids in the case of transporting people participating in accident. On the

[32] Fritz Friedersdorf, Jeff Demo, Conrad Andrews, M. Putic, "Sensor suite for monitoring atmospheric corrosion", NACE - International Corrosion Conference, 2012, Series 5:3558-3572

other hand, inspecting the area under the floor is very expensive. It is related to the work of dismantling the floor, checking the elements of the structure, and then carrying out the necessary repairs. This causes the aircraft to be excluded from flying for quite a long time. The CHMS will make it possible to determine, with a high degree of probability, the conditions that prevail in a closed and inaccessible space, which will enable the determination of inspection needs (increasing inspection intervals) also detection of the moment at which additional inspections should be performed in order to avoid serious damage to the structure.

Contact:

Marcin Kurdelski Marcin.Kurdelski@itwl.pl